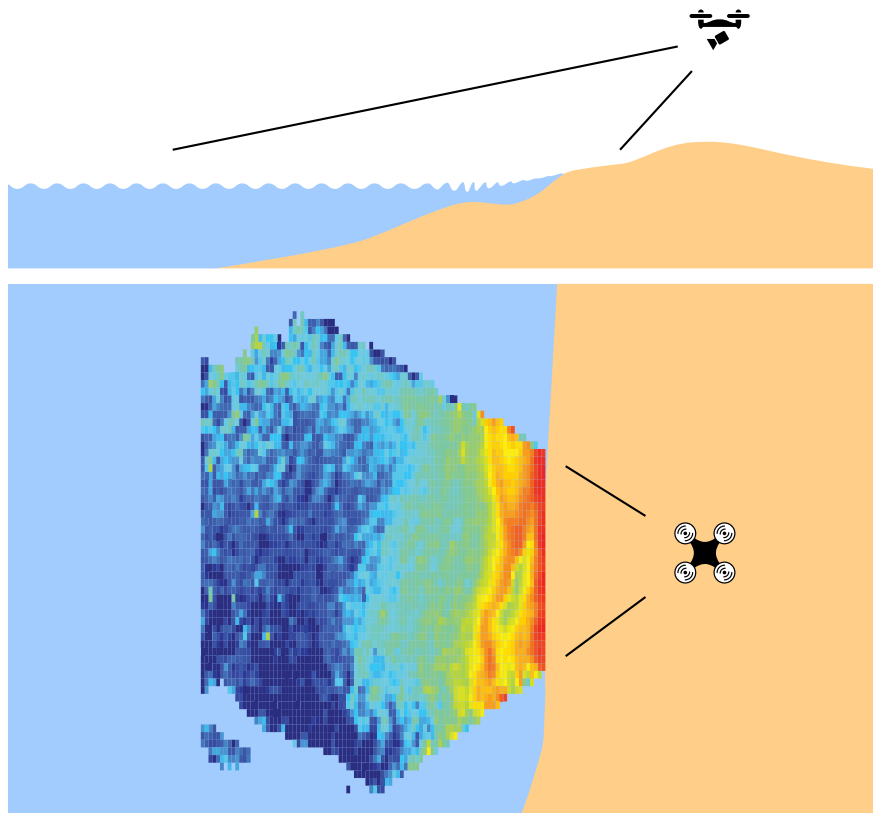


Bathymetry Mapping using Drone Imagery

Coastal Engineering MSc Thesis



Author
J.L. AARNINK

Supervisors
Prof. dr. ir. S.G.J. AARNINKHOF
Dr. ir. S. DE VRIES
Ir. R. DE ZEEUW
Dr. ir. D.C. SLOBBE

July 2, 2017

Contents

1	Introduction	1
2	Literature Review	5
2.1	History of Coastal Monitoring	5
2.2	Direct Bathymetry Mapping	6
2.2.1	Long Term Projects	8
2.3	Video Monitoring	8
2.4	Indirect Bathymetry Mapping	10
2.4.1	Wave Parameters	11
2.4.2	Depth Inversion using Wave Celerity	12
2.5	Image Stabilization	17
2.5.1	Optical Image Stabilization (OIS)	18
2.5.2	Digital Image Stabilization (DIS)	18
2.5.3	Rectified Video Stability	19
2.6	Societal Impact	19
2.7	Summary	19
3	Methodology	21
3.1	Conceptual Model	21
3.2	Data Acquisition	22
3.2.1	Bathymetry Calculation	22
3.2.2	Variables	22
3.2.3	Process	25
3.3	Image Undistortion (Intrinsic)	25
3.3.1	Theory	26
3.3.2	DJI Camera Matrix Calibration	27
3.4	Image Rectification (Extrinsic)	27
3.4.1	Theory	28
3.4.2	Rectification Test	28
3.4.3	Scenario's	29
3.5	Depth Inversion Algorithm	32
3.5.1	Wave Celerity and Water Depth	32
3.5.2	cBathy	33
3.6	Field Survey Plan	35
3.7	Summary	36
4	Results	37
4.1	Data Gathered	37
4.1.1	Day 1	37
4.1.2	Day 2	39
4.1.3	Reference Jetski Measurements	40
4.2	Rectification Process	40
4.2.1	Coordinate Analysis	41
4.2.2	Automatic Ground Control Point Detection	41
4.2.3	Rectification	42
4.2.4	Grid Rotation	42
4.2.5	Rectification Accuracy	43
4.2.6	Optical Signal	45
4.3	Depth Inversion through cBathy Algorithm	47
4.3.1	Base Scenario	47
4.3.2	First Results	48
4.4	Fine Tuning cBathy Settings	51
4.5	Summary	58

5	Discussion	59
5.1	Rectification Process Parameters	59
5.2	Measurement Setup	61
5.3	Wave Signal	61
5.3.1	Signal Analysis for Specific Locations	61
5.3.2	Spatial Parameters of Signal Analysis	65
5.3.3	Conclusions Signal Analysis	68
5.4	Influence of Longshore Current	68
5.5	Absolute Rectification Error	70
5.5.1	GCP Usage	70
5.5.2	Wrongful Wave Length Estimation	73
5.5.3	Plotting the Depth at the Wrong Location	74
5.5.4	Summary Geometry Error	75
5.6	UAV Bathymetry Mapping Performance	75
5.7	cBathy Adjustments	76
5.8	Future Research	76
5.8.1	Testing cBathy	76
5.8.2	Variance Decrease	76
5.8.3	Accuracy Increase	77
5.9	Practices	77
5.9.1	Drone Stability	78
5.9.2	Limitations	79
6	Conclusions & Recommendations	81

Bathymetry Mapping using Drone Imagery

J.L. Aarnink

Delft University of Technology

Abstract

As extensive efforts from consumer drone manufacturers resulted in inexpensive aircrafts that can capture high quality video imagery, drones are increasingly considered to be beneficial for scientific purposes. In the recent past, video imagery has been used to analyze waves in terms of several hydrodynamic parameters and to indicate matching coastal features. Whereas these measurements have been acquired using static cameras mounted on large poles situated at beaches, this report exploits a recently developed method using Unmanned Aerial Vehicles (UAVs) as a means to map coastal morphology. After recording aerial imagery in combination with several Ground Control Points (GCPs), several time series of georectified coastal images are compiled. Subsequently, for all of the points in a predefined grid, pixel intensities are stored throughout the time of the recording. Consequently, hydrodynamic data like wave celerity and phase are estimated, which in turn are used to invert water depths for every location in a predetermined area of interest using an algorithm called cBathy. Using reference measurements with an accuracy in the order of five centimeters, this report benchmarks the bathymetry as computed using the drone imagery by calculating the root mean squared error, the root mean squared error divided by the water depth and the mean error of three different sub areas within the area of interest. After calibrating parameters as used by the cBathy algorithm, it is shown that the best computation yielded a bathymetry with a root mean squared error of 0.37 meters for a total area of approximately 2500 square meters. It is also shown that the other datasets yield errors of approximately twice the error of the best dataset. It is shown that the total error can to a large extent be attributed to errors in the rectification part of the algorithm. The large errors and the large discrepancy between the errors make the method currently unsuitable for coastal monitoring purposes. Hence, before the UAV bathymetry mapping method is to replace traditional methods, more research should focus on standardizing the process and thereby decrease the variance between the errors of different datasets.

1 Introduction

Until recently, the most commonly used way of measuring beach profiles (see figure 1) was driving into the sea with a tall vehicle and reading its giant ruler. This so-called Coastal Research Amphibious Buggy (CRAB) is used to monitor the evolution of our coast. In the past decades, a growing interest in coastal data has subsequently increased the drive to acquire data more efficiently.



Figure 1: Beach Profile with Respect to Reference Level

The increasing amount of bathymetric data have increased our knowledge of the coastal system and its processes. This knowledge in turn can help acquire data more efficiently. In this study, a newly adopted bathymetry mapping method is exploited.

The method uses video imagery acquired by an Unmanned Aerial Vehicle (UAV) to track the celerity of different wave frequencies in a pre-determined offshore area stretching from the waterline to approximately 500 meter in cross shore direction. By comparing observed wave frequencies and their celerity, water depth can be inverted. This report endeavors to contribute to a more efficient way of gathering beach transacts with the use of UAVs.

Background Beach profiles include bottom location measurements as compared to a certain reference level. These transacts are acquired in a straight line perpendicular to the coast. In the Netherlands the reference level commonly used is the "Normaal Amsterdams Peil" (NAP). Depths are acquired up to a certain predetermined depth or offshore distance, depending on the coastal features in which the users are interested. When collecting multiple beach profiles that are located next to each other, a three-dimensional under water geography can be mapped, which is called a bathymetry. When analyzing the bathymetry of a certain beach over a certain period of time, changes in sediment budgets of the coastal system can be determined.

The changing bathymetry alters the movement of bodies of water over the beach floor. The changing water movement in its turn causes erosion and/or sedimentation leading to a different bathymetry. This interaction is captured in a dynamic process called morphodynamics. In summary, bathymetric data help scientists understand coastal dynamics by monitoring sediment budgets.

The study of morphodynamics is gaining increasing interest in the scientific community for a number of reasons. Apart from for instance predicting siltation of nearshore shipping lanes, keeping track of erosion and/or accretion of sediment can help governments to make decisions regarding safety against flooding. The continuous measuring of the amount of sand in the coastal system is called coastal monitoring. In Europe, Australia and the United States it has been practiced for over a century. These developed countries are relatively well prepared against the effects of climate change. On the other hand, there are many less developed countries with large populations in lower lying deltaic areas. These coastal regions are facing increasing humanitarian and financial risks induced by the rising sea level.

The dunes are part of the dynamic coastal system as described above. During storm events, dune sand is replaced in offshore direction. Subsequently, during calm weather conditions, the dunes are naturally rebuild. Therefore, structural erosion can result in land loss and even dune breaches during storm events once the dunes do not have enough sand to be transported offshore. Hence, for the governments of developing countries, acquiring bathymetric data can assist in identifying coastal areas that are prone to above mentioned risks.

An increase in efficiency when gathering bathymetric data can provide the scientific community with faster assessments and subsequently a better understanding of coastal processes. Furthermore, it can be a useful tool for less developed countries to monitor their coasts and make decisions to increase the safety of their population.

Previous Research Whereas up until the 1990s, bathymetry surveys were generally conducted using the before mentioned CRAB, scientists have since been exploring new methods. Echo sounders have been mounted at ships and smaller water-based vehicles to collect water depths at specific locations. Also, satellite data and radars were proposed as a more efficient solutions for acquiring bathymetric data. The data acquisition is a trade-off between

accuracy and spatial coverage¹. Echo sounders for instance have an accuracy of a couple of centimeters. However, the process is location bound and therefore expensive when surveying a larger area. On the other end of the spectrum, satellites increase the spatial scale significantly. However, the accuracy lower and not usable for sediment budget calculations.

A more recent technology that monitors a stretch of coast of approximately one kilometer exploits the quality increase of video footage. Tall poles equipped with video cameras for multi-directional coastal surveying, called Argus stations, take images with a certain predetermined interval. From these images, wave peaks can be obtained and subsequently wave celerity and phase data is gathered. As parts of the hydrodynamic behavior of incoming waves are known, scientists from the Oregon State University have been able to write an algorithm that uses this data to calculate water depth and therefore compute a bathymetry. This method reportedly yielded a root mean squared error of 0.44 meters for an area of approximately 500 meters in cross shore direction by 1000 meters in long shore direction².

Currently, consumer UAVs are capable of capturing video from a high and relatively stable viewpoint. Therefore, when using the above described video-based bathymetry mapping method, Argus stations and UAVs are seemingly interchangeable. Drone surveys can potentially benefit from a larger flexibility and a higher altitude at which footage can be recorded. Efforts are made to use the same wave tracking methodology for UAV imagery instead of Argus footage. Rob Holman, of the Oregon State University, indicated in a personal communication that first results are promising. The method of inverting water depth from UAV video imagery basically entails three steps. The first step regards the field survey. Subsequently during step 2, the captured images are rectified after which in step 3 the water depths are computed. All of these steps entail errors which add up to the total error of the method.

Regarding the data collection, UAVs are widely operational and have advantages over fixed Argus stations. Drone manufacturers are investing significant efforts to improve their products up to the point where flying a drone becomes effortless. Furthermore, research is still improving the performance of drone cameras which has resulted in the capability of capturing 4K videos. The most signif-

¹(van Son et al., 2009; Li et al., 2016)

²(Holman et al., 2013)

icant advantage of UAVs over Argus Stations however, is their flexibility. Drones can fly anywhere whereas Argus Stations have a fixed location. Potentially, when bathymetric data of a certain location is required, a simple drone flight could suffice. Also, using a drone enables carrying out multiple scenarios with different angles at which the area of interest can be captured.

The second step regards the image rectification process which links the observed waves in the video to a specific location in a user defined three dimensional grid system. Undistorting and rectifying images is a process widely researched in the study of geodesy. An essential part of this process entails the calibration of the drone camera. Whereas the angles of incidence of all 4096 x 2160 pixels are captured by 9 parameters, there will always be room for incremental improvements. The rectification determines the three dimensional coordinates for every pixel in each individual video snapshot. The two dimensional 4096 x 2160 photo pixel matrix is converted into a user specified three dimensional coordinate system. In this research four ground control points (GCPs) are used to calculate a coordinate for every pixel. In this step, inaccuracies of the automatic detection of GCPs together with the rectification algorithm add to the error budget of the determined bathymetry.

Finally, an algorithm called cBathy is used to convert the rectified images into water depths. In coastal regions where the water is shallower than 1/20 the size of the wave length, the speed at which a wave travels is related to the water depth. This relation is used to estimate the bathymetry of the area of which the drone imagery is taken. When waves are behaving linearly, the relation between their celerity and the water depth is indicated by a linear dispersion relation. However, when higher waves introduce turbulence which can be observed by white foam caps, the dispersion relation is less prevalent. Therefore, this part of the process is also expected to add to the overall error of the eventual computed bathymetry.

Purpose This report discusses the advantages and disadvantages of different bathymetry mapping technologies and elaborates the UAV video method. It will indicate the role of the newly acquired method within the realm of existing bathymetry mapping methods. As all different technologies have advantages and disadvantages, the potential future use and limitations of UAV imagery as indicated by this research can help in the comparison with other methods and give it a role in future coastal engi-

neering practices. Furthermore, as there are virtually endless possibilities for the setup of such an UAV survey, the choices made in this report are extensively elaborated and could therefore serve as a guideline to enable swift bathymetry mapping for inexperienced users. Also, an indication is given on what magnitude of water depth error is to be expected for the current state of the technology.

The report subsequently analyses each of the steps in the proposed method in terms of their contributions to the total error of the bathymetric measurements. Lastly, suggestions are made on how to increase consistency and eventually decrease the error magnitude.

Hypothesis Because the use of UAVs requires little labor at low cost, it is expected that mapping bathymetry using drone imagery can be a substitute for traditional methods in the future of coastal monitoring. It is hypothesized that the method yields results sufficiently accurate for coastal monitoring purposes.

Research Questions

- **Main Question:** Is it valuable to intensify researching efforts regarding UAV Bathymetry Mapping for future use in Coastal Monitoring?
- **Sub Question:** What is the depth inversion accuracy in the current state of the technology for coastal conditions in the Netherlands?
- **Sub Question:** Does the depth inversion process yield consistent results within 0.2 meters root mean squared error?
- **Sub Question:** Which step in the UAV depth inversion process is the largest contributor to the water depth error budget?
- **Sub Question:** On which aspect of the UAV bathymetry mapping method should future research be focused to increase its accuracy?

Method To compare the UAV bathymetry mapping method with conventional bathymetry mapping technologies, a comprehensive survey of a small part of the Dutch coast at Scheveningen is conducted. An accurate water depth is measured using a jetski with an echo sounder. As the jetski acquires data with an accuracy of a couple of centimeters (van Son et al., 2009), this data can be used as reference data. Subsequently, several videos of

the same area are taken with a drone. The drone footage is used to compute water depths. The report elaborates on the different steps of the UAV depth inversion process and show the intermediate data, ranging from GPS loggers to automatically detected GCPs. The error budget of each step is described and compared between four different field measurements conducted with a consumer UAV.

Several surveying scenarios have been compiled that differ with respect to drone position or using different Ground Control Points. As wave and light conditions change, other variables that can vary throughout the scenarios are for example the date or time of day at which the survey takes place. As the total accuracy of the method is the results of the accuracy of the different steps of the method, this report aims at indicating the error in each part and finally showing its sensitive areas. Different measurement and computation scenarios are used to find the largest error contributors. Whereas Rob Holman of the Oregon State University already elaborated on the use of differing amounts of GCPs and thereby potentially making the data gathering process easier, this report verifies the computed bathymetry with ground truth. Hence, a valuable analysis on the accuracy of the depth inversion can be done giving the root mean squared error. When comparing the final bathymetry error budget with the errors which are observed for the individual steps in the process, an indication of the potential future error of the method can be given.

Content The following chapter discusses literature regarding societal aspects and the history of coastal monitoring. Also, the advantages and disadvantages of different coastal surveying methods are elaborated in a graphical comparison. Subsequently, developments in the use of video imagery for coastal research are elaborated as well as the depth inversion algorithm cBathy. In the final part of the literature review, the hypotheses are introduced. Chapter 3 entails the methodology of the research. One by one the different steps in the UAV bathymetry mapping process are elaborated. For each step in the UAV bathymetry mapping method the data is shown that is transferred to the next step. Furthermore, a small test regarding the rectification accuracy of subsequent images is conducted. Thereby support is created for decisions regarding the setup of the final survey for this research. Subsequently, section 4 shows the results of the bathymetry mapping process. A base scenario is established that specifies the settings for the different steps in the process. The results chapter

also indicates the observed error of the bathymetry after it has been computed according to the settings in the base scenario. Subsequently, chapter 5 elaborates on the conclusions that can be drawn from the results as indicated by the base scenario. The largest error contributing steps in the process are identified based on the composition of the data as indicated in chapter 4. Thereafter, they are investigated to be able to increase the total bathymetry accuracy. Lastly, in chapter 6, conclusions are drawn.

2 Literature Review

After reviewing the history of coastal monitoring, this section of the report shows different methods for coastal monitoring. It gives an indication of the usefulness of the different methods based on several parameters. It subsequently briefly shows societal impacts after which a conceptual model for UAV depth inversion is shown.

2.1 History of Coastal Monitoring

Whereas societies around the world have always been dealing with protecting their land against the sea, coastal morphodynamics has not been understood very well throughout time. It has only been since the beginning of the 20th century with both the understanding of physics and the increase in computing power to the disposal of researchers that knowledge of our coastal system has evolved significantly. Several researchers have contributed to increasing monitoring techniques and predicting skills. Initially, this section will give a brief overview regarding the research that has already been done with respect to coastal monitoring. Subsequently, it lists both direct and indirect bathymetry measuring technologies.

One of the first researches which specifically focused on coastal morphology was induced by the second world war. To make a landing on enemy beaches, bathymetric knowledge was regarded to be valuable information. Therefore, Williams (1947) researched the mapping of beaches from aerial images. He took wave propagation and phase speed into account. This research was based on an early stage remote sensing technology using time lapse images of the water surface. Subsequently during the seventies, large scale research was conducted to gather data regarding hydrodynamics, beach profiles and sediment transport for several beach segments across coasts of Florida and California in the United States (Gorsline, 1966; Ingle, 1966; Komar and Inman, 1970). Large quantities of data helped coastal engineers gather knowledge about coastal situations in both high and low energy coasts. Later, coastal engineers started focusing on creating equipment that made it easier and cheaper to gather beach profiles (e.g. the Coastal Research Amphibious Buggy (Birkemeier et al., 1984)).

After the development of these new technologies together with an accumulation of interest in the coastal engineering field of study, researchers started focusing on the (repetitive) migration of sand bars, nearshore wave statistics and suspended

matter in coastal areas (Lippmann and Holman, 1989, 1991; Holland, 1992; Lippmann et al., 1993; Leu et al., 1998; Kutser et al., 1998). As the monitoring had been going on for several decades, different studies found controlling variables for coastal behaviour and started researching inter annual variability with a data set of over 14.000 nearshore profiles (Wijnberg and Terwindt, 1995; Lippmann and Holman, 1990). It was discovered that the most frequently observed bar is the longshore periodic bar. These bars are highly unstable as their average residence time was about two days. Therefore, unlike regular geology, the coastal system is highly dynamic and requires intense monitoring.

According to Plant et al. (2002), due to the narrow band of spatial and temporal scales, morphological studies are generally prone to sampling errors. Therefore, a spectral analysis can be used to decrease these errors by configuring an appropriate scale-controlled interpolation method. Concurrently, increasing availability in computing power initiated the rise of computer models for the prediction of morphological development. With these tools, researchers could start implementing their accumulated knowledge into predictive algorithms. Meanwhile, different measuring techniques started being used for the purpose of coastal monitoring (e.g. radar installation (Young et al., 1985; Teague, 1986) and Argus Coastal Monitoring Systems (Holman and Stanley, 2007)). All of these technologies serves a similar purpose but yet the majority seems to survive and coexist. This is due to the different nature of the specific measuring technologies. Some are efficient in capturing a bathymetry with an accuracy of five centimeters or higher. These measurements are generally used for sediment budget calculations for a specific stretch of coast on a specific moment in time. Other technologies have a lower accuracy but a higher spatial scale and could therefore still be used to monitor coastal features over a longer period of time.

Bathymetry mapping is used for several purposes. The International Hydrographic Organization (IHO) established general accuracy standards for water depths (Mills, 1998). The standard for shallow water was set at 25 cm. This accuracy is sufficient for long term monitoring of coastal features like for instance sand bars. However, calculations of sediment budgets as done by Shore Monitoring are generally done with data accurate within five centimeters. With these numbers taken into account, for a new technology to (partly) take over from existing methods, an error of approximately 25 cm is required.

2.2 Direct Bathymetry Mapping

The following coastal monitoring technologies are capable of mapping a bathymetry. They instantaneously collect location and water depth, and after a simple compilation of the data, a nearshore morphology can be mapped. These technologies do however require researchers to physically be at the location of interest. Therefore, during extreme conditions like for instance a storm, it is usually impossible to do research. The following analysis will elaborate on different coastal monitoring methods and assign a score to six different measures:

- **Flexibility:** Whether the technology can easily be used on several different stretches of coast within a short period of time.
- **Low Cost:** The amount of financial resources it requires.
- **Accuracy:** The indicated error of the mapped bathymetry as compared to the real world situation.
- **Spatial Range:** How large a stretch of coast the technology can measure at once.
- **Temporal Range:** The ease of doing near-constant measurements over long periods of time.
- **Low Effort:** The labor intensity of the technology.

CRAB During the twentieth century, researchers usually used a sea sledge in combination with a fathometer to compile a comprehensive bathymetry. As this traditional way of mapping was time consuming, scientists focused on increasing the efficiency of these measurements. Birkemeier et al. (1984) created a device to survey nearshore data more efficiently. The device was called the Coastal Research Amphibious Buggy (CRAB, see figure 2 & 3) and was basically a motorized tripod which could measure water depths up to 9 meters by driving over the sea floor. At the time, this was a revolutionary design which also sparked the invention of similar devices. This new way of gathering coastal data was primarily more cost effective than conventional ways of measurement. Birkemeier et al. (1984) state that the CRAB reduced the surveying cost by about 18 times. The reduced costs were primarily a result of the decrease in the required personnel and time.



Figure 2: Coastal Research Amphibious Buggy

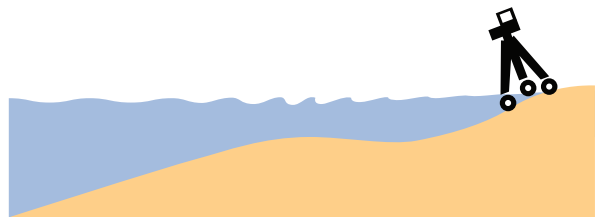


Figure 3: Method CRAB

Even though at the time this measuring technology was innovative and more efficient than conventional measurements, the CRAB is not considered to perform well based on the six predetermined measures (see figure 4) by current standards:

- **Flexibility:** The machine is large and hard to transport. Therefore, it cannot be deployed swiftly.
- **Low Cost:** The utilization of the device is specific to bathymetry mapping. As there were not a lot of manufacturers, the product was expensive.
- **Accuracy:** The CRAB has a high accuracy. Because it rides on the actual sea bottom, the measurements are not influenced by suspended sediment properties like for instance light rays traveling through the water.

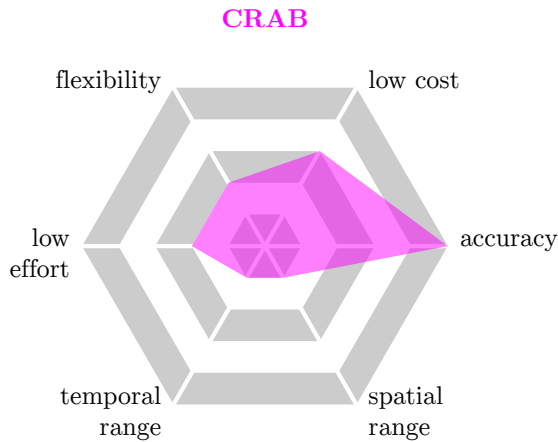


Figure 4: Rating CRAB

- **Spatial Range:** As the machine is slow, the stretch of coast it can measure per day is limited. To be able to do extensive surveys, several CRABs are needed.
- **Temporal Range:** For the same reason as mentioned above, to be able to measure the development of a morphology, the low amount of data the CRAB can gather really limits temporal measurements.
- **Low Effort:** As the machine is specific to bathymetry mapping, extensive training is necessary to operate the CRAB. Also, it required several people to operate. Therefore, it takes a significant amount of effort.

Jetski with Echo Sounder Later, an accurate way of measuring coastal bathymetry was developed using an echo sounder mounted behind a jetski (see figure 5 & 6). Due to the use of a centimeter-accurate Real Time Kinematic Global Positioning System (RTK GPS) sensor, this mapping technique produces maps with depths within a couple of centimeters accuracy (van Son et al., 2009).

Nowadays, if a research project requires an accurate map of the coastal situation, the jetski echo sounder is usually the equipment that is used. The technology has pushed the CRAB out of existence because it scores similarly or better on every point (see figure 7):

- **Flexibility:** Although it is much easier to move a jetski than a CRAB, it is still hard to transfer it across the planet. Therefore, it has an average score in flexibility.



Figure 5: Jetski With Echo Sounder

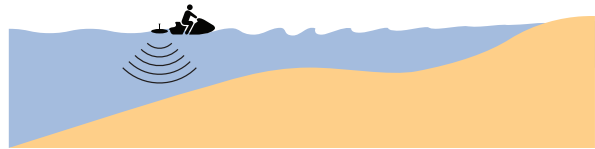


Figure 6: Method Jetski

- **Low Cost:** As the data gathering is faster than the CRAB, the manpower and therefore the cost is lower. However, it still requires rather specialized equipment.
- **Accuracy:** Through the use of an RTK GPS and an echo sounder, the error of measurements is approximately only a couple of centimeters. This is extremely accurate for coastal monitoring purposes.
- **Spatial Range:** On the other hand, due to the high amount of effort and specialized equipment necessary, measuring a more extensive stretch of coast becomes far more time consuming compared to other measuring techniques.
- **Temporal Range:** Like mentioned above and like the CRAB, the amount of effort going into data gathering makes it unattractive for long term measurements. Especially if daily data is required.
- **Low Effort:** Due to the need for an operator on every jetski and people needed for support activities, the amount of effort that is required for measuring with jetski's is significant.

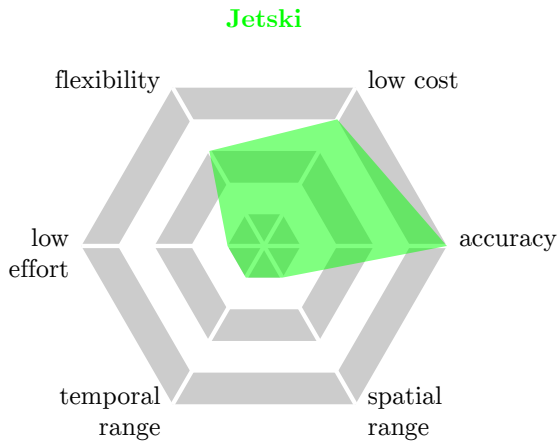


Figure 7: Rating Jetski

2.2.1 Long Term Projects

Similar to the sand engine at the Monster coast in the Netherlands, there are multiple test sites at which extensive sets of coastal data are available. At Duck, in North Carolina, there have been multiple studies. Furthermore, there has been a beach morphology monitoring program along the Columbia River littoral cell. These locations are located at the coasts of Oregon and Washington, USA. At the latter location, Ruggiero et al. (2005) researched the seasonal and interannual morphological variability of a highly dissipative beach. The research used real-time kinematic differential global positioning system survey methods, which included the use of GPS receivers in terms of a hand-held data logger, a jetski mounted GPS logger and a vehicle mounted GPS logger. Whereas seasonal variability was discovered and described, the report states that distinct differences in large-scale coastal behavior is still not understood.

Furthermore, Lippmann et al. (1993) researched the sand bar system at the above mentioned United States Army Corps of Engineers Field Research Facility at Duck, North Carolina. The bars were measured daily for a five year period. For the inner bar, conventional methods were used. However, for the outer bar, video methods were used where wave breaking indicated the position of the bars qualitatively. Also, research into long term sand bar behavior which gathered data from the Dutch, US and Japanese coast described the proportionality of depth variations in the coastal region (Ruessink et al., 2003b). Once again, this report states that linear regression analysis between bar parameters and hydrodynamic parameters are inconclusive.

As coastal behavior is still not understood extensively, in combination with future societal coastal challenges, the need for research is still growing. Subsequently, the need for data is also growing. Therefore, is it still beneficial to put effort in researching new data collection methods.

2.3 Video Monitoring

Throughout the twentieth century, different scientists have started using new technologies to gather coastal data. As early as in 1989, Lippmann and Holman wrote about using video imagery for coastal surveying. They used the imagery for quantifying sand bar morphology. By indicating dissipation of wind waves and swell over the crest of a breaker bar, their location could be indicated with errors of less than 35 %. Later, these researchers from Oregon State University pioneered the Argus camera framework to standardize coastal video monitoring.

Argus Camera System Coastal video systems were developed with the primary aim of improving our scientific understanding of diverse nearshore systems and how they respond to forcing by waves and tides. This was the primary motivation for the initiation of the Argus Programme (Holman and Sallenger, 1986; Holman et al., 1993a,b; Aarninkhof and Holman, 1999; Holman et al., 2003). The system is basically a multitude of cameras mounted on a tower that monitors a stretch of coast (see figure 8). It was by using this technology that it became possible to constantly monitor a coastal stretch of about 5 km. In the early stages of Argus, among other purposes it was used for detecting coastlines (Plant and Holman, 1997).

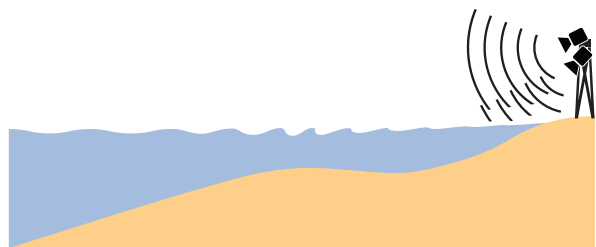


Figure 8: Method Argus System

Apart from gathering data on itself, video imagery can also be used to improve other coastal monitoring programs. Smit et al. (2007) explored video-imagery for the purpose of coastal evolution. They found that the inclusion of monthly video-derived data was found to improve confidence inter-

vals for predicted shoreline evolution, and also facilitate more sophisticated data exploration. The research focused on indicating intertidal coastline location (TICL) and the intertidal momentary coastline (MICL). The Argus imagery was found to significantly decrease the width of the confidence interval. Lastly, they found that intertidal bathymetrical data could be beneficial to nearshore flow and sediment transport forecasts. Also using Argus, Aarninkhof et al. (2003) researched video imagery to map intertidal beach bathymetry. Automated pixel clustering was used to identify a boundary. Thereafter, concurrent tide and wave data was used to calculate the elevation of the intertidal shoreline. According to this research, the method is accurate up to 15 cm. Currently, data from Argus stations is used in combinations with a water depth inversion algorithm called cBathy. In this was, an Argus station acquired data from which a bathymetry is calculated a couple of times per day.

When comparing the Argus system with other mapping techniques, there are clear distinctions between their scores (see figure 9):

- **Flexibility:** As the Argus system has to be constructed and is fixed at a certain location, its flexibility is limited.
- **Low Cost:** Also, due to the use of specialized equipment the construction cost especially makes it financially intensive.
- **Accuracy:** Whereas there is still an inversion error because the water depth is not directly measured, due to the high temporal range, the water depths can be estimated relatively well.
- **Spatial Range:** The system cannot easily be moved. However, it can monitor a stretch of coast of a couple of kilometers. Therefore, the methods score in terms of spatial range is average.
- **Temporal Range:** When looking at the temporal range, the Argus system scores well. This is because the monitoring is constant for years on end.
- **Low Effort:** Whereas there is theoretically not a lot of effort going into gathering images once the system is operational, getting the system operational and creating useful data from these images still takes effort.

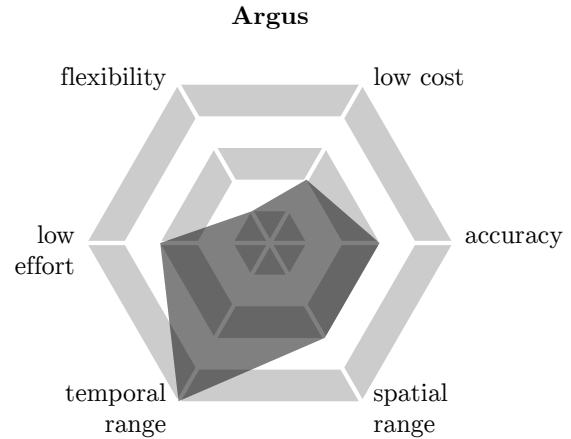


Figure 9: Rating Argus System

Other Video Monitoring Efforts About 20 years after the innovation of Argus stations, a similar camera setup was developed by Taborda and Silva (2012) which they called COSMOS. This technology comprehends a lightweight video monitoring system. It is portable, low-cost, robust and easy to install and can be used to monitors several coastal features. A further goal for the surveillance system is to expand its features and create a coastal hazard warning system.

Also attached to the Oregon State University, Holland (1992) used video monitoring to quantify the celerity of overwash waves. The images indicated that the maximum overwash celerity exceeded 2 m/s. Also, the wave direction was easily accessible through the video imagery. Another Argus video method to estimate intertidal coastal properties uses a CMYK color model (Sobral et al., 2013). With this technique, the intensity of the different color bandwidths Cyan, Magenta, Yellow and Key are compared. This method was found to be highly usable to distinguish water surface from beach surface, and thereby indicate the waterline.

A different use of optical monitoring is the optical current meter. According to Chickadel et al. (2003) an optical current meter can measure the longshore component in nearshore currents. This method uses short videos. A model of the velocity spectrum is used to calibrate the observed data with the longshore velocity.

Generally, a lot of research is done regarding the exact coastline position. Kroon et al. (2007) have researched the general application of video systems for coastline management. They developed video-derived parameters to monitor the evolution of the coastline. These parameters were called Coastal

State Indicators (CSIs). Primarily the shoreline position is discussed as indicator. According to this research, the waterline positions can be used to determine shoreline contours and beach volumes. It was shown that the Coastal State Indicators facilitate the measurement of coastline evolution. It is stressed that especially the ability to measure closely before and after an extreme event makes videos valuable to coastal zone management.

It has been established that coastal morphologies are highly dynamic and therefore variate in both the temporal as the spatial scale. By using remote sensing imagery, Ruessink et al. (2013) monitored the longshore variability of sandbars. They used numerical modelling and data-model integration to further research the finite-amplitude behavior of sandbars and found that the straightening (morphological reset) of alongshore variable sandbars not only happens when waves are erosive and highly energetic, but also in low-energy situations.

Unmanned Aerial Vehicles Also developed for military purposes are Unmanned Aerial Vehicles (UAVs). There are several types of UAVs. The first ones were air balloons and were used as early as 1849. Other types are stationary winged and rotary winged UAVs. Whereas the stationary winged UAVs are more energy efficient and used often by the army, rotary winged UAVs have the advantage that they are able to hover at a specific location. Therefore, in coastal monitoring it is usually the latter type that is used.

Due to the dynamic nature of coastal areas, researching it requires the ability to do quick measurements (Holland et al., 2010; Brouwer et al., 2015; Turner et al., 2016). Unmanned Aircraft Systems are shown to be a reliable and adaptive way of measuring. These researchers show that by using an optical sensor, several coastal parameters can be measured, including wave period, wave direction, nearshore currents and bathymetry.

Satellite In coastal monitoring there are several ways of using satellite data. A regular (passive) optical sensor that captures a single photo can indicate wave direction and length but also pollutants, algae (Stumpf et al., 2003) and bathymetry (Li et al., 2016). To be able to track pollutants, Kutser et al. (1998) used passive optical sensors that can be gathered from satellites to monitor coastal waters. They found that a spectrometer could distinguish several types of suspended matter in the water.

Radar / Lidar Whereas passive optical sensors only record the radiation waves that are reflected by the earth's surface, active sensors like radar first emit a signal and capture what is left of it after it has reflected off the earth. Lidar uses the same technology as radar, however, it uses light waves instead of radio waves (Guenther et al., 2000).

Radar images have been used to determine ocean wave direction and surface currents (Young et al., 1985; Teague, 1986; Son et al., 2007), but also oil spills and shallow bathymetric data (Johannessen, 2000). Furthermore, Trebossen et al. (2005) looked at sedimentation and erosion processes and found that with the use of radar, coastal monitoring could also be done during cloudy circumstances.

Young et al. (1985) used a marine radar to record spatial images. Using these images, a three dimensional wave spectrum was compiled. After indicating the discrepancy between the spectral energy and the dispersion relation, they found the surface current induced by the Doppler shift of the wave frequency. Whereas this research was done using micro wave radar images, Barrick (1980) and Teague (1986) used high frequency radars to research the Doppler shift and estimate wave height.

Lidar has also been used to quantify beach topography Sallenger et al. (2003). The researchers used data from NASA's Airborne Topographic Mapper (ATM) which was compared to measurement acquired by more conventional methods. As the total error they found in their research was approximately 15 cm, one could argue that also wave height could be estimated by this type of measuring.

2.4 Indirect Bathymetry Mapping

Instead of analyzing coastal systems directly, the video based depth inversion technology uses indirect observations to estimate coastal features. In this report, especially the water depth in a coastal system is elaborated. There are two main techniques to compile a bathymetry through remotely sensed data. The first one uses the different spectral bands to estimate water depth and compile a bathymetry. It uses the difference in water penetrating performance of the spectral bands from which (after calibration) water depth can be inverted. The other method analyzes hydrodynamic observations after which it estimates water depth based on known physical processes in the nearshore.

Multispectral Imaging The first method for estimating water depth just uses the different col-

lected spectra of photographs. This method is called multispectral bathymetry mapping and uses the different color bands of a camera’s spectrum. As different colors penetrate through water with a different depth, the difference can give an indication regarding the water depth. A simple method for estimating water depth with multispectral imagery is proposed by Lyzenga et al. (2006). Whereas water pollution and density variations could be influencing measurements, the report states that the results are accurate with an aggregate root mean square error (rmse) of 2.3 m over all datasets. Also, Pacheco et al. (2015) uses a similar technology to map a relatively complex coastal situation with a barrier island. The rmse was found to be 0.89 m in waters up to 12 meters of depth.

A similar technology is spectral matching (Mobley et al., 2005). This method acquires an electromagnetic spectrum and compares its intensity with a look-up-table. The authors created a database which matches water depths with remote-sensing reflectance (R_{rs}). Thereafter, these Inherent Optical Properties are used to invert water depth from the measured spectrum. When compared to echo sounder data, this report shows that the proposed technology is accurate up to 5%. The difference between an approach like this and remote sensing with UAVs is the need for specialty equipment. Even though the Ocean Portable Hyperspectral Imager for Low-Light Spectroscopy (Ocean PHILLS) which was used in the research existed entirely of commercially available products (Davis et al., 2002), it is still an intensive effort to build one.

Furthermore, a different research covered wave breaking patterns through remote sensing. This study was done by Van Enckevort and Ruessink (2001) who used time exposure video images to derive the high-intensity color bands, which they found to be suitable to monitor large scale and long term sand bar movement. Even though this seemed to work well, they also note that there is a discrepancy between the high-intensity bands and the actual sand bar position of about $O(10\text{m})$.

2.4.1 Wave Parameters

Hydrodynamic factors in coastal imagery can also be used to analyze sub-surface processes. For instance, the way waves move through coastal waters could indicate certain features of the particular system. This is less of an observing and more of a calculating strategy as it always requires a certain algorithm to compile depth data from the images which are actually recorded.

When trying to induce water depth from remotely sensed imagery, some conversions need to be determined. An obvious step that links physically observable phenomena with depth are wave parameters. As the nearshore consists of intermediate (wave length / water depth > 2) to shallow (wave length / water depth > 20) water, the celerity at which the waves propagate is related to the water depth. For shallow water conditions and assuming a constant water depth, waves would propagate according to the following relation (Holthuijsen, 2014):

$$c = \sqrt{gh} \quad (1)$$

Where c is the wave celerity, g is the gravitational acceleration and h is the water depth. However, due to hydrodynamic effect in the surf zone like dissipation and shoaling, this theory does not hold. When regarding wave height in relation to the water depth, Ruessink et al. (2003a) empirically derived a new functional form for the wave height-to-depth ratio (γ). The research states that γ is not constant cross shore, but depends on the product of the local wave number k and water depth h .

Holthuijsen (2014) shows the following relation between wave number, frequency and water depth.

$$c = L/T = \sigma/k \quad (2)$$

$$\sigma = 2\pi/T \quad (3)$$

$$k = 2\pi/L \quad (4)$$

$$\sigma^2 = g \cdot k \cdot \tanh(k \cdot h) \quad (5)$$

$$h = \frac{1}{k} \cdot \text{tanh}^{-1}\left(\frac{\sigma^2}{g \cdot k}\right) \quad (6)$$

Therefore, the wave frequency (sigma) and the wave number (k) are required for water depth calculations.

Also, Holman (1981) investigated onshore and longshore velocities with onshore instruments. The research focused on the infra gravity energy of waves in the surf zone. The research showed that the infra gravity amplitude approximately linearly varied with the incident wave amplitude.

Wave Shoaling When wave groups enter shallow water, the group velocity decreases. This is because wave celerity is related to water depth. As the energy travels with the group velocity which is

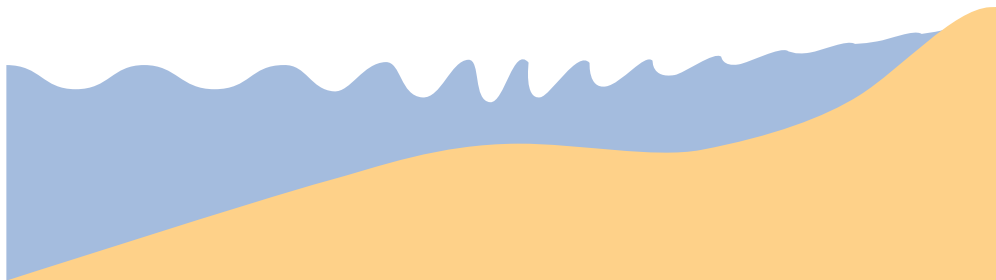


Figure 10: Coastal Hydrodynamic Processes

decreasing, conservation of energy results in an increase in wave height. As a result, also the wave length decreases. This phenomenon is called shoaling (see figure 10). Lippmann and Holman (1991) used time series of image intensities at known locations, which they compared to in situ pressure gages. They found that their measurements of phase speed and wave angles were consistent with the first order shoaling theory.

Wave Number Another hydrodynamic factor is the wave number. This measure is indicated as the spatial frequency. It counts how many waves there are in a particular distance. Plant et al. (2008) have reviewed approaches to estimate ocean wavenumbers from time series imagery. They elaborate on two fundamentally different approaches to estimate the wavenumbers. The first one they mention is a so-called power spectral density approach, which identifies wavenumbers where image intensity variance is maximized. The second approach identifies wavenumbers where intensity coherence is maximized. This approach uses cross-spectral correlation. The research found that the latter approach generates a resolution which is a factor ten times better than the first approach. Furthermore, a rule of thumb is provided which states that the short-scale cross-shore patterns may be resolved if they are about ten times longer than the average water depth over the pattern. This means that in a water depth of about 0.5 m, spatial patterns with a length of 5 meters could be indicated.

2.4.2 Depth Inversion using Wave Celerity

Inversion of depth through (aerial) imagery has been attempted for a long time. According to Williams (1947), if the frequency of dominant narrow-banded swell is known, a single photograph could be enough to estimate water depth.

Also, Dugan et al. (2001) state that without knowledge of the dominant frequency, a mere two

photographs is enough to deduce the water depth. This can be done by calculating the wave celerity. The depth is obtained by the surface gravity wave dispersion relation:

$$\omega = (g \cdot \kappa \cdot \tanh[\kappa h])^{1/2} + U \cdot \underline{\kappa} \quad (7)$$

Where ω is the frequency ($2\pi/T$), κ is the scalar wave number magnitude ($2\pi/\lambda$), $\underline{\kappa}$ is the wave number vector, g is the acceleration due to gravity, U is the water velocity vector (assumed constant), h is the local water depth and the celerity c is ω/κ .

On similar notes, as wave length and period have been used to induce water depth on multiple occasions (Piotrowski and Dugan, 2002; Stockdon and Holman, 2000), most of the focus has remained on celerity. Especially phase speed of shoaling waves has been used to deduce water depth using the dispersion relation. Multiple researchers have adopted the use of a variety of video imagery for this purpose. Stockdon and Holman (2000) used remotely operated video cameras to estimate the shoreward propagation speed of waves. They used linear wave theory's dispersion relation to infer water depth. An error was found of approximately 13% of the water depth. However, it was established that nonlinearities in waves accounted for a significant part of the error. They also found that the performance of the model increased during low amplitude swell.

Also Holland (2001) researched depth inversion. He also used the linear dispersion relation to calculate water depth and found an accuracy of 3 to 9 % of the observed water depth. This was done by measuring phase speed of shoaling waves with pressure gauges. According to the author, gauge data can be used similarly to remotely sensed imagery.

Other research primarily focusing on the intertidal beach profile was done by Aarninkhof (2003). He focused on the visible signature of nearshore processes, which can be monitored remotely. According to his research, it could be worthwhile trad-

ing some accuracy for the cost-efficiency of remote sensing technologies. A Intertidal Beach Mapper was created to make a three-dimensional beach image between low and high tide. This method was shown to be up to 15 cm accurate along a coastal stretch of two kilometers. Furthermore, a Subtidal Beach Mapper was created to quantify surf zone bathymetry from video intensities cross shore. The bathymetry was updated/calibrated by comparing the Mapper's wave dissipation measurements with common wave dissipation models and adjusting the bottom profile as such. The bathymetry errors were found to be between 20 and 80 cm throughout the nearshore.

Also using wave dissipation, Van Dongeren et al. (2008) created a data-model assimilation method called Beach Wizard. The model uses estimations of wave dissipation and wave celerity to calculate subtidal bathymetry. They state that the advantages of their technique is that it is based on multiple sources of data and depends on few parameters.

cBathy To be able to map nearshore bathymetry, Holman et al. (2013) developed an algorithm that converts wave surface motions into water depths which they called cBathy. Dominant wave frequencies are estimated by Fourier transformations and also wave numbers are derived. The frequencies and wave numbers are paired and coupled to water depth. The bias of their depth estimates was 0.19 and the root-mean-square error 0.51 m. It was shown that the algorithm works better for smaller waves. It is based on long time series observations of surface wave motions and is constructed in three parts:

1. Frequency-dependent analyses of several wave parameters.
2. Frequency-independent estimation of the best single depth.
3. Estimation of running-averaged depths.

In the first phase, dominant frequencies are estimated by Fourier transformations for the coordinates of a certain area of interest. Also, wave numbers are derived. The spatial resolution is kept high and coherent spatial structures at each frequency are extracted. The second phase depths are estimated to fit the pairs of frequencies and wave numbers in accordance with the linear dispersion relation. Lastly, phase three uses a so called Kalman filter to smooth out the depths found in phase two.

Indirect Bathymetry Mapping with Radar / Lidar Instead of satellite and aircraft data, also radar and lidar data has been used to induced water depth. An application of marine radar imagery to indicate wave dispersion was done by Trizna (2001). Like in similar reports, in relatively deep water (deeper than 5 m) and with low to moderate wave heights, this technique managed to retrieve the correct depth.

Instead of using the commonly known relation between linear wave dispersion and water depth, Senet et al. (2008) suggested a new approach which they call the Dispersive Surface Classifier (DiSC). The method uses the nautical X-band radar image sequences of sea surface waves to estimate the water depth. They used a ground-based radar to acquire the data which were verified by echo sounder measurements. Whereas this technology seems promising, it still requires significant financial resources when compared to UAV measurements.

As light waves have different properties than radio waves, lidar technology is generally used for indicating altitude properties. The US Army Corps of Engineers created the SHOALS system, which includes the use of lidar for coastal monitoring purposes. Because the lidar is mounted to an airplane, this technology increases the survey speed and scope (Irish and Lillycrop, 1999). The technology has a stated vertical accuracy of 15 cm and can map bathymetry through depths of up to 40 m (Irish et al., 2000).

Indirect Bathymetry Mapping with Satellites Satellites are generally used in combination with radar or lidar equipment. Several scientists have used satellite data to indicate water depth (see figure 11). For instance, the SPOT (Satellite Pour l'Observation de la Terre) is a french initiative to support scientists. It entails multiple satellites launched between 1986 and 2014 to monitor the earth's surface. Essentially using the same technique as Williams back in 1947, Leu et al. (1998) and Wu and Juang (1996) did similar research using data from SPOT satellites instead of aircraft imagery. Wave spectra were analyzed from the high resolution images obtained by the satellite and used to infer water depth. Errors in estimating water depth of about 10% were found.

When comparing satellite bathymetry mapping with other methods, the most striking features is a more extensive temporal and spatial range (see figure 12). On the other hand, the accuracy is regarded to be low:

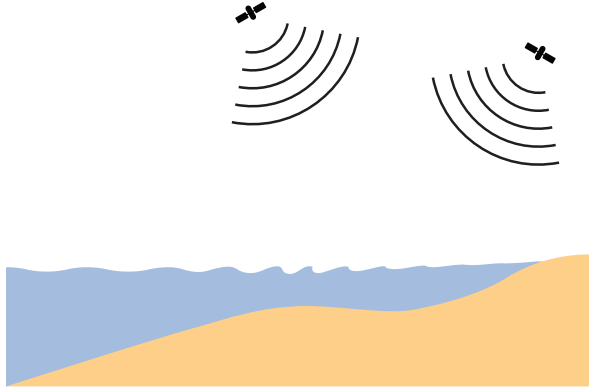


Figure 11: Method Satellite

- **Flexibility:** As satellite images are extensively available, there are a lot of coastal areas of which data can be found. However, this data is mostly limited to one photograph. Therefore, the data is not always usable and the flexibility is relatively low.
- **Low Cost:** Launching a satellite for the sole purpose of coastal monitoring is extremely expensive. However, because images taken from satellites can be shared between different fields of study, the cost drops significantly.
- **Accuracy:** Because the satellite is not involved in direct measurement of water depth but only records signals reflected by the earth, it is difficult to estimate bathymetry.
- **Spatial Range:** Due to the availability of an extensive data set, images from across the planet can be collected.
- **Temporal Range:** Because satellites keep on orbiting, they can be used to collect data of a certain location regularly. Therefore, similar images can be found of the same area over time.
- **Low Effort:** Collecting the data is relatively straightforward. However, there need to be parties that have data available of the specific location. Also, as the data is acquired differently between satellites, using these images to compile a bathymetry takes effort.

Apart from mapping water depths by using wave celerity, satellite images can also be used for multi-spectral imaging (see section 2.4). This technology is more direct, but requires calibration due to suspended sediments.

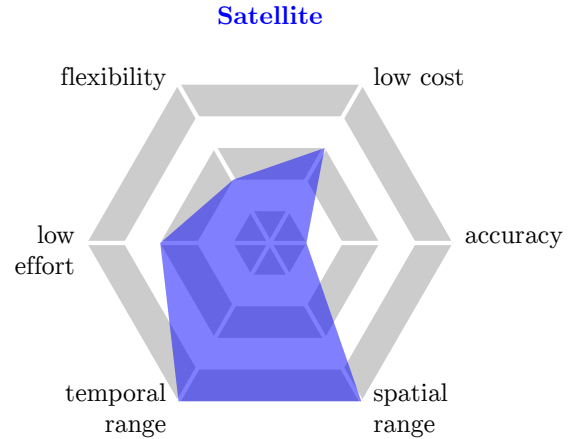


Figure 12: Rating Satellite

Indirect Bathymetry Mapping with Aerial Vehicles Where dry parts of the earth's surface get eroded by rain and wind, the coastal area is influenced by the water movements induced by waves and tides. As the latter mechanism is far more energetic, the coastal system is much more dynamic and can change from day to day. Therefore, the coastal area requires more and quicker monitoring techniques. Throughout time, aviation has been considered a resourceful area of monitoring (see figure 13). Due to its relatively dynamic employability it can capture data rapidly. For coastal monitoring different kinds of aerial vehicles can be used.

Dugan et al. (2001) used optical measurements captured from an aircraft to research water depth and surface currents. They used images of nearshore shoaling waves. Location data from a GPS/INS (Internal Navigation System) is used to adjust the image to a rectilinear grid, after which waves can be identified. After a Fourier transform, they obtained frequency-wave number spectra. From these spectra, the wave length, frequencies and propagation speed could be estimated. After this, the researchers estimated the water depth, using a best fit approach between the theoretical dispersion relation. Also, airborne vehicles have been used in combination with lidar (Guenther et al., 2000).

When compiling a rating for the use of traditional aerial vehicles for coastal monitoring, especially the extend of the spatial range is notable (see figure 14):

- **Flexibility:** Gathering data by traditional aerial vehicles is by no means flexible. It takes a severity of permits and organization to get a plane airborne.

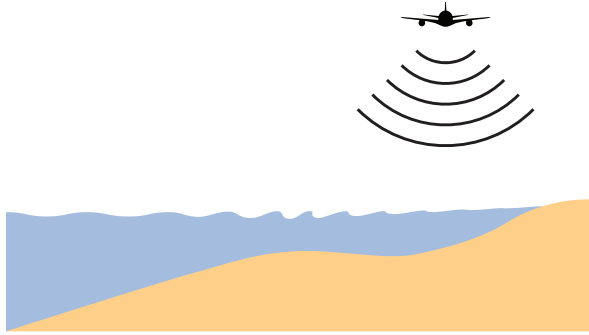


Figure 13: Method Aerial Vehicle

- **Low Cost:** Also, airplanes required a significant amount of financial resources.
- **Accuracy:** Furthermore, as also airplanes do not measure water depths directly, they need to be calculated. This goes hand in hand with significant errors.
- **Spatial Range:** Once an airplane is airborne, the recorded data can span an extremely large area.
- **Temporal Range:** Like with Jetks e.g., as the pictures taken by plane are a single effort, temporal monitoring will involve chartering a plane on a month to month (or year to year) basis. It is not a constant monitoring system.
- **Low Effort:** Lastly, getting an airplane with monitoring equipment operational, is an activity which involves a significant amount of effort.

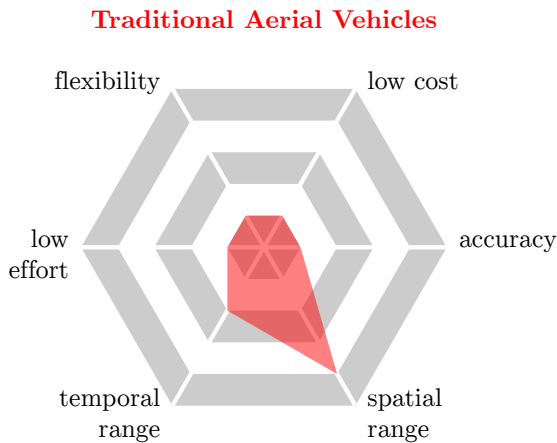


Figure 14: Rating Traditional Aerial Vehicle

UAV Bathymetry Mapping With the rise of rotary Unmanned Aerial Vehicles, new data collection methods were introduced (see figure 15). When compared to fixed wing aerial vehicles, instead of having a constant speed, UAVs can hover and record steady imagery. The data captured by a UAV was comparable to the data acquired by Argus stations. Holland et al. (2010) first rectifies the images, after which pixel intensity is used to determine spatial relationships. Subsequently, linear wave dispersion was applied to calculate water depth. Also Vousdoukas et al. (2011) created a (semi automatic) technique for environmental assessment using a UAV. They focused on mapping sand bars, rip channels and dimensions of the surf zone.

Holman et al. (2011) more specifically looked into bathymetries. They also researched the use of wave celerity to estimate nearshore bathymetry. Compared to fixed onshore cameras, UAV videos are less steady and the data is generally shorter due to limitations in the UAV battery life. These disadvantages were researched and it was found that video images captured for a short of 50 seconds could already have sufficient data for bathymetry analysis. Even if only 50% of the record would stay intact (due to unsteady recordings), a full Fourier transform could be implemented, leading to the desired bathymetry. Also, navigational errors can be stabilized by using reference points. Test runs yielded results which had errors of 0.51 m (standard deviation) in shallow water (0-4 m), and 1.19 m in deeper water (6 m). 73% of estimates in the nearshore were within 1 m of actual depths.

Advantages of the UAV method over fixed Argus stations are especially its flexibility. Whereas it taken extensive effort to set up an Argus station, a drone flight can be done within a couple of hours. Furthermore, as in the Netherlands drones can legally reach altitudes of 120 meters, their viewpoint is higher than Argus towers. This could indicate that in the acquired drone data, waves could potentially be analyzed in a more accurate manner. Also, due to the altitude, offshore locations would have a different spatial resolution.

When looking as UAVs as a way of gathering scientific data, there are a number of ratings in which it stands out (see figure 16):

- **Flexibility:** As a drone fits in a suitcase, it can travel anywhere a human can. Therefore, it is highly flexible. Another part of the flexibility is that it is a consumer vehicle. As drones are widely available, one could also

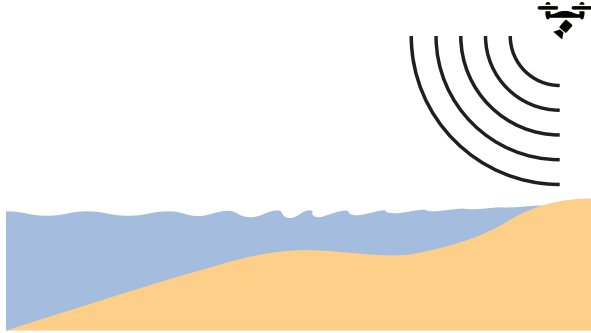


Figure 15: Method Consumer UAV

instruct someone to acquire drone footage remotely on another part of the world without a lot of effort.

- **Low Cost:** The consumer drone market is growing rapidly. Due to the rise in demand, the industry is getting increasingly efficient and prices of relatively well engineered potential measuring equipment drop. As an affordable consumer drone comes with a lot of internal sensors which have a lot of potential for scientific research, this method is relatively inexpensive.
- **Accuracy:** Similar to aerial and satellite observations, the drone images do not measure water depth directly. The inversion algorithm is estimated to give a relatively large error.
- **Spatial Range:** The space that is measured is limited to what is captured by the drone. And due to the limited range of the battery it is hard to cover a whole stretch of coast quickly. However, as the altitude of the drone is much higher than that of an Argus station, larger areas can be monitored by one camera.
- **Temporal Range:** Like jetki echo sounders, the bathymetry collected by the UAV is a snapshot of the coastal situation. Therefore, to measure a stretch of coast on a longer term, more individual measurements have to be done.
- **Low Effort:** As measuring potentially just involves going to the beach and flying the drone, the amount of effort it takes is relatively low.

In a more recent study, Brouwer et al. (2015) indicated that UAVs are extensively suitable for monitoring the surfzone. They stress that especially the

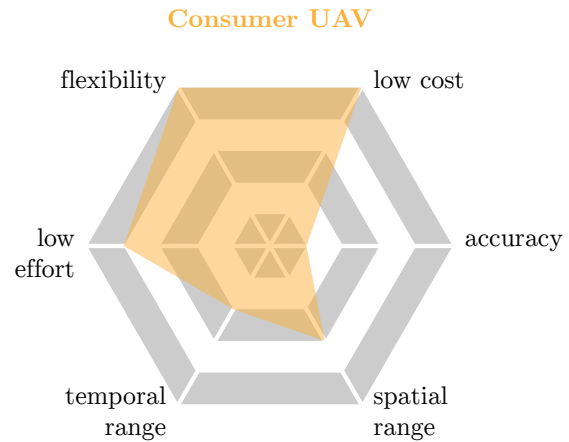


Figure 16: Rating Consumer UAV

flexibility is an advantage of UAVs over more conventional surveying methods. The pixel resolution can be georectified to between 0.01 and 1 m and the technology has a reprojection error of $O(1m)$. Even though their spatial resolution is moderate, due to the high temporal resolution it is stated that the method is especially suitable for researching surf-zone kinematics, and dispersion/advection of pollutants.

Also Turner et al. (2016) focused on coastal monitoring using UAVs. They focus on on off-the-shelf drones, and state that UAVs with RTK-GPS systems have sufficient accuracy to eliminate the need for on-ground control points. Furthermore, it is stated that UAVs are rapidly usable for post-storm measurements.

Consumer UAV vs Conventional Bathymetry Mapping Methods

When comparing the UAV technology to its substitutes technologies (e.g. jetkis with echo sounders & Argus systems), it is shown that especially the amount of flexibility and the low amount of effort and cost stand out (see figure 17). Its ratings are lower in terms of accuracy, and temporal and spatial range. However, in a significant amount of coastal monitoring issues, these factors are not crucial. UAV bathymetry mapping could be used in a number of occasions. One could hypothetically ask someone in a random country without any available data to take a video of a specific coastal region and distract a full bathymetry from these images. This would make coastal monitoring far more flexible and increase to possibility to gather a significant amount of data without a lot of effort.

**Envelope of (CRAB; Jetski; Satellite;
Traditional Aerial Vehicle; Argus)
Consumer UAV**

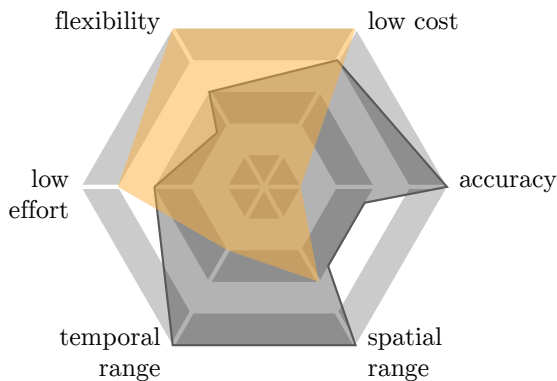


Figure 17: Rating Comparison

The UAV technology can be beneficial for certain future coastal monitoring purposes. It exploits a product which is ever increasing in efficiency due to its growth in the consumer market. In the following, some specific features of the UAV bathymetry mapping method are elaborated.

Grid Resolution The resolution of the grid that is used for coastal research directly influences the usability of the results. Plant et al. (2009) researched bathymetric filtering on nearshore process model results. They found that the sensitivity of wave height and flow to different bathymetric resolutions varies. Especially the cross shore variability seemed to be influencing wave height predictions, whereas the longshore variability influenced the flow predictions.

Camera Properties Each camera has different properties in terms of e.g. pixel resolution and capture angle. Holland et al. (1997) developed an approach to quantify nearshore physical processes. They describe a way to convert image coordinates into ground coordinates. In the article, calibration of the camera model, which can be used for several fields of study, is discussed. Topics that can be researched according to them:

- nearshore fluid processes
- sand bar length scales
- foreshore topography
- drifter motions

On the same topic, Holman et al. (1993) elaborated on the use of rectified time-exposure images. At that time, researchers were solving the problem of rectifying images taken by Argus camera's. According to their research, these images are a great help to long term studies regarding morphological variability. However, the use of video imagery begins with the physical understanding of a camera (Holman and Stanley, 2007). Also, it is important to understand the relation between the optical signals and the geophysical signals they represent.

When regarding the frequency and pixel size, Piotrowski and Dugan (2002) did extensive research. According to them, when estimating bathymetry, pixel sizes of 3 to 4 m and framing rates of approximately 0.5 Hz (one picture every two seconds) are sufficient for providing adequate results.

Backend Improvement It might also be possible to increase efficiency of the results afterwards by combining data from different sources. Moulton et al. (2014) developed a method to increase spatial density and map the evolution of the bathymetry throughout time. The method updates watercraft echo sounder data which is infrequent with the use of nearly continuous sampling altimeters. According to the research, the updated maps are more accurate than maps obtained by using either conventional water crafts or maps created by using altimeters alone. However, questions could be raised whether it is worth it going through the efforts of setting up the altimeters, when a quick and rough estimate would suffice.

2.5 Image Stabilization

In both the scientific community as the entertainment industry, a disturbed (shaky) image is considered to be undesirable. Unstable imagery is characterized by changes in camera orientation in an unorderly fashion up until the point that limited to no data can be distracted from the images. To be able to eliminate these disturbances, the main method of stabilization is mitigating sudden movements of the recording device.

There are two basic ways of keeping video's from being unstable. Firstly, there is a hardware-based stabilization comprising of a camera sensor that is detached from the base of the camera, which is assumed to be the cause of the instabilities. This method is applied during the recording sessions. In addition, post-recording stabilization comprises software-based methodology.

2.5.1 Optical Image Stabilization (OIS)

One of the most basic ways of increasing stabilization of video footage entails the decrease in movement of the camera aim. This can be achieved by simply putting the camera on a tripod or laying it down on solid ground. In some practices (e.g. handheld devices or drones), above mentions methods are inconvenient as the device that the camera is attached to is generally in motion. Therefore, in the past decades, researchers have been focusing on OIS. In contrast to digital stabilization, OIS is a hardware-based solution that reacts to movements in real time. The method ensures that the camera lens and the camera sensor are aligned, and is based upon movements of the device registered by internal gyroscopes or linear accelerometers (Algrain and Quinn, 1993). These sensors are called Internal Measuring Units (IMUs). The registered movements are compensated by adjusting the angle of either the lens or the image sensor.

The first type of OIS is a lens-based application. This method adjusts the axis of the lens to keep the image tracked on the sensor. As the potential movement of the lens is limited, the effectiveness of this method is also limited to correcting small movements. The second type is a sensor-based application, which changes the angle of the sensor based upon the gyroscopic readouts. Furthermore, the whole camera (lens and sensor) can be detached from the body of the device and stabilized externally. This type of stabilization device is called a gimbal (Windau and Itti, 2011).

2.5.2 Digital Image Stabilization (DIS)

Contrary to OIS, DIS is a software-based image stabilization. This can be done either with or without the readouts of the IMU's. When the readouts are used real time, the technology is called Electric Image Stabilization (EIS). Subsequent images are shifted from frame to frame to counteract sudden motions (Chereau and Breckon, 2013). To be able to shift the images, a buffer zone on the edge of the image is used and cropped where necessary. This leads to a decrease of information.

Lin and Fuh (2006) described several different types of DIS. The first one is similar to the technique described above which they called DIS by Moving Window. Subsequently, they described a method that stabilizes imagery by using higher ISO speed. By raising the ISO speed up to 620, 800 or higher, the faster shutter speed can provide more stable imagery. They do note whether with this method the image quality decreases.

Another method of DIS is described by Chen and Fuh (2005). The authors elaborate on a super resolution concept to reconstruct blurred images. Two input images are used in combination to create a sharp image. The method works well for images that are only partially blurred. However, when both are blurry throughout the image, the sharpness will not increase.

Furthermore, Litvin et al. (2003) created a probabilistic image stabilization method. They used a probabilistic estimation framework to separate unwanted vibrations from intentional camera motion. Their method analyses changes in subsequent frames and through estimated parameters makes a distinction between accidental and incidental motions.

According to Matsushita et al. (2006), most DIS methods, although being effective, decrease the size of the stabilized video. Therefore, they propose a method that does not alter the video resolution or size, whilst still stabilizing the image. The technique naturally fills up the missing image parts when comparing the blurry frame to the neighboring frames.

Pixel References In coastal engineering, there has been an extensive desire to measure particle flow speed. This data is used to estimate dynamic hydraulic models or river flow rates with subsequently its sediment transport. On the topic of particle image velocimetry, the use of an optically transparent test section with an illuminating light source, a recording device and a computer for post-processing was proposed. In this way, in a very controlled environment, flow rates were automatically detected (Dill et al., 1995). Based on a similar technique, Fujita et al. (2007) developed a method aiming to identify velocity fields in laboratory, but also in field conditions. They called the method Large-Scale Particle Image Velocimetry (LSPIV) and used it to measure floodplain flow in a full-scale river. For the real world testing, a transformation needed to be done between the captured coordinates and the physical coordinates. Following these efforts, Fujita et al. (2017) developed image stabilization for the application of river flow measurements. This technique creates masks of individual snapshots and compares it to a reference image mask, after which it can be lined out and adjusted. This method is shown to also work when the UAV is moving, provided that the image is taken almost normal to the water surface.

2.5.3 Rectified Video Stability

Where image stabilization has been severely improved over the last couple of years, the video taken by a DJI Phantom 4 consumer UAV can be considered to be sufficiently stable for coastal monitoring purposes. Therefore, the transformation from pixel coordinates to three dimensional coordinates between subsequent images should ideally also be sufficiently stable. However, as in current use, the images are rectified individually, any error in rectification accuracy, which is generally the case for situations with limited Ground Control Points, will result in instabilities in the rectified video. Small changes in the calculation of the geometry can introduce an instability with the same frequency as the sampling frequency.

Efforts can be made to utilize neighboring images when rectifying videos. Image stabilization methods can be explored which are similar to above mentioned techniques. However, instead of analyzing pixels in subsequent images like Matsushita et al. (2006) proposed, the research will focus on analyzing pixel coordinates in subsequent images.

2.6 Societal Impact

Coastal monitoring influences a severity of people in the coastal zone sometimes without them even knowing it. It is for the benefit of the coastal society as a whole that the monitoring process continues in an efficient manner. Researching effort can provide useful tools to keep the population in these specific areas safe.

When looking at societal impacts and the relation between scientists and end user, Van Koningsveld et al. (2003) state that coastal research programs are often too short due to divergence in perceptions between the users of the knowledge and the developers of the knowledge gathering techniques. Between the on the one end purely scientific approach and the on the other end purely customer/user approach, a hybrid form is stated to be a so-called 'driven' approach. The driven part of UAV monitoring is the extensive need for coastal projects to determine water depths. Both in case where a structure is proposed in the nearshore (e.g. port, closure dam) and in assessing the risk of flooding for the hinterland, several parties are focusing on water depth mapping.

Furthermore, coastal monitoring can help in decision making. Turner and Anderson (2007) focus on the interaction between constant coastal observation systems and political decision makers. A web-based beach management system is therefore

elaborated. A helpful tool is the CoastView project. It uses video images to derive Coastal State Indicators (CSIs) (Davidson et al., 2007). According to this research, it is important for engineers and coastal decision makers to collaborate in establishing the CSIs as they directly initiate managerial decisions.

Another use for video images which can help improve CSIs is to manage dynamic navigational channels (Medina et al., 2007). In navigation, the consequences of a collision are significant. Therefore, the channels need comprehensive monitoring. This report quantifies Coastal State Indicators which can be used to monitor the channels. In the cases which are reported on, video systems are shown to evaluate CSIs in a broad range of time scales.

Coastal monitoring can also be used to monitor leisure activities. In their research, Jiminez et al. (2007) define CSIs for beach recreation planning using video imagery. The two variables specified are the level of beach use and the safety. Managerial frameworks are presented for both variables, which use the capabilities of Argus cameras.

Like described above, imagery of the coastal zone can be used for more than just bathymetry mapping. All different uses of these images can help create a more comprehensive set of CSIs and therefore support decision makers in a more effective way. However, it is not guaranteed that these tools are effective. According to Van Koningsveld et al. (2007), even though Coastal State Indicators are effective support tools for coastal decision making, the transfer of useful methodologies is not guaranteed. The research shows that especially simplicity and robustness of CSIs is important.

2.7 Summary

This section of the report briefly elaborated on the history of coastal monitoring as well as the purpose of coastal monitoring. Also, the difference was shown between direct and indirect bathymetry mapping after which bathymetry accuracy and spatial scales were attributed to the different methods. Furthermore, a distinction was made between coastal monitoring with passive camera sensors and a coastal monitoring with active radar or lidar. Subsequently, coastal hydrodynamic processes were briefly explained after which it was shown that it is possible to calculate water depths from video imagery.

3 Methodology

In the previous section, it has been established that bathymetric data is useful for several purposes in coastal monitoring. Therefore, to explore the process and indicate potential improvements, this section will elaborate on the different steps of the UAV bathymetry mapping method.

3.1 Conceptual Model

The conceptual model as shown in figure 18 describes the way a bathymetry gets estimated using video footage recorded by an Unmanned Aerial Vehicle (UAV). At first, a stationary flying drone collects a video of a specified nearshore coastal region for approximately 15 minutes. Ground control points with high visibility will be located in the area which are used for the image rectification in the second phase. The rectification step links the two dimensional UV coordinates of the pixels in the recorded footage to their particular three dimensional coordinates in a user specified grid system. The rectification will be done for every one of the approximately 2000 recorded images. From the geo rectified video, wave characteristics like frequency, wave number and angle of incidence can be used to match water depths and wave celerity based

upon the dispersion relation. Lastly, a bathymetry is mapped by combining the water depths of every single coordinate in a spatial structure.

The conceptual model shows several variables to which in this section the characteristics are elaborated. In each of the steps of the proposed method, there are potential factors which could influence the accuracy of the eventual bathymetry that is mapped. This research proposes to give a preliminary analysis to indicate which of these factors could be the largest contributor to the mapping error.

Population & Sample As mentioned before, compiling data in nearshore shallow water is an extremely resourceful activity. The literature review states different techniques to gather this information essential for coastal monitoring purposes. However, not every technology can be commonly used in any coastal situation. The proposed method of UAV bathymetry mapping regards hydrodynamic physical processes in a nearshore environment. These processes are considered to be valid throughout the world and could in theory be applied anywhere. For this research however, the stretch of beach in Scheveningen, the Netherlands will be used.

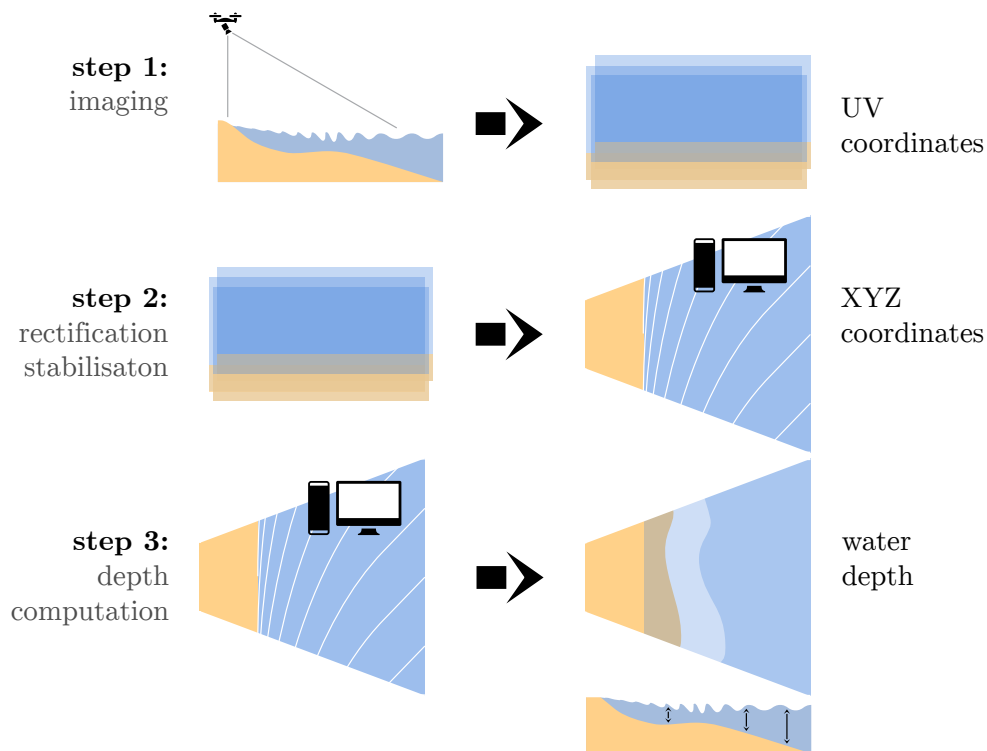


Figure 18: Conceptual Model

3.2 Data Acquisition

The proposed method uses an Unmanned Aerial Vehicle to capture video imagery of a specific coastal region. The acquired data regards a passive video, captured with the camera that comes standard with the UAV. This setup is primarily chosen to make the surveying technique as generic as possible and applicable by anyone owning a consumer UAV.

DJI Phantom 4 The UAV that was chosen for this research is the DJI Phantom 4. DJI is widely known as the most popular consumer drone manufacturer at the moment of writing. Its Phantom 4 is situated in the higher end of their consumer product segment and retails around 1500 euros.

Surveying Date To be able to validate the mapping method in the most efficient way, the imagery was collected on and around the date when also detailed jetski surveying was done. On Thursday the 9th and Friday the 10th of February 2017 the data was collected.

Benchmark There are services which offer global bathymetry maps through satellite data. However, within meters, the error of this technology is relatively high. Therefore, the computed bathymetry data will be compared to an echo sounder survey which will be conducted on the same day or in the same week.

Analyzing Wave Data After for every image taken by the UAV a projection was calculated, the projections were displayed subsequently creating a video of the wave conditions. Thereafter, for every point in the area of interest, the pixel intensity was analyzed. Subsequently, wave data like celerity, phase, period and length was compiled.

3.2.1 Bathymetry Calculation

Throughout the last couple of decades, scientists have put effort in creating several different methods for using hydrodynamic processes in the nearshore to estimate water depth.

Comparison As the bathymetry influences the motion of water flowing through it, there are different techniques which distract water depth from wave characteristics. The first stages of such technologies mapped the intertidal area of the beaches (Aarninkhof et al., 2003). Subsequently in 2008, Van Dongeren et al. created a Beach Wizard that

uses the estimation of wave dissipation and compares it to numeral test bathymetries. They state that the advantages of their technology is that it depends on only a few parameters. Furthermore, several scientists used a method based on the depth relationship with wave celerity (see equation 7) (Holland, 2001). Similarly utilizing the relation between wave celerity and water depth is the cBathy algorithm which is describes in the literature review (Holman et al., 2013).

The latter algorithm is considered the most advanced and accurate depth induction method. As the technology is considered to be most promising, this report focuses on the use of the cBathy method for bathymetry estimation.

3.2.2 Variables

When considering data acquisition, in every step of the process there are factors which could negatively influence the results. In the following section, a comprehensive set of variables are elaborated.



GPS Accuracy UAVs provide a moderate spatial resolution (Brouwer et al., 2015). It is essential to assign a correct coordinate to each individual pixel in the image. Depending on the method, when rectifying an image, especially the coordinates of particular Ground Control Points provide detrimental information. If these coordinates do not represent their actual location well, every pixel in the entire image would decrease in positional accuracy.

Whereas in theory the exact location of the drone itself does not even need to be known, Turner et al. (2016) elaborate on the decrease of GCPs by equipping the UAV with a RTK-GPS. Whereas their study seemed promising, the intensified financial resources needed for such an upgrade are not aligned with the purpose of this study.

UAV Errors For the drone to be able to compensate for movements and indicate its takeoff location, it is equipped with several sensors. The sensors record the drone's position in X, Y and Z direction (see the errors in figure 19). Depending

on the method, this data can be used to solve unknowns in the calculation of the coordinate conversion matrix.

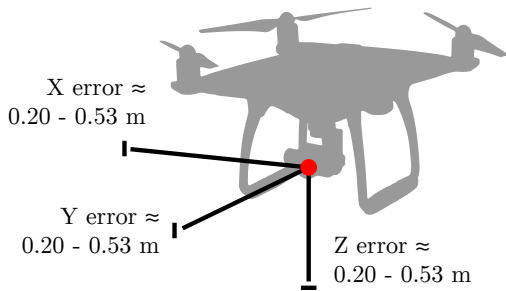


Figure 19: Drone Position Errors

Furthermore, the pitch, roll and heave are recorded for flying stability. The errors are shown in figure 20. Also this data can be used to even further decrease to amount of ground control points necessary.

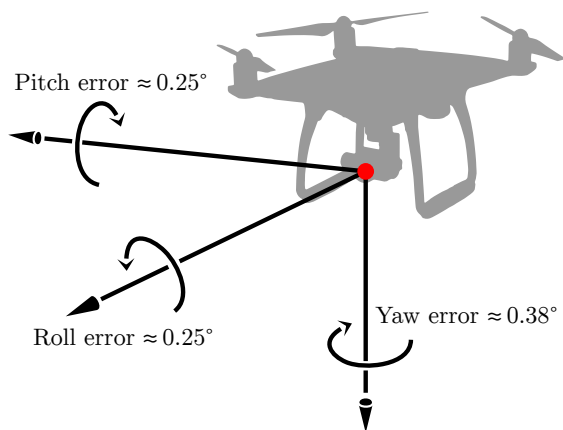


Figure 20: Drone Angle Errors



Video Time & Frequency Coastal processes usually have a time frame in the order of seconds to minutes (Brouwer et al., 2015). Therefore, approximately 10 minutes of imagery is estimated to be sufficient to indicate hydrodynamic factors after which depth can be inverted. However, longer recordings give the depth inversion algorithm more data and ideally makes the inversion more accurate. According to wave climate theory, for the an-

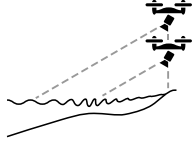
alyzed frequencies in the spectrum to converge to a statistically stationary situation, a measurement of around 15 minutes is needed. As the DJI Phantom 4 has a flight time of approximately 24 minutes per charge, the duration of the video footage is not considered to have negative influence on the eventual depth estimation.

Also the sampling frequency has to be taken into account. A study from Piotrowski and Dugan in 2002 indicates that a frame rate of approximately 0.5 Hz is sufficient. Whereas decreasing the frequency might result in a decreased accuracy as not all of the frequencies in the wave spectrum could be detected, increasing the sampling rate is not considered to have negative consequences. The only downside is that it does increase the amount of data that needs to be processed. In a later stage of the report, an analysis is done whether differences in sampling rate influence the eventual bathymetry accuracy.

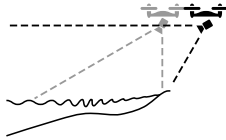


Number of GCP's As stated in section 3.2.2, GCP's are used for the rectification of the images recorded by the UAV. Arguably as the calculation of the coordinate conversion matrix would have more information to solve the unknowns, more GCPs can make the measurement more accurate. On the other hand, when using too many GCPs, this method would become too labor intensive. According to Aarninkhof (2003), to be able to rectify images from an Argus camera, only two GCPs are needed. However, the exact location of Argus cameras is known whereas the drone constantly moves.

Furthermore, according to Turner et al. (2016), the need for extensive GCPs could be reaching its end, as Real Time Kinematic GPS equipped drones are accurate enough for the purpose of coastal monitoring. This would on the other hand not be the case for consumer drones. Due to the lack of consensus in the literature regarding the amount of GCPs to use, for security reasons this research uses a fairly extensive amount. This is because it is always possible to decrease the number of GCPs used. Furthermore, the GCPs should be spread out as much as possible, which is difficult if only non-floating GCPs are used.



Drone Altitude The altitude of the UAV is directly related to the surface area it can capture. However when capturing a larger area, the pixel density decreases. Furthermore, different altitudes yield different angles from which the wave front is captured. It is not known whether these changes have a beneficial or negative impact on the accuracy of the UAV bathymetry mapping method.



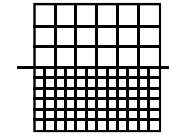
Video Angle The angle at which the image is captured indicates whether or not the horizon of water body will be captured. Capturing the horizon could result in the need for less GCPs, and could therefore be desired. Furthermore, if the horizon is captured that means that the location of the drone is farther inland resulting in the area of interest being captured by fewer pixels. Also, with a position farther inland the wave front is captured with a sharper angle in a way that is similar to the (generally lower) Argus stations. As the cBathy algorithm is written for Argus data, this could potentially yield better results. The altitude and location have different effects on the data. It is not clear whether the more Argus-like camera angle or the increased amount of pixels is more important for accurate depth inversion.



Wave Height & Water Depth The accuracy of tracking waves is influenced by the wave height and water depth. Higher waves or shallower water cause more non-linear wave energy dissipation and therefore the inverting algorithm is less accurate. According to Trizna (2001), who used radar

imagery to analyse waves, in relatively deep water (deeper than 5 meter) and with low to moderate wave heights, their wave dissipation inversion technique managed to retrieve the correct depth. He found that a root mean square wave height increase from 1 to 3.5 meter made the depth estimation significantly poorer. Also, Stockdon and Holman (2000) found that lower waves yielded better results and Holland (2001) indicated that in the shallower regions, errors of over 50% were found. On the other hand, only in shallow water is the depth related to the wave celerity. Waves that are too small are not influenced by the sea bottom. Therefore, small waves are also assumed to yield bad results.

Camera/ Grid Resolution



Similar to the above mentioned drone altitude, the camera resolution influences the quality of captures imagery. It could be beneficial to upgrade the camera that is attached to the drone if the desired pixel resolution is not reached for usually the coordinates far away from the drone camera. For the purpose of this research the method is attempted to be kept as generic as possible. Therefore, this research uses the camera that comes standard with the UAV. Subsequently, the specified spatial resolution of the grid that is used for bathymetry mapping is also assumed to influence the final result. For instance if only few grid point are chosen, does probably not give a high enough spatial resolution to plot a map of the bathymetry with the desired level of detail. Also, when the grid points are chosen with an extremely high spatial resolution, the model could require too much resources.

Although they did not invert water depth, according to Plant et al. (2009), especially the cross shore variability in resolution seems to be influencing wave height predictions, whereas the longshore variability mainly influences flow predictions. As especially wave conditions are used for the depth inversion, the cross shore component seems to be most important.

In a later part of this research, different grid resolutions are compared in terms of the accuracy they yield.



Inversion Accuracy The final step in the proposed process involves using the wave frequencies and their corresponding wave numbers for computer water depth according to the dispersion relation. As there are many dynamic mechanisms in the nearshore coastal area, it is challenging to model them accurately.

3.2.3 Process

To do meaningful measurements with the use of video imagery, a couple of steps need to be taken.

Camera Calibration Together with GPS and water level measurements, drone imagery is the only data that is gathered for this method. Therefore, it is necessary to specifically know different parameters that distort the images which are taken and thereby calibrate the drone camera. These parameters are called intrinsic camera parameters and can be calculated using software specifically written for this purpose. Section 3.3 will go into the specifics of this process.

Image Rectification The images are stored in a two dimensional UV matrix, and every pixel in the image has a different distance to the next pixel in the the three dimensional space (center to center, see image 21). As the algorithm that is used requires estimates of wave conditions like frequency and wave number, of every single pixel in every single image the three dimensional coordinates need to be determined. This process is called image rectification and will be elaborated in section 3.4.

Depth Inversion The last step of the process involves tracking of the observed waves and calculating the water depth in the spatial range of the imagery. The specific algorithm used for this process will be elaborated in section 3.5.

3.3 Image Undistortion (Intrinsic)

Light rays pass through the camera's lens after which they are registered by a sensor. The passing through the lens will almost always cause some kind of distortion in the captured image. Sometimes, as

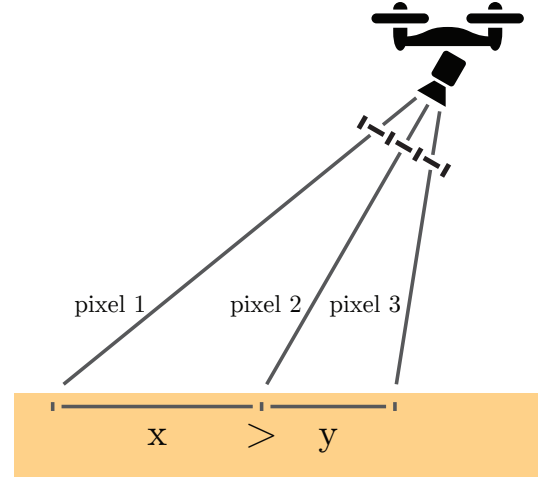


Figure 21: Pixel Distance

is the case with so-called fish-eye cameras, it is a really significant effect and can therefore be observed by the naked eye. For example, lines that are in the real world straight will be captured as a line with a curvature. For the recording to be able to portray the waves as accurate as possible, these distortion effects need to be compensated. This can be done when several parameters of a lens are known. These parameters can be found with a camera calibration.

Coordinate Systems Whereas the real world is experienced in three spatial dimensions (X, Y and Z), images are captured on a two dimensional plane. During this conversion, information is lost because of the decrease in dimensions. A method to reproject a two dimensional image in a three dimensional grid is called image rectification and will be further elaborated in this chapter.

Intrinsic Camera Parameters The extend to which images are distorted by the lens are quantified by the intrinsic camera parameters and the distortion coefficients. These intrinsic camera parameters are stored in a 3 by 3 camera matrix and entail the following:

- **Focal length (f_u) in U direction**
- **Focal length (f_v) in V direction**
- **U coordinate of the principal point (U_0):** the location of the light ray that reaches the film perpendicularly in U direction (from the origin of the photo)
- **V coordinate of the principal point (V_0):** the location of the light ray that reaches the

film perpendicularly in V direction (from the origin of the photo)

- **Image skewness (s):** the discrepancy between angles as observed in the real world and on the image (see image 22)



Figure 22: Skewness

3.3.1 Theory

Depending on the tolerances of the manufacturing equipment, each camera lens has its own distortions. Even lenses from the same batch are usually different. Because the error is in the equipment, there is no way of knowing the camera parameters beforehand. Therefore, it is necessary to calibrate the camera manually.

The above mentioned Intrinsic Camera Parameters are stored in a matrix (K):

$$K = \begin{bmatrix} f_u & s & U_0 \\ 0 & f_v & V_0 \\ 0 & 0 & 1 \end{bmatrix} \quad (8)$$

The camera parameter matrix is structured in such a way that, in combination with the distortion parameters, of all the pixels the angles of incidence are known (see figure 23). The calibration process therefore incorporates finding the relation between pixels and their specific angle of incidence. This can be done using a checkerboard of which the dimensions are known by the algorithm. As the software can identify the corners of every square on the checkerboard and compare the location with the supposed three dimensional locations, it can calculate distortions in the lens. Around 20 images of a particular checkerboard from different angles are generally used per calibration. During the calibration, the 5 unknowns in the camera parameter matrix are calculated and stored.

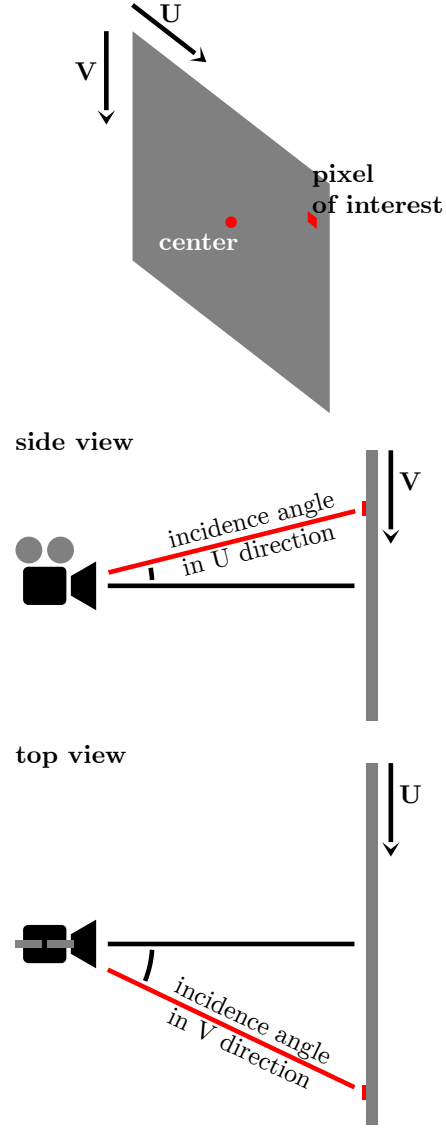


Figure 23: Angle of Incidence

Radial Lens Distortion Apart from the camera parameter matrix, also distortion coefficients are calculated by comparing the checkerboard image to the pixels locations (Zhang, 2002). Camera manufacturers usually distort the camera image by intension for the user to be able to have a wider field of view. These distortion coefficients comprehend the intentional distortion.

For regular lenses, 5 distortion coefficients are sufficient to calculate the angle of incidence for every pixel. However, for fish eye lenses generally 8 distortion coefficients are needed.

3.3.2 DJI Camera Matrix Calibration

In the beginning of this research, the camera parameters were calculated for the camera of the DJI Phantom 4 (P4). After a couple of month however, the drone was crashed and a new one was purchased. As an experiment, the internal camera parameter matrix of the crashed P4 was used to try and undistort the images, but the results were extremely poor. Therefore it was assumed that indeed every camera produced by the same company (or even maybe in the same batch) differs and needs to be calibrated individually.

Several different approaches were used for calibrating the camera. Firstly, a checkerboard was displayed on a computer screen and 20 images were sampled. However, the software used for the calibration had difficulties detecting the edges on a computer screen, after which a printed checkerboard was used. The first calibration based on an A3 paper with 11 by 5 squares (see image 24) generated a reasonable results based on naked eye qualifications. The computer algorithm automatically recognizes (see the red circles in the image) every point that lies in between 4 squares and therefore this is really a 10 by 4 checkerboard. (Herrera et al., 2012; Zhang and Pless, 2004)

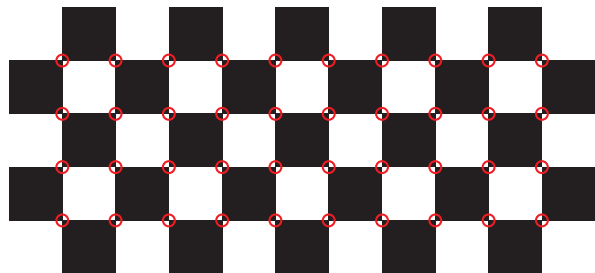


Figure 24: Checkerboard 11 by 5

However, as it was assumed that the factor which could potentially render the largest improvement was not the algorithm, more checkerboard calibration images and settings were used to improve the final internal camera parameter matrix. In the calibration process, there are an extensive amount of parameters that can be altered and therefore there will always be a matrix that better represents the parameters of the lens. The final setup used in this research was a 26 by 18 checkerboard printed on a A0 piece of paper. The internal camera parameters found are shown in the following matrix.

$$K = \begin{bmatrix} 2.33e + 03 & 0 & 1.97e + 03 \\ 0 & 2.34e + 03 & 1.45e + 03 \\ 0 & 0 & 1 \end{bmatrix} \quad (9)$$

And the 5 distortion coefficients found are:

$$distortion = \begin{bmatrix} 3.30e - 03 \\ -1.81e - 02 \\ -1.25e - 03 \\ 1.11e - 04 \\ 1.10e - 02 \end{bmatrix} \quad (10)$$

Whereas the undistorted images already looked more representable than the images found using the 11 by 5 A3 checkerboard, the settings were not ideal. As the A0 paper is large, it was stuck against a wall outside. However, due to the windy conditions of that day, the middle part of the paper sometimes moved, although not very extensively, in the Z-direction. Hence, it can be argued that even after this calibration, an efficiency gain can be made in this part of the process.

3.4 Image Rectification (Extrinsic)

Now the camera parameters are known, the external unknowns can be solved. Image rectification basically entails converting a two dimensional pixel image to a map with each pixel of the photo portraying its location in a user specified three dimensional grid system. This is done by using the intrinsic camera parameters which are summarized in the K-matrix. Furthermore, the camera direction, stated in a direction matrix, needs to be known/solved (Monasse et al., 2010; de Vries et al., 2011). Ground control points indicated in the image are used as a reference for the determination of the coordinates. Subsequently, every pixel in the image can be allocated a coordinate and a projection can be made.

Whereas it is most accurate to spread the GCPs evenly across the area of interest, in moving water this proposed a challenge. Even so, in their research, Brouwer et al. (2015) found that the reprojection error of approximately one meter.

Extrinsic Camera Parameters As the internal camera parameter matrix incorporated the angles of incidence of every single pixel in the image, also the extrinsic parameters need to be solved. The camera direction needs to be calculated by the use of ground control points of which the pixel location and the three dimensional location is known. This calculation solves the pitch, roll and heave of the camera.

3.4.1 Theory

Transforming pixel coordinates to three dimensional coordinates involves calculating a camera projection matrix P . Equation 11 shows the camera model.

$$\begin{bmatrix} U \\ V \\ 1 \end{bmatrix} = P \begin{bmatrix} x \\ y \\ z \\ 1 \end{bmatrix} \quad (11)$$

If the camera projection model is known, for all the 2d coordinates, 3d coordinates can be calculated and vice versa. The above mentioned projection matrix has several components which are shown in equation 12 (de Vries et al., 2011).

$$P = KR [I \quad -C] \quad (12)$$

Where I is a 3 by 3 identity matrix, K are the internal camera parameters as described in equation 8. The other parameter represent the extrinsic camera parameters. C is the (X, Y, Z) camera location within the user specified three dimensional grid system. Finally, R represents the 3 by 3 rotation matrix including the pitch, roll and heave.

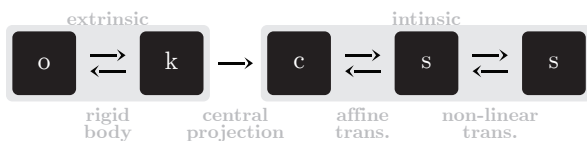


Figure 25: Extrinsic and Intrinsic

Furthermore, the previously mentioned distortion parameters are accounted for resulting in a projection of the pixel coordinates on a plane in a three dimensional grid system.

3.4.2 Rectification Test

To analyze the rectification, a test was performed. The rectification test was set up to discover the accuracy of rectifying images with the algorithm used in this research. The plan consisted of simulating an area of interest with a flat surface area and rectifying this area with the algorithm. In the area, several Ground Control Points (GCPs) would be located of which the location is known (see figure 26). Subsequently, the location of the automatically identified GCPs is calculated through rectification. For every GCPs, the location found through rectification is compared to the measured locations (by RTK GPS) and the data is analyzed.

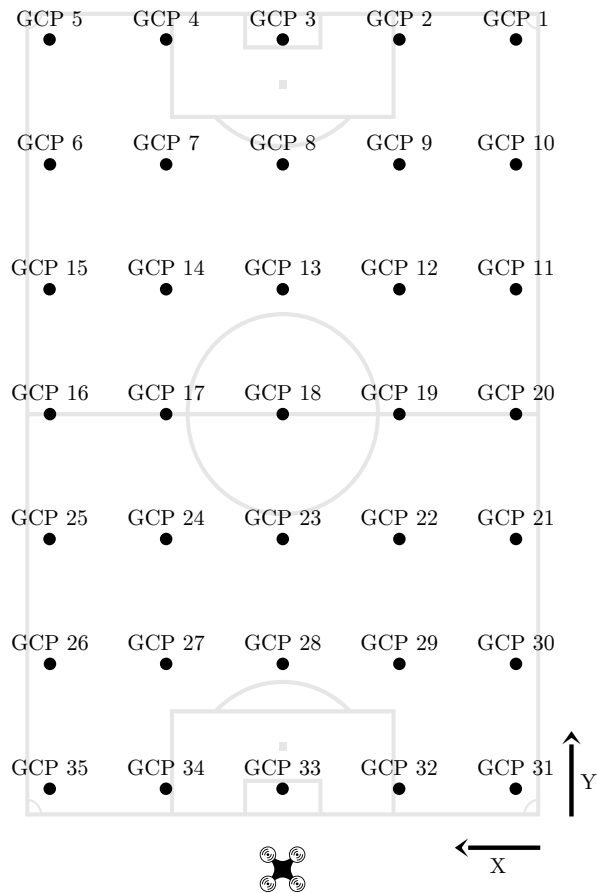


Figure 26: Setup 1

Test Location As Delft lays within the Rotterdam-the Hague Airport no-fly zone, the location of Naaldwijk was chosen. As a football field is relatively flat, the test was conducted at the artificial grass field of V.V. Naaldwijk (Football Club Naaldwijk).

Ground Control Points At the football field, a grid of 35 GCPs were laid out on the field. With a Real Time Kinematic GPS receiver, the exact locations of the GCPs were determined.

Error Scaling Because the rectification software uses the angles of incidence of the pixels that represent the ground control points, this process is mainly focused on solving a set of triangles to determine the drone location. As the proportions of the triangles stay the same throughout the lifespan of the drone camera, it is assumed that the errors found in this preliminary rectification research can be scaled proportionally to final observations that will be made in the coastal area.

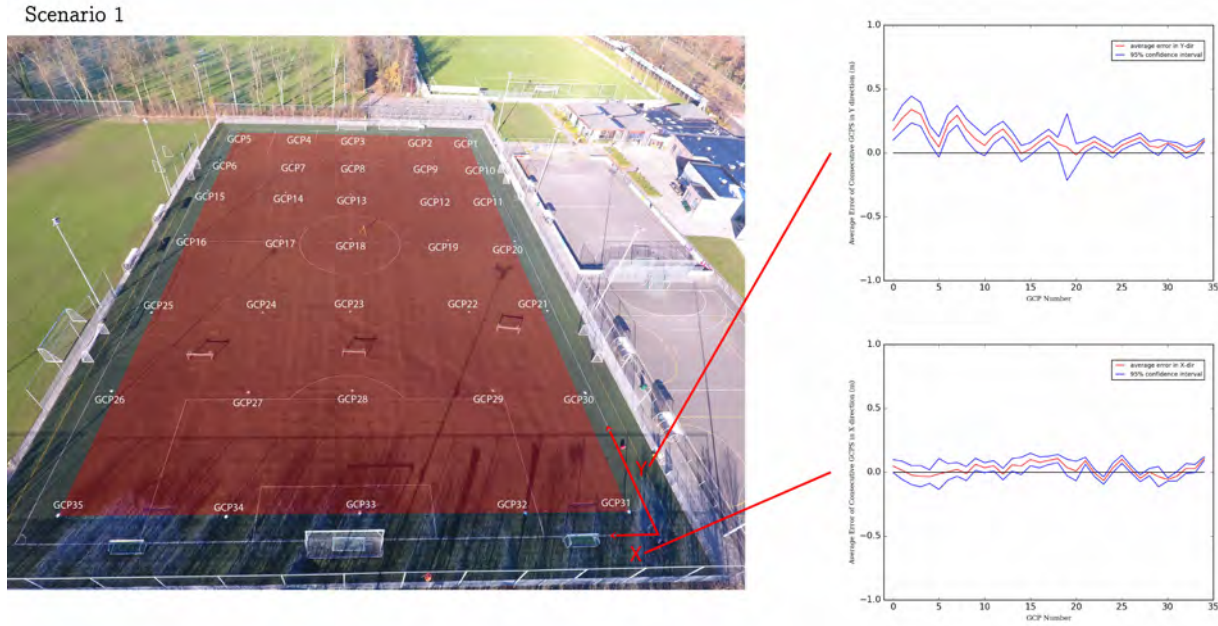


Figure 27: Error for Scenario 1, Top Right Corner: Y errors, Bottom Right Corner: X-errors

Scenarios For every different scenario, four different GCPs are used as control points for the rectification of all of the images taken. This is done to analyze which setup should be used in the final field research.

Data During rectification, all of the positions of the GCPs are estimated by the computer vision software. These locations can be compared to the RTK GPS locations of the GCPs after which the rectification error is analysed. Therefore, for every GCP, an average rectification error and its 95% confidence interval can be calculated and plotted. This is done for the Y-direction (parallel to the side lines of the football field) and for the X-direction (parallel to the goal line of the football field).

Dataset 1 For the first test, the drone was hovering over the football field at the location of the goal. A total of 644 images were used. Therefore, a total of $644 * 35 = 22.540$ errors were calculated.

GCP 19 Some of the scenarios show a large standard deviation for GCP 19 (see figure 27). It is unknown where exactly this discrepancy in the data can be attributed to. It could be that, although it was briefly manually checked, the automatic GCP detection did not find the correct location in some of the 644 images for this particular GCP.

3.4.3 Scenario's

To make a first estimation on the efficiency in the data recording process, several scenarios of GCP configuration are analyzed in the following section. Whereas 23 scenarios were researched, only the most important ones are elaborated.

Scenario 1 (figure 28) In the first scenario, the four outer-most corner GCPs were used for to be the reference control points for the rectification (see figure 28). These four GCPs are assumed to be the most effective combination of control points as they span the largest area of the field. It can be observed that especially the X-direction is accurate. The average error in the X-direction is 0.15 max and the standard deviation generally stays within 0.3 meters. On the other hand, the computer vision software is less accurate when it comes to the Y-direction. The errors in this direction have a fairly systematic rhythm and the rectification is fairly accurate at the far end close to the side lines of the football field (GCPs 1, 5, 6 and 10). In the center of the field on the far end (GCPs 3, 8 and 13) are less well projected with an average error up to 0.35 meters. Arguably, this is due to inefficiencies with respect to the Internal Camera Parameters used. Probably, the distortion in the width of the camera is not corrected as accurately as possible leading to a rhythm in the average errors. This can be ar-

gued because the standard deviation is small (up to 0.3 meters at the far end). The small variance also means that whereas the pixel is projected with a small error, the error will stay the same throughout the dataset and therefore it can be argued that the images will still be usable for depth inversion in a later stage.

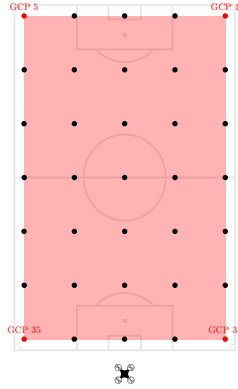


Figure 28: Scenario 1

Scenario 5 (figure 29) Scenario 5 still shows the strange variance phenomenon regarding GCP 19. Furthermore, generally the same rhythm as in scenario 1 is observed. It can be assumed that this setup would yield no problems when inverting water depth. This is mainly due to the small standard deviation, which shows that the pixels plotted in certain locations will probably be rectified in a close proximity of that location throughout the dataset.

Scenario 6 (figure 30) In terms of lowering labor intensity, it is easier to use 4 control points located on the beach then having to use floating GCPs. This scenario mimics 4 GCPs on the beach with the drone flying over land. Whereas the errors in the Y-direction on the far end of the field are large, the confidence interval does not exceed 1 meter.

The errors are shown in figure 35. In the X-direction the confidence interval around GCP 4 seems to increase. This could either be the result of wrong camera parameters or a systematic error in pinpointing the right location of GCP 26 and/or 35. The GCPs on the close end of the field cover a significant amount of pixel, and it could be that the computer vision software selected a pixel a bit off of the center of the GCP.

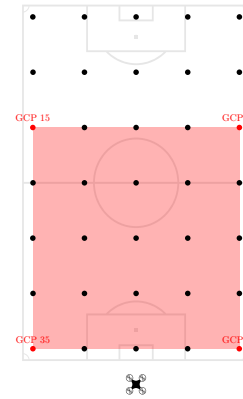


Figure 29: Scenario 5

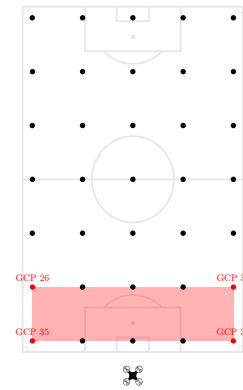


Figure 30: Scenario 6

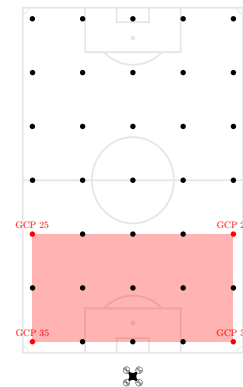


Figure 31: Scenario 7

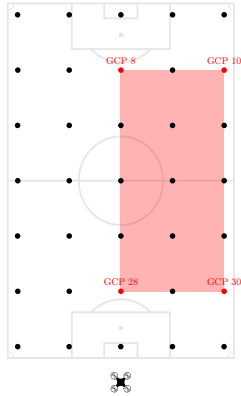


Figure 32: Scenario 14

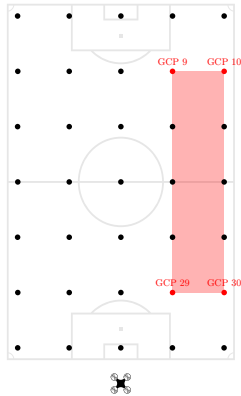


Figure 33: Scenario 15

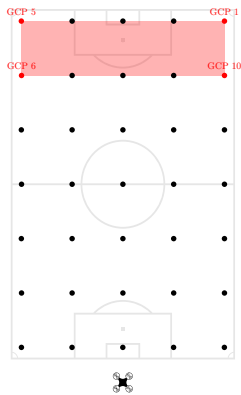


Figure 34: Scenario 21

Scenario 7 (figure 31) Scenario 7 represents the same setup as scenario 6. However, the fictional beach is now captured by a larger part of the video. This results in a smaller average error, but does only seem to decrease the standard deviation in the X-direction. This is a strange result as the area is only extended in the Y-direction.

Scenario 14 (figure 32) The alongshore distance that the rectification covers has been decreased in this scenario. Where the average errors seem different than the previous scenario, they are not necessarily worse. The standard deviation does seem to increase a bit in both directions (especially around the GCPs furthest from the drone camera), albeit not significantly.

Scenario 15 (figure 33) In this scenario GCPs 9, 10, 29 and 30 are used for rectification. This reduction in rectification area does render worse results than the previous scenario. However, the average error and the standard deviation do not seem bad in terms of usability. This scenario again shows that only having GCPs on the beach and taking imagery from the side might potentially yield good bathymetric accuracy.

Scenario 21 (figure 34) When flying the drone over water and using GCPs on the beach, scenario 21 represents a rectification area far away from the beach. The Y-direction rectification seems to be fine with the 95% confidence interval staying within meter. However, in the X-direction the standard deviation seems to get worse the closer it gets to the drone camera.

Conclusions It can be argued that the shape of the area used for rectification should be close to a square. The above results show that in this case the rectification stays as predictable as possible. Whereas the average error is not always smallest when using a square, the standard deviation seems better than for other shapes. Not using a rectangle or a square as the rectification area could result in random unpredictable distortions that might decrease the depth inversion accuracy as the wave celerity might not be estimated in a correct way. In the case that due to labor intensity reasons it is preferred to only use GCPs on the beach, there will always be an increasing error the further seawards the rectification stretches.

It was also shown that the error in the Y-direction is in some cases positive (reprojected too far away

Scenario 6

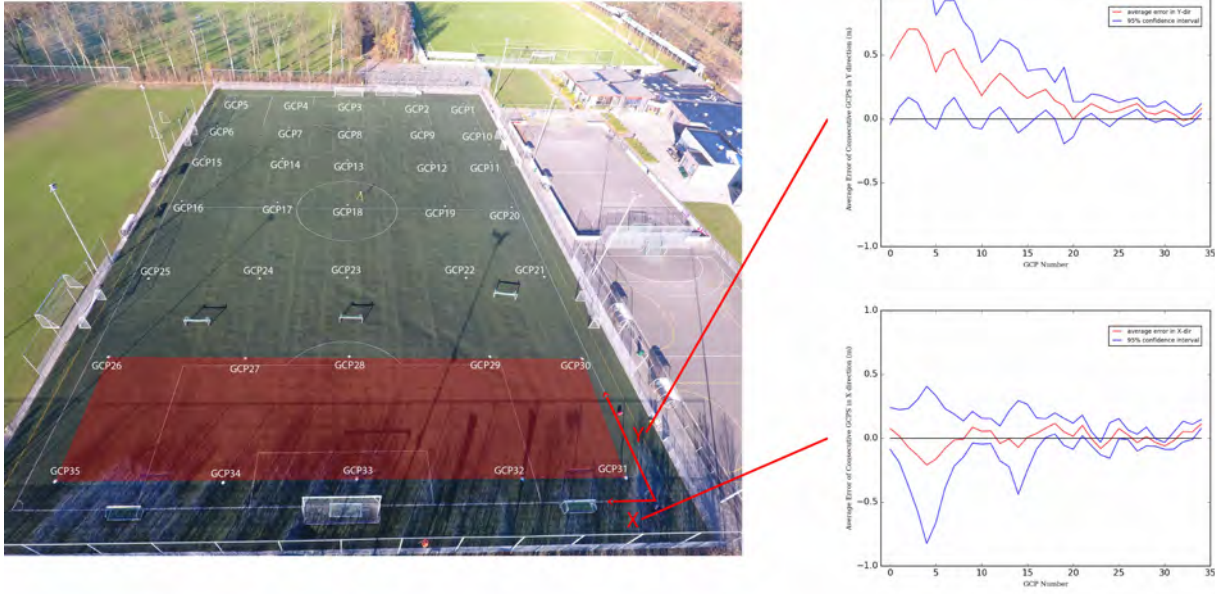


Figure 35: Error for Scenario 6, Top Right Corner: Y errors, Top Left Corner: X-errors

from the camera position) and in some cases negative (reprojected too close to the camera position). This effect seems to be arbitrary and therefore cannot be accounted for in the planning of the final coastal surveillance.

Furthermore as expected is the surface area correlated with the accuracy of the rectification. However, whilst it seems to be correlated to the average error, it is not necessarily the case for the standard deviation. Also, the distance of the rectified area to the GCPs seems to be correlated with the accuracy of the rectification. Subsequently, the amount of distance the rectification area covers in a certain direction (for instance X) is directly related to the accuracy of the rectification in that particular direction. This is the case even when the analyzed coordinates are located far from the area in the other direction (for instance Y).

Whereas above mentioned correlations generally seem to hold, there are several exceptions found in the 23 scenarios. This means that there is always an uncertainty in the accuracy when keeping the boundary conditions the same as the above described testing setup. It will probably be the case that in the future, especially with even further improved cameras and resolutions, the rectification would get more accurate. However, for this research, this uncertainty should be taken into account.

When the drone is faces shoreward, only using GCPs on the beach does seem to render good results. However, the results get worse when the distance of the total rectified area exceeds three times the beach width. In practice, this technology is created to map bathymetry well beyond the breaker line and therefore in is uncertain whether this scenario will fulfill the needs of the depth inversion software in practice. A further practical complication for this method is the battery life of the UAV and the margin of safety to use when flying it back to the beach after a recording.

3.5 Depth Inversion Algorithm

The cBathy algorithm that is used in this research for water depth inversion uses physical knowledge of the interactions between bathymetry and movements of water bodies. More specifically, water depth has a restriction on the wave celerity in the water on top of it.

3.5.1 Wave Celerity and Water Depth

There is a difference in hydraulic behavior in oceanic (deep) waters when compared to coastal (intermediate to shallow) waters. Whereas the water depth in oceans is too large to have any impact on the behavior of waves, in coastal waters the movements of waves are limited by the bottom.

Wave Celerity The speed at which a wave propagates through a water body can be determined by its length divided by the time it takes (the wave period). This can also be captured by dividing the radial frequency (ω) by the wave number (k).

$$c = \frac{L}{T} = \frac{\omega}{k} = Lf \quad (13)$$

As:

$$\omega = \frac{2\pi}{T} \quad (14)$$

$$k = \frac{2\pi}{L} \quad (15)$$

$$f = \frac{1}{T} \quad (16)$$

Where L is the wave length, T the wave period and f is the frequency. To be able to calculate water depth from wave celerity, the following known depth-celerity relations can be used.

Deep Water In deep water, the wave motions do not get influence by the bottom. Generally, water is considered to be deep when it fulfills the following requirements.

$$\frac{1}{2} < \frac{h}{L} \quad (17)$$

Because the waves do not 'feel' the bottom, the wave celerity is not influenced by water depth. Rather, it is limited to its frequency.

$$c = \frac{L}{T} = \frac{gT}{2\pi} = \frac{g}{\omega} (\approx 1.56T) \quad (18)$$

Where g is the gravitational constant.

Shallow Water On the other hand, waves in shallow water behave differently. Water is considered to be shallow if:

$$\frac{h}{L} < \frac{1}{20} \quad (19)$$

This indicates that water this is considered shallow for some waves, might not be considered shallow for other waves. Subsequently, in shallow water the wave celerity is only dependent on the water depth.

$$c = \frac{L}{T} = \frac{\omega}{k} = \sqrt{gh} \quad (20)$$

Intermediate Water When waves penetrate into coastal waters, before the water is shallow enough to be considered shallow water, there is an intermediate part. Intermediate water has the following characteristics:

$$\frac{1}{20} < \frac{h}{L} < \frac{1}{2} \quad (21)$$

Furthermore according to Holthuijsen (2014), the relation between wave celerity and water depth in intermediate water is:

$$c = \frac{L}{T} = \frac{\omega}{k} = \sqrt{\frac{g}{k} \tanh(kh)} = \frac{gT}{2\pi} \tanh(kh) \quad (22)$$

With this dispersion relation, the following algorithm can iteratively determine water depths in the nearshore by tracking incoming waves as described in the subsequent section.

3.5.2 cBathy

As described in the literature review, the cBahty algorithm consists of three phases. The first phase involves a frequency-dependent analyses of wave frequencies (f_b), wave numbers (k), wave directions (α) and corresponding water depths (\tilde{h}). The second phase uses the analyzed wave numbers for several frequencies to make a frequency-independent estimation of the best single depth (\hat{h}). Lastly, the third phase estimates a running-averaged depth (\bar{h}). The last phase however, is only possible when multiple measurements of one particular location are taken, and is therefore commonly used for Argus stations that do measurements a couple of times each day.

Phase 1 From equation 22, it can be distracted that a depth can be calculated when the angular frequency (ω) and the corresponding wave number (k) are known. This relation is shown in the following equation.

$$h = \frac{1}{k} \operatorname{arctanh}\left(\frac{\omega^2}{gk}\right) \quad (23)$$

Therefore, the first phase of the cBathy algorithm analyses waves and tries to find a wave number for every single wave frequency. The frequencies are user-specified and ideally involve all of the present bandwidths of the wave spectrum in that particular location. Where in the North Sea the wave spectrum generally includes 3 to 12 second waves, at the East Coast of the US 3 to 18 second waves are observed.

It is assumed that the optical pixel intensity portrays the physical waves and therefore a Fourier analysis on a specific coordinate for the full time series can distinguish the presence of certain wave frequencies in the wave domain. Per frequency, the wave phase is compared to the phases at the coordinates in the proximity of the coordinate of interest for a predefined area (tile) $[x_m \pm L_x, y_m \pm L_y]$. When these frequencies are combined for the area, a so-called cross-spectral matrix can be computed. This matrix is instrumental to finding different wave patterns with different frequencies. From this matrix, eigenvectors and values can be extracted that indicate the coherence of a particular frequency. The higher the magnitude of the absolute value of the real part of the eigenvalue, the more coherent (dominant) the signal.

From these wave patterns, the angle of incidence and the wave number can be found. Thereafter, per frequency the found angle of incidence and wave number can be used to model a wave field which is compared to the observed wave field. If the modeled wave field closely resembles the observed wave field, the component is assumed to be present and therefore to yield good depth inversion results. To analyze whether the modeled signal resembles the observed signal, a skill value is used that represents the percentage of variance in the wave signal that can be explained by fitting the local phase data to a planar surface. This value is used as a threshold value (skill values under 0.5 get rejected) for further computations.

From the found frequencies and their corresponding wave number, water depths can be calculated. Eventually, the algorithm computes depths of the 4 wave frequencies with the highest total coherence (highest normalized eigenvalue) over the tile. These depths are only temporary values that can be used to identify whether correct signals are picked up by the algorithm. In this so-called debugging mode, observed and modeled phase maps are shown for the 4 most dominant frequencies in a particular location. Also, among others, the estimated wave number, angle of incidence, skill value and error in the preliminary water depth of the 4 frequencies are shown. These values can be used to verify the wave climate as estimated by the algorithm.

Phase 2 The second phase of the depth inversion algorithm entails using the 4 estimated dominant frequencies found in phase 1 to estimate water depth. For these 4 frequencies, the wave numbers are used to search for a single water depth that provides the best weighted fit for the dispersion re-

lation (equation 23). The weight of the frequencies are determined by using a Hann filter that includes coordinates in proximity of the coordinate of interest in combination with the in phase 1 found magnitude of the eigenvalue and skill parameter (in that order). In this way, the most coherent frequency signal contributes to a larger part of the depth estimation. The found single depths are then stored in a matrix which compiles to a bathymetry.

Phase 3 Finally, the third phase uses a so-called Kalman filter to increase accuracy in the plotted bathymetry by comparing measurements of the same area to each other. This is commonly used for Argus stations as these stations are capable of taken 15-minute recordings multiple time each day. It identifies the well performing areas of each recording (if there even are any) by analyzing the phase 1 quality indicators and only uses the good data to update the bathymetry. In this way, rare disturbances such as storms, clouds or rain drops on the camera lens will get filtered out. Phase three is only usable when near-continuous measurements are taken. Although it could also be beneficial to drone bathymetry inversion as taking two or three recordings of a specific area is achievable on a single day, this research focuses on the accuracy of the phase two depths.

Wave Climate Analysis According to Holthuisen (2014), as wave climates constantly change, measurements of wave frequency domains should not be too long as the climate might have changed throughout the measurement. On the other hand, to be able to accurately analyze every different wave component, averaging over a longer period yields better results as it converges to the required statistical stationary state. Therefore, the optimum is described as measurements between 15 and 30 minutes. As according to the cBathy developers, much shorter recordings can also yield accurate bathymetries, it could be argued that cutting up a 15 minute recording in a couple of sections and using a Kalman filter might be beneficial for the accuracy of the eventual bathymetry.

Potential Limitations In the UAV bathymetry mapping method, optical signals are observed instead of physical signals. So even with a good skill value, it means that it can accurately recreate the optical signal. This does not necessarily mean that the underlying physical signal is detected.

3.6 Field Survey Plan

To gather data for the final part of this research, in February 2017, a field review was conducted. Several measurements acquired footage of the surfzone with visible Ground Control Points. From these videos frames were cut with a two hertz frequency and rectified. In this way, waves were tracked in a predetermined coordinate system.

The goal was to test different settings for the usage of drone imagery in combination with the cBathy algorithm to determine water depths in the nearshore area. Therefore, the proposed measurements were done as elaborate as possible. With an extensive amount of Ground Control Points and different camera angles, different scenarios can be elaborated and compared in terms of accuracy of bottom depth estimation.

Location As it is in close proximity of the testing equipment, for this project the beach of Scheveningen is chosen as a location. The Noorderstrand (Northern Beach) was chosen as due to bad weather it would not be too busy, and it lies within close proximity of Shore Monitoring's office.

Wave Conditions According to the literature review, for the cBathy algorithm, small waves yield the best result. However, the wave climate taken into account by that specific research is significantly different from the Dutch wave climate. Although during small wave conditions, there are far less non-linearities that interfere with the movement of the waves, on the other end of the spectrum the drone camera still has to be able to make a distinction between the wave peaks and the wave troughs. Current Argus systems have a hard time implementing the cBathy algorithm when the waves are high. This is partly because of the non-linearities and partly because of the limited visibility behind the high waves. This is because Argus stations usually have a limited height. Because of the higher altitude, the limited recording height is considered to be less of a problem when using drones.

Furthermore, the main limitation on wave length is the pixel resolution of the drone camera. The camera has to be able to record the length of the wave. As wave lengths are usually tens of meters, the resolution of the rectified images will most probably be sufficient for most wave lengths.

Ground Control Points To enable the above mentioned comprehensive amount of scenarios, a

so-called 'overkill' of GCPs will be used. As officially only 4 are needed to be able to rectify each image, several more will be used. This is also because there might be a malfunction. The GCPs will be spatially divided in a grid system and the following amount of points.

- 4 water GCPs
- 8 beach GCPs

However due to a lack of time and supplies, on the first day of measuring only 4 beach GCPs were used.

Flight Specifications The cBathy algorithm generally uses 17 minutes of images. Probably it will also work for time periods as short as five to ten minutes. However to be comprehensive, this test will conduct static videos as long as possible.

Furthermore, two drone batteries and two microSD cards were used throughout the day. While the drone is measuring using one of the two available batteries and microSD cards, the other will be charged and downloaded respectively. In this way, the four below mentioned drone positions can be used in that order.

- Position:
 - In cross shore direction towards the sea (hovering over land)
 - In cross shore direction towards the sea, further inland (hovering over land)
 - In long shore direction (hovering over water)
- Height: 120 meters
- Duration: 10-20 minutes per position
- Drone: DJI Phantom 4 (4K filming)
 - 2 16GB microSD cards
 - Charger
 - Extra battery

Also, the saturation of the video that is taken should be taken into account. Pixel intensity is measured a couple of times per second (original Argus cBathy algorithms use a frequency of 2 Hz). An automatic ISO can correct for scenarios when lighting by the sun changes significantly throughout the 20-minute measuring interval (for instance on a cloudy day). Subsequently, the flight logs with GPS location and GPS time were captured in an SRT file by the drone.

Camera Ideally, individual pictures are taken a couple of times per second with a resolution of 4000 by 3000. However, due to limitations in the firmware, there is no function to automatically shoot pictures with a fixed interval. Therefore a video was taken, out of which different snapshots were subtracted.

Lastly, the highest video resolutions available on the DJI Phantom 4 are either 4096 by 2160 or 3840 by 2160. The advantage of the slightly lower resolution is the higher frequency of 30 Hz (instead of 24 Hz). However, cBathy frequencies are significantly lower and therefore the higher pixel count is preferred.

- ISO: auto (check with white balance indicator)
- Resolution: 4096 x 2160 pixels

3.7 Summary

This section elaborated on the different steps in the UAV bathymetry mapping method as described by the conceptual model. The data acquisition was reviewed and the potential influence of a large amount of parameters on the eventual bathymetry accuracy was indicated. Subsequently, the internal and external camera parameters were described after which a rectification process was proposed. Different rectification strategies were reviewed after which the depth inversion algorithm was elaborated. The above mentioned survey plan was based on literature and preliminary tests regarding drone flights and experience. Once the data was gathered on the 9th and 10th of February 2017, it was analyzed. The following section of the report elaborates on the preparation of the data and eventually the depth inversion.

4 Results

Whereas the previous section elaborated on the process of depth inversion using drone imagery, this section shows the data that has been observed in the field survey. It also shows the computed bathymetries based on base scenario settings. Thereafter, different parameters in the cBathy algorithm are tweaked in a sensitivity analysis to optimize the results. The section consists of three main parts. Initially in section 4.1, the data gathering process describes the layout of the measurement location on both the survey dates. All general information regarding the hydraulic and UAV conditions are elaborated. Thereafter, section 4.2 portrays the process which was followed during the first part of the data analysis. This section includes preparing the data using a computer vision plugin for python by automatically detecting the Ground Control Points and calculating a projection for every single image taken during the data gathering process. Lastly, section 4.3 shows the settings that were used for inverting water depth by means of the cBathy algorithm.

4.1 Data Gathered

The data for this research was gathered on Thursday the 9th and Friday the 10th of February, 2017. Where on the first day, due to time limitations two drone flight were conducted, the second day consisted of five collections. However, noise in the wave field due to the reference bathymetry survey with a Jetski rendered the last two flight useless for inverting water depth. Therefore, the two usable measurements on day one and three on day two are referred to as datasets 1.1, 1.2, 2.1, 2.2 and 2.3.



Figure 36: A Frame of Dataset 1.1



Figure 37: A Frame of Dataset 1.2

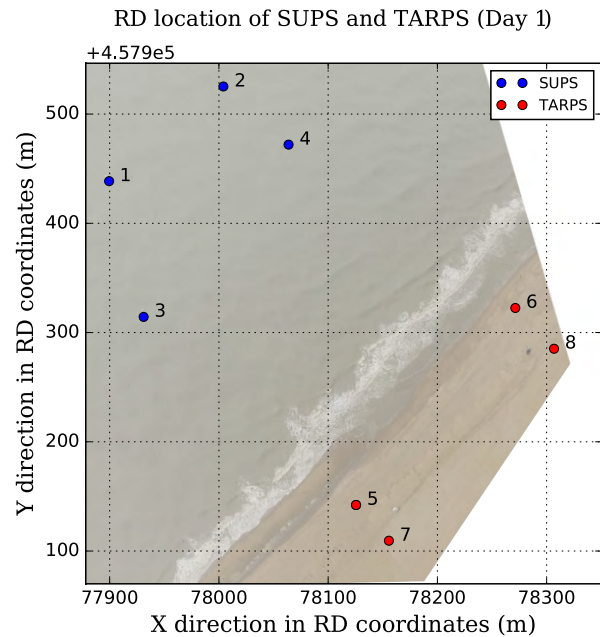


Figure 38: Ground Control Points Day 1

4.1.1 Day 1

On the first day a clean swell generated in Norway and Denmark reached the beach of Scheveningen from the North (see figure 36 & 37). In the south of the Netherlands, waves were reported to break, whilst in Scheveningen limited to no breaking on the bars was observed. Table 1 shows the conditions in which the data was gathered. The offshore water level was collected from the water information website of Rijkswaterstaat (Rijkswaterstaat, 2017a) for the location of Scheveningen. Also, figure 39 shows the specific phase in the tidal movement at which the recordings were acquired. For the recordings on day one, there was a strong tidal flow directed to the North. Also, as there was no data available for the location of Scheveningen,

Table 1: General Survey Information

Data set	Date	Start Time (GMT)	End Time (GMT)	Water Level (m)	Wave Height (m)	Wave Length (m)	Wave Number (m^{-1})	Tidal Current (m/s)
1.1	09-02-2017	14:28:56	14:44:57	.48	.97	50	.13	-.6
1.2	09-02-2017	14:58:30	15:17:11	.30	.92	50	.13	-.8
2.1	10-02-2017	11:57:28	12:12:55	-.13	.85	40	.16	.7
2.2	10-02-2017	12:38:29	12:53:30	.55	.80	40	.16	.6
2.3	10-02-2017	13:23:06	13:40:17	1.03	.79	35	.18	0

Table 2: Drone Information

Data set	Drone Position in RD (X,Y) (m)	Video Duration (s)	Height by Barometer (m)	ISO	Shutter Speed (s^{-1})
1.1	(78331, 458010)	963	120	100	1/160 - 1/100
1.2	(78270, 458045)	1122	120	100	1/120 - 1/100
2.1	(78310, 457999)	890	118	100	1/320
2.2	(78263, 458045)	902	120	100	1/240 - 1/200
2.3	(77995, 457971)	1032	120	100	1/200 - 1/160

the Wave height was averaged by combining three offshore measuring stations (Lichteland Goeree, Ijmuiden Munitiestortplaats & Ijmuiden Stroommeetpaal, (Rijkswaterstaat, 2017b)). Hence, wave heights are indicated far offshore and at remote locations and therefore might not be accurate for the exact Scheveningen beach location. Where in video 1.1 no breaking waves were observed apart from the first 50 meters offshore, the second video (1.2) shows some foam in the area of interest. Furthermore, based the rectified images, the wave length on the first day was visually estimated at 50 meters, leading to an estimated angular wave number in the order of .13 for both datasets 1.1 and 1.2.

On the beach, located approximately 50 meters from the waterline, 4 blue tarps were functioning as static ground control points (GCPS) and 4 SUP boards were equipped with two GPS loggers each as floating GCPS. The boards were equipped with two GPS logging to be able to afterwards analyze discrepancies in the data. As all of the devices had been functioning throughout all of the datasets and no discrepancies were found, the positions of each board could be determined by averaging the locations. Figure 38 shows the GCP locations projected on the dutch Rijks Driehoek (RD) reference system. Although the SUPS moved a couple of meters during the recordings on day one, contrary to the surveys on day two, all of the floating GCPS seemed

to have a relatively stable location.

Despite the fact that a medium to heavy fog made an absolute recognition impossible, both dataset 1.1 and 1.2 captured the horizon (see figures 36 & 37). The difference between the two however was the drone position and camera orientation. During the first measurement (1.1), the drone was located in such a position that all 4 beach GCPS were visible throughout the video. The second measurement (1.2) included a drone position closer to the waterline. Therefore, is it only registered two of the four beach GCPS. Also, during the first measurement, the camera was tilted further upwards than during the second measurement, capturing more sky.

When looking at the drone settings during the recordings of the video (see Table 2), it can be shown that most variables were kept constant. As UAV position and height varied throughout the observations, this table gives an indication of the average numbers. The only variable that differed significantly when comparing the datasets was the shutter speed. During the first measurement, approximately the first 25 percent of the footage was taken with a shutter speed of 1/120 whilst the last 75 percent was taken with a shutter speed of 1/100. The second recording had a shutter speed of 1/100 for the first 95 percent and 1/160 for the last 5 percent. Throughout all recordings, the exposure value was +1/3 and the F number was 2.8.

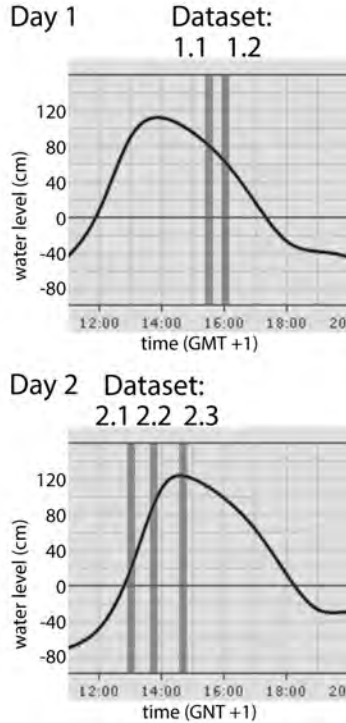


Figure 39: Tidal Phases During Data Acquisition

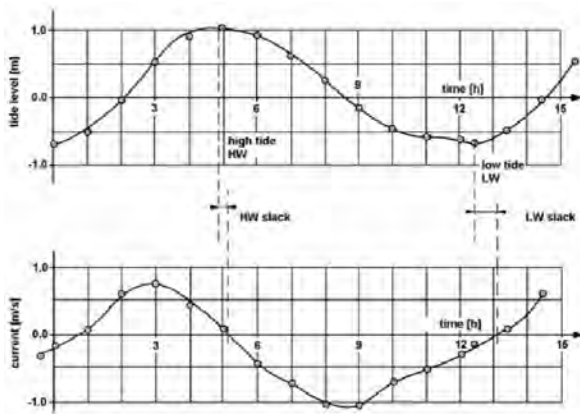


Figure 40: Water Level and Tidal Flow off the Coast of Rotterdam



Figure 41: A Frame of Dataset 2.1



Figure 42: A Frame of Dataset 2.2

4.1.2 Day 2

The second day consisted of a slightly decreased wave height due to a reduction of swell from the north. When looking at the conditions at which the three datasets were gathered, the range in water level was larger than the day before. These datasets were recorded a little before tidal flow reversal. During the first dataset (2.1), the low water level resulted in some significant wave breaking close to the water line (no farther than 150 meters offshore). In datasets 2.2 and 2.3, no significant wave breaking farther than 50 meters offshore was observed. The length of the waves on day two was estimated at around 40 meters. Hence, the angular wave numbers were estimated at .16 and .18 respectively.

Furthermore, a medium to heavy fog was observed. Similar to the surveys on day one, the first dataset (2.1) captured the horizon as well as two rows of beach GCPs (see figure 41). During the second dataset (2.2), shown in figure 42, the camera was tilted further downward with as result the lack of a captured horizon. Also, it captured only 1 row of beach GCPs. Remarkably, the video taken in the dataset seems to have a bluish tint whereas the other videos seem more yellow.



Figure 43: A Frame of Dataset 2.3

For dataset 2.3 (figure 43), a new observation strategy was executed. Instead of positioning the UAV above the beach and recording a video perpendicular to the water line, the camera was positioned alongshore and captured three floating GCPs, the first and a part of the second row of beach GCPs. Similar to the first day, regarding the drone settings, especially the shutter speed varies when comparing the datasets. The data of the first survey contained a significant decrease in video brightness in the first couple of seconds caused by a decrease in shutter speed. The decrease in brightness lasted for around 13 frames which indicates a period of 6.5 seconds (a frequency of 0.15 Hz). As the cBathy algorithm was set to analyzing wave lengths between 3 and 12 seconds, this interfered with the spectral analysis. As this prevented the cBathy algorithm from rendering good results, the first 8 seconds of this recording were not included in the analyses. In dataset 2.2, the first 5 percent of the captured video had a shutter speed of 1/200 whilst the rest has a shutter speed of 1/240. The final dataset was recorded with a shutter speed of 1/200 during the first 75 percent of the recording and 1/160 during the last 25 percent.

The difference in setup between the first and the second day was an increase in the amount of GCPs located on the beach. Instead of 4, 12 were configured (see figure 44). Subsequently, the same floating GCPs were used as the day before. However, as during the second day the floating GCPs were positioned by a Jetski, their eventual location had a closer resemblance to the grid as planned. Due to the low water level during the first measurement (2.1), the third floating GCP migrated approximately 40 meters throughout the particular survey (see figure 45). A similar floating GCP migration was observed for GCP 1 and 4 of dataset 2.3. For the rest of the datasets, the SUPS seemed to stay in position more steadily.

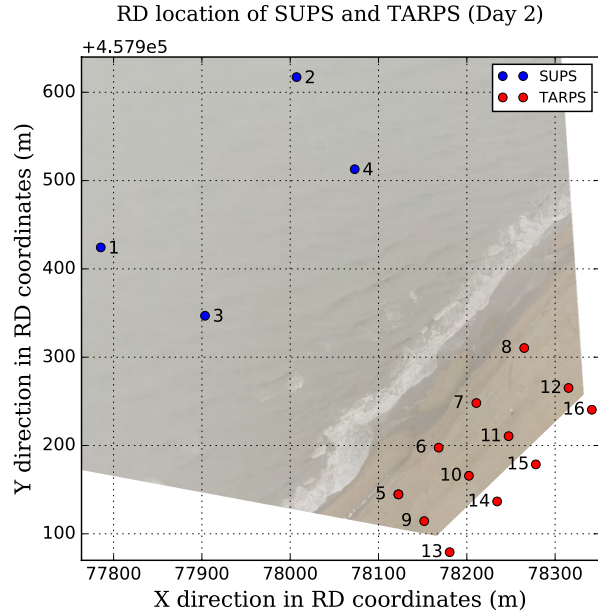


Figure 44: Ground Control Points Day 2

Finally, the tidal current was estimated. This was done by determining the specific phase of the tidal cycle during every recording using figure 40. Thereafter, based on measurements off of the coast of Rotterdam (figure 40) an indication of the velocity was made. Whereas the exact currents could differ, these estimations could still be used to analyze relative changes in wave characteristics.

4.1.3 Reference Jetski Measurements

To do an accuracy analysis comparing the UAV bathymetry mapping method with reference data, on the second day the water depth of the area of interest was measured by means of a jetski echo sounder as described in the literature review. As these measurements are up to a couple of centimeters accurate, for bench marking the method proposed in this report, they will be sufficient.

4.2 Rectification Process

The following section will elaborate on the preparation of the gathered data to be able afterwards determine the water depth. After analyzing their coordinates, the GCPs are automatically detected and used to calculate a projection. This projection is made for every single image in the specific dataset after which a video is created for a quantitative analysis. After the projections are put in a specific coordinate system a time series of a specific

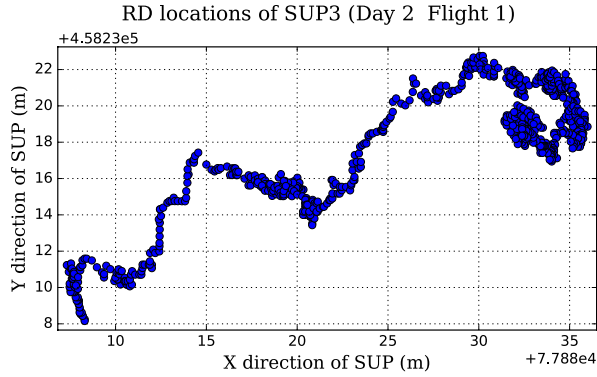


Figure 45: (Extreme) Position Change SUP 3 During Dataset 2.1

grid is made specifically to be used by the cBathy algorithm.

4.2.1 Coordinate Analysis

After acquiring the data in the field and the 4K videos were cut into frames with a two hertz frequency, the first step to be able to rectify the images was processing the coordinates of the beach and floating GCPs. Every floating GCP had two GPS loggers recording data. Commonly used by windsurfers, the GT-31 of brand Locosys seemed to be a good fit to the setup. As these loggers are financially on the low end of the spectrum, not a lot of risk was involved. However, where the loggers were located right next to each other on the boards, some of the recordings differed up to a couple of meters. Also the noise ratio differed between the devices. Figure 46 shows the X location of a specific floating GCP as recorded by its two GPS loggers. The image shows a discrepancy of up to three meters. As no reference data was gathered, and therefore no estimations could be made for every individual logger, the mean of the devices was used as the location for the floating control points. Lastly, the GPS data was converted to the Dutch Amersfoort Reference Grid, also known as the Rijks Driehoek (RD) system. The RD system is the most commonly used system in the Netherlands. Furthermore, the water levels are displayed based on the Normaal Amsterdams Peil (NAP).

4.2.2 Automatic Ground Control Point Detection

The next step is to identify the Ground Control Points in every frame. Due to limitations in the

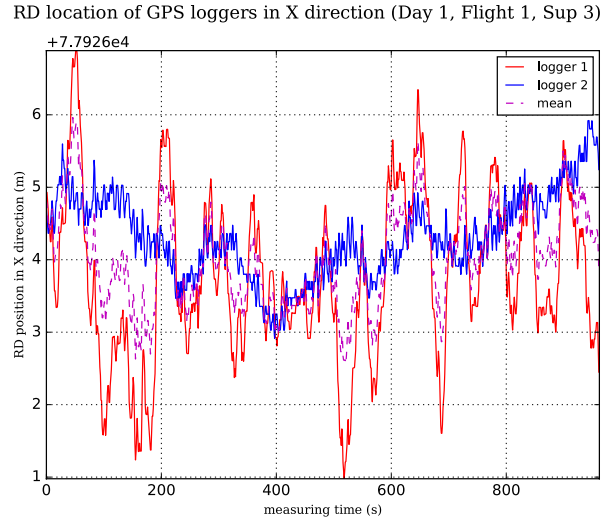


Figure 46: GPS Logger Data SUP 3 During Dataset 1.1

firmware of the DJI Phantom 4, after about 9 minutes the drone stopped recording the video and started recording a second one. Therefore, two videos were analyzed per dataset in terms of GCP recognition. Table 3 shows the results of the automatic GCP detection. It shows how many of the GCPs were left undetected. As differences in drone position throughout the datasets resulted in a differing amount of GCPs in view, the total number of points to be detected also varied.

In the first image loaded by the GCP detection algorithm, the user needs to identify the location of the control points manually. Thereafter, for each point for each subsequent image, the search area gets cropped around the GCP location of the previous frame. The GCP detection uses grayscale and HSV masks for floating and beach GCPs respectively. As the boards at sea were generally either lighter or darker than the sea surface, the grayscale mask generally showed a large blob. In some masked search areas, some parts of the water surface were either too light or too dark and therefore were not filtered by the mask. After filtering this noise by means of the computer visions erode function, in most cases the script was able to detect the GCP. As the tarps located on the beach all had a blue color, a Hue Saturation Value (HSV) color mask was used in a similar way.

The highest percentage of undetected GCPs for all of the videos is 3.2 percent. Therefore, a simple interpolation could fill up the data. On a couple of occasions the algorithm could not detect a GCP for

a maximum of 6 frames in a row, but after checking these occurrences manually, due to the steady drone footage, the interpolation seemed to still be identifying the correct pixel. The end of this step yields a matrix that includes the pixel location of all of the detectable control points in every single frame.

Table 3: Number of GCPS Not Detected

Data set	Video 1 / (out of)	Video 2 / (out of)	Average %
1.1	258 (8968)	224 (6296)	3.2
1.2	30 (6720)	79 (6732)	0.8
2.1	121 (5525)	126 (3370)	2.8
2.2	200 (8952)	35 (5464)	1.6
2.3	271 (10098)	264 (8478)	2.9

4.2.3 Rectification

The rectification process associates the geographical location of 4 (or more) specific detected Ground Control Points to their respective pixel location. For the floating GCPS, the specific time (GMT) at which the frame was taken is compared to the time as indicated by the GPS loggers and thereby the locations are linked. As the beach based GCPS had a fixed location, the time was not taken into account.

Through the internal camera parameter matrix described in section 3.4, of every individual pixel that is captured in a single frame the angle of incidence is known. After linking the four locations of the Ground Control Points in the user specified three dimensional grid to their pixel locations in the image, these camera parameters are used to calculate the three dimensional location of all of the other pixels in the image. When these locations are known, they can be appointed the pixel intensity captured in the image after which a projection of the frame is mapped (see figure 47).

The base rectification scenario used 4 GCPS of which two were located offshore and two on the beach. As on the first day, GCP 2 and 3 had a relatively large spread in the Y-direction (see figure 38), these were used and combined with two beach based control points. For dataset 1.1 GCPS 7 and 8 were used and as the second measurement did not include those, in this occasion GCPS 5 and 6 were used (see table 4).

On the second day, as the floating GCPS better represented pre-determined grid, the base scenario included floating GCPS 1 and 2. During the first



Figure 47: Projection of Figure 36 on RD Grid System

Table 4: GCPS Used for Rectification (see figure 38 & 44)

Data set	Floating GCPS Used	Beach GCPS Used
1.1	2,3	7,8
1.2	2,3	5,6
2.1	1,2	9,12
2.2	1,2	5,8
2.3	2,3	5,12

dataset, to keep the area between the 4 points used for rectification as large as possible, GCPS 9 and 12 were used as beach control points. For dataset 2.1, 5 and 8 were used. The difference in position of the third recording resulted in GCP 1 and 16 not being visible in the frames. Therefore, points 2, 3, 5 and 12 were used.

4.2.4 Grid Rotation

To be able to calculate water depth, the cBathy algorithm needs a specific grid layout with the beach line parallel to the y-axis. Therefore, before the images get rectified, the base of the measuring area on the beach gets arbitrarily chosen as (78200, 458130) in RD coordinates. Subsequently, the coordinates

Table 5: Absolute Errors and Errors in X and Y Direction (Real Location - Estimated Location, m) of GCPS

Data set	GCP 1		GCP 2		GCP 3		GCP 4	
	abs	(x, y)	abs	(x, y)	abs	(x, y)	abs	(x, y)
1.1	19.5	(-19.5, 0.7)	18.6	(-18.6, 0.0)	15.8	(-15.7, 0.6)	15.5	(-15.4, -1.2)
1.2	27.4	(-27.1, 3.8)	26.1	(-25.8, 3.7)	18.9	(-18.5, 3.6)	19.8	(-19.6, 2.9)
2.1	28.7	(-19.8, 20.6)	37.7	(-30.5, 22.0)	<i>n.a.*</i>	<i>n.a.*</i>	<i>n.a.*</i>	<i>n.a.*</i>
2.2	35.4	(-15.1, 4.9)	34.7	(-24.5, 3.7)	23.3	(-23.0, 3.9)	29.1	(-26.4, 6.0)
2.3	<i>n.a.**</i>	<i>n.a.**</i>	44.9	(-4.0, 44.6)	3.3	(0.9, -3.2)	36.3	(6.5, 35.7)

*The script was not able to automatically detect GCP 3 and 4 in dataset 2.1. **GCP 1 was not in field of view during dataset 2.3.

are rotated with an angle of 221 degree with respect to this position which results in the required grid layout for the algorithm with the beach situated on the left side of the grid.

4.2.5 Rectification Accuracy

To be able to analyze wave celerity based on the projections of the video frames, the definition of speed being meters per second insinuates that two variables are important. Firstly, the time which is recorded by GPS loggers on both the drone as the SUPS. Therefore, as all GPS loggers use the same satellites as a time reference, it is assumed that there is no error between them. On the other hand, location is important, as a difference in location divided by the time results in celerity. Therefore, it is valuable to take the rectification accuracy into account both in terms of the absolute error of the pixels projected on the pre-determined coordinate system as the stability of the coordinates.

Grid The depth inversion algorithm requires the data to be stored in time stacks which are indicated by specific coordinates chosen by the user. As Argus stations are reportedly using around three meters of grid interval in the X direction (cross shore) and 10 meters in the Y direction (along shore), for the base scenario of this research, a grid size of 3 by 3 meters is chosen. In a later stage of the research, this grid is altered to be able to identify the bathymetry accuracy in/decrease accordingly.

Absolute Rectification Error In section 3.4, some preliminary tests elaborated on the error in the rectification process based upon measurement of a measured grid of GCPs spread out on a football field. These measurements gave an indication of the accuracy of rectification using several mea-

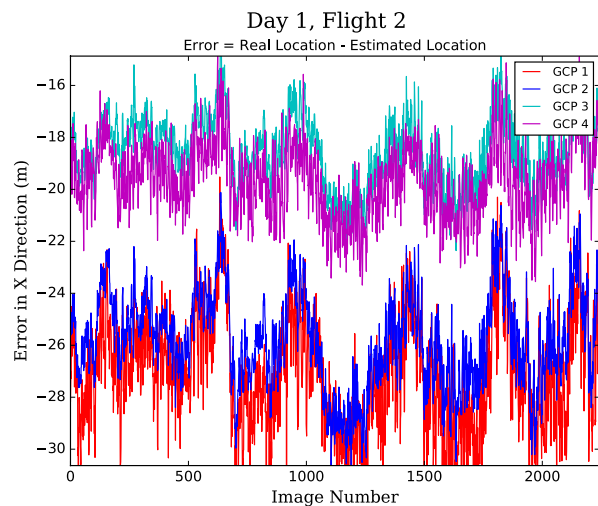


Figure 48: Error in X Direction of floating GCPS during Dataset 1.2

suring setups. As the survey of 9 and 10 February did not include a comprehensive grid of ground control points, only the 4 point located offshore are used as a reference for the absolute error. Table 5 shows the eventual absolute rectification error of the floating control point as well as the error in X and Y direction. This error is calculated by comparing the position of the floating GCPS to their position in the projection that is calculated by the rectification script. The table shows a consequent underestimation of the locations in the X direction and a significantly increasing error in the direction of the pointed camera when the distance between the measured point and camera gets expanded. It should be noted that the floating GCPs had a different location (further offshore) on the second day than on the first day. Generally, locations farther offshore have a larger rectification error. On the

other hand, as also the homography is determined with means of those same control points the rectification should generally be better.

When looking at the error in X direction more specifically, figure 48 shows the error for dataset 1.2. It can be argued that although the error is quite significant, it is relatively stable and generally stays the same throughout the dataset. This seems to be the case for all the dataset. The maximum difference in X error for 1 GCP throughout the dataset is around 10 meters.

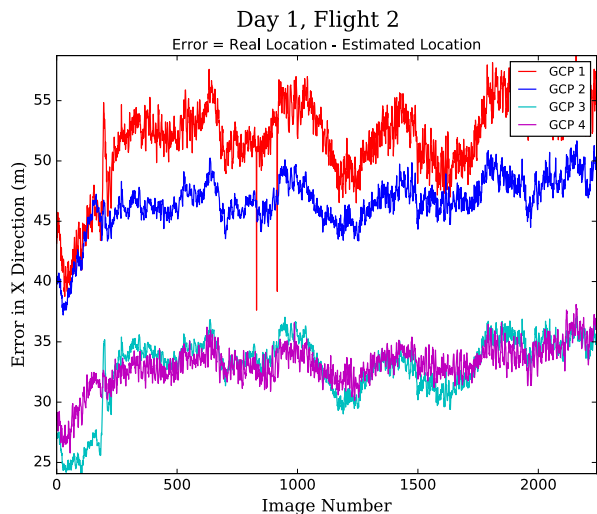


Figure 49: Error in X Direction of floating GCPS during Dataset 1.2 Using Different Internal Camera Parameters

These errors are a combination of discrepancies in the internal camera parameter matrix and the rectification script and could therefore potentially be decreased by intensifying the effort of calibrating the camera. For instance, when using a different internal camera parameter matrix which was collected in a different (less comprehensive) calibration, the errors increase and change sign (see figure 49). This matrix yields significantly different rectification results. It could be argued that purely from a rectification point of view, the results could still be drastically improved.

Rectification Stability The absolute error alone might not be sufficient in determining the quality of the rectification process. For instance, if the error fluctuates around zero with a great variability, the value might still be low or even close to zero, while the only thing that is captured in the final data is the noise in rectification accuracy. There-

fore, apart from the absolute rectification error also the rectification stability is analyzed. However, as the exact location of the individual pixels is not known it is not merely a question of comparing exact location with the calculated projection location and analyzing the standard deviation. Therefore, a new measure for stability is created and described in this section.

Qualitatively analyzed, the drone footage is relatively stable. Therefore, it is assumed that the location of a specific pixel in a subsequent frame can not differ too strongly. However, in contrast to Argus cameras which are fixed to a sturdy structure, it is acknowledged that the drone angle does move throughout the recording as a result persistent winds and the drone not being able to keep the camera pointed at one specific location. These movements have a relatively long time span and should therefore only be visible when analyzing a longer time period. These longer term movements can be captured in a certain trend line. Subsequently when taking a closer look around this trend line, smaller scale signal deviations are observed. As these deviations suggest that a specific pixel has moved several tens of meters within half a second after which it has moved back in the subsequent half a second, they can arguably be discarded and indicated as noise invoked by the rectification process.

To capture the above mentioned noise in the signal, a custom stability analysis method has been implemented. At first, a grid is specified at which points the stability will be analyzed. As these points lay within the area which is eventually used as input for the cBathy algorithm, 9 points with X coordinates (500, 750 and 1000) and Y coordinates (-250, 0 and 250) are specified to be analyzed. However, as these coordinates do not have a specific pixel which is assigned to them throughout the dataset, a representative pixel is chosen by calculating the average pixel that portrays the coordinate for the first 9 minutes of the recording. Once this pixel is found, its coordinate throughout time as calculated by the rectification algorithm is plotted. The location is calculated by adding both the X and Y coordinate squared after which the square root is taken. It therefore represents the distance of the specific location from the specific point (0,0). A part of the location data of pixel (2545, 117), representing coordinate (1000, -250) in dataset 2.2 is plotted in figure 50. An arbitrary time series of 250 of the 1808 frames is plotted to give visual support for the described stability analysis method. The blue line represents the location of the specific

Table 6: Arbitrary Rectification Stability Numbers (lower is better)

Data set	All Coordinates	Coordinate (500, -250)	Coordinate (1000, -250)	Coordinate (750, 0)	Coordinate (500, 250)	Coordinate (1000, 250)
1.1	9.89	6.14	17.99	8.11	4.85	14.24
1.2	7.99	4.90	13.89	6.57	4.22	11.84
2.1	8.86	5.07	10.03	7.57	5.51	14.39
2.2	7.80	4.33	11.90	6.57	4.54	12.82

pixel as calculated by the rectification algorithm throughout time for each subsequent frame. The red line indicates the above described trend line after signal smoothing with a Savitzky Golay filter. The signal noise variable is indicated by subtracting these signals from each other. As More extreme deviations are arguably a larger contributor to the signal instability, the root mean squared error is calculated as a quantification. However, as the settings of the signal filtering that is chosen are arbitrary, three different filters are used and the above mentioned rmse is averaged. The average rmse is calculated for the 9 predetermined coordinates for every dataset. Subsequently, the 9 rmses are averaged to give a single stability indicator for every dataset. Five of the nine values are portrayed by table 6. The table shows that according to the predetermined indicator, dataset 2.2 has the most stable images while dataset 1.1 is the noisiest. It is also shown that after rectification, the datasets during the first day of measuring have a relatively more stable signal for positive Y coordinate values (points on the left side of video) whilst for the second day it is the other way around. This seems to

be the case for both locations closer to shore and location farther offshore.

4.2.6 Optical Signal

After the frames have been rectified and compiled into a specific grid, the pixel intensity signal of specific areas and coordinates can be analyzed. As the pixels are supposed to portray the actual wave field, their intensities and standard deviations give an indication of the signal strength.

Figure 51 shows the mean values of the pixel intensity of a specific cross section ($Y = -1$ m) for datasets 1.1 trough to 2.2. Furthermore, figure 52 gives an overview of the mean values for the entire grid in dataset 1.1.

It is shown that datasets 1.1 and 2.1, which were surveyed with a similar layout (see section 4.1), have the lowest values especially when analyzing areas farther offshore. However, when taken into account that the survey on day two has relatively lighter pixels closer to shore, its pixel intensity interval over the X-axis is narrower. Datasets 1.2 and 2.2 seem to have a similar signal intensity,

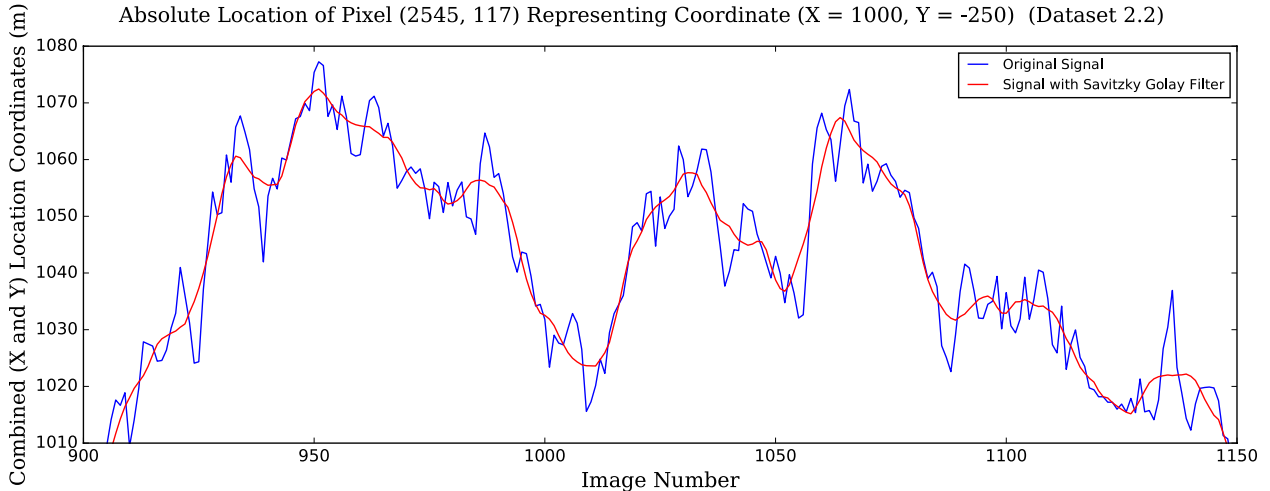


Figure 50: Rectified Signal Filtering

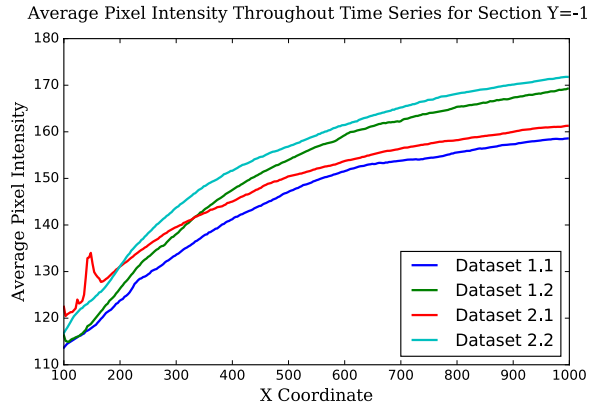


Figure 51: Average Pixel Intensity of Datasets in Section $Y = -1$

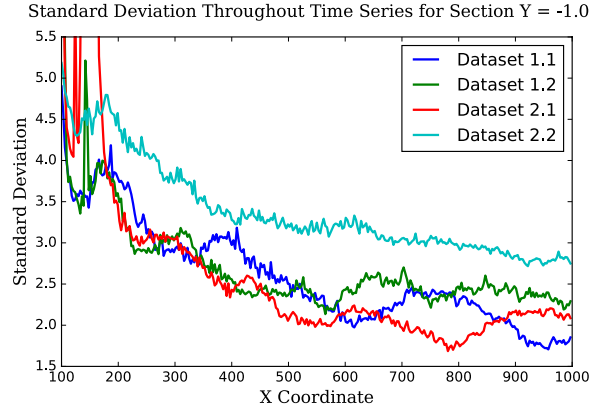


Figure 53: Standard Deviation of Pixel Intensities for Datasets in Section $Y = -1$

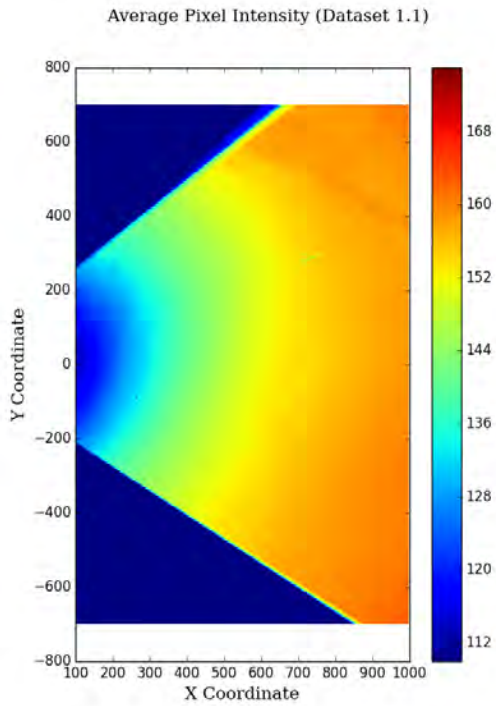


Figure 52: Average Pixel Intensity Throughout Dataset 1.1

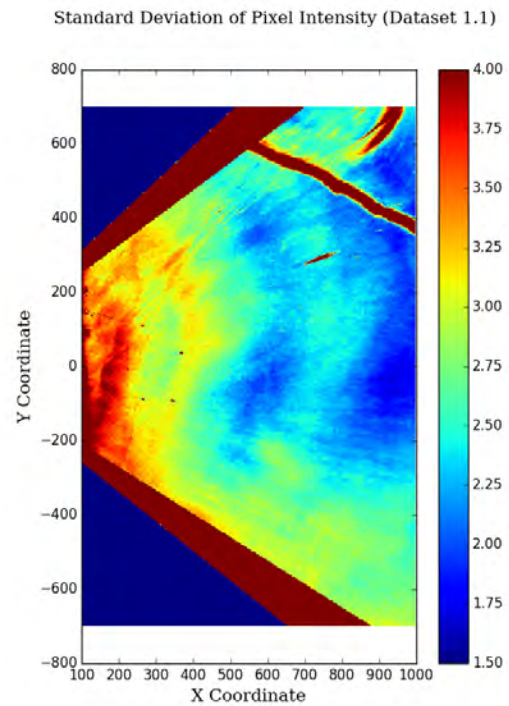


Figure 54: Standard Deviation Pixel Intensity Throughout Dataset 1.1

while being shifted by about a value of 5 throughout the section. Regarding figure 51, the relatively high values in the bank area around X coordinate 150 for dataset 2.1 clearly indicate waves breaking as is also shown in figure 41. As breaking creates white foam for a couple of second at a time, the average gray scale pixel intensity of the location significantly increases. When looking at figure 52, the only deviations in terms of variance can be found in the upper right corner of the projection. Because it is darker then the sea surface, the blue spot indicates the position of the buoy close to the Scheveningen breakwater. On the other hand, as a foam trail of a sailing ship midway through the measurement has lighter pixels then the sea surface, a straight darker orange line can be detected around coordinate (900, 400).

In a similar way, figure 53 shows the standard deviation of pixel intensities for all the datasets at cross section $Y = -1$. Subsequently, figure 54 displays the standard deviation throughout the recording time for every coordinate in dataset 1.1. The general trends is a decrease in standard deviation when analyzing coordinates increasingly farther offshore. This decrease in variance might make wave motions undetectable by the cBathy algorithm. In figure 54, is it shown that although standard deviations seem higher closer to shore than offshore, just as was displayed by figure 53, the differences are not as uniformly distributed as the average pixel intensity. Furthermore, relatively close to the beach, the 4 floating ground control points are shown by dark red dots. Farther offshore in the top right corner of the image, the same buoy and ship trail as in the average pixel intensity plot are indicated by a dark red color. Also, the bend line indicated by a dark red color around coordinate (900, 600) is created by a ship that started moving during the recording of the video.

4.3 Depth Inversion through cBathy Algorithm

Once the data is prepared and saved in a specific way, the cBathy algorithm will analyze the waves which are in field of view and subsequently calculate water depths at the specified coordinates.

Debugging In resemblance to the analyses as performed in part 4.2.6, before computing a bathymetry, the cBathy algorithm can be used in debugging mode to analyze in input data. To determine whether the cBathy algorithm actually recognizes the different waves in the datasetst, a spectral analysis is

performed. A wave field consists of several different wave frequencies of which the signals are assimilated into 1 signal representing the water level signal. In debugging mode, the cBathy algorithm analyses the full length of the dataset and tries to identify the different wave frequencies through a Fourier transform. Images are shown that indicate the phase map of a specific frequency over the entire domain. The wave peaks are indicated by a yellow color and the wave trough by a blue color. If the user can observe a wave field for a specific frequency, it means that the input data actually consists of a wave component in the specific frequency. When comparing the different datasets, it was found that, as common to the dutch wave climate, wave lengths ranged between 3 and 12 seconds. For the analysis of waves in between 1/12 and 1/3 hertz, wave fronts were visually detected. However, it should be noted that not all datasets consisted of equally prevalent and obvious patterns. Figure 55 shows the identified waves phases in dataset 1.1 based on a frequency of 0.167 hertz. Subsequently in figure 56, for the same dataset the 0.0833 hertz frequency is shown. The figure shows a less pronounced pattern. Again, in the top right corner, signal interference is observed caused by a ship calling the Scheveningen harbor. The ship clearly causes distortions which make the frequency undetectable by the Fourier transform. For all of the datasets, the 0.167 Hz wave frequency showed clear phase maps which means that 6 second waves were consistently present in the acquired data.

4.3.1 Base Scenario

As the signal analysis shows that there should be a signal for the cBathy algorithm to analyze, the cBathy settings toolbox is elaborated. The toolbox enables the user to tweak some of its waves field analysis parameters. Therefore, together with the previously mentioned 3 by 3 meters rectified grid and 2 Hz image frequency, also for the last step, some standard parameters were used to benchmark preliminary results.

Firstly, the domain spacing for analysis was 10 meters in the X (cross shore) direction and 20 meters in the Y (long shore) direction. These parameters indicate that for the analysis of one specific coordinate, the data within a tile of 10 by 20 meters is used. The area to be analyzed was arbitrarily chosen to be 900 meters in cross shore direction and 1400 meters in long shore direction, so that it would significantly overlap the reference measurement. Furthermore, the minimum number of k-k

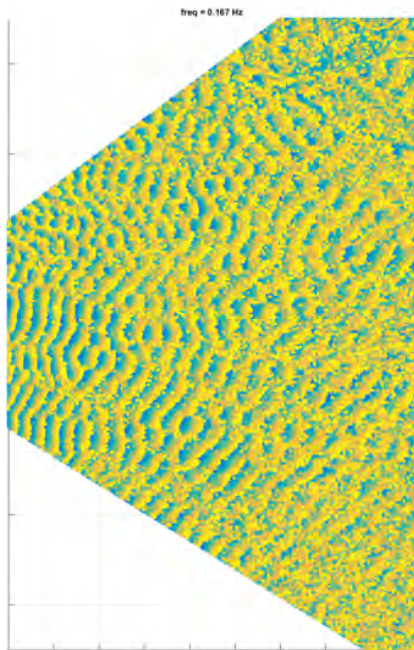


Figure 55: Wave Phase Analysis at 0.167 Hz for Dataset 1.1

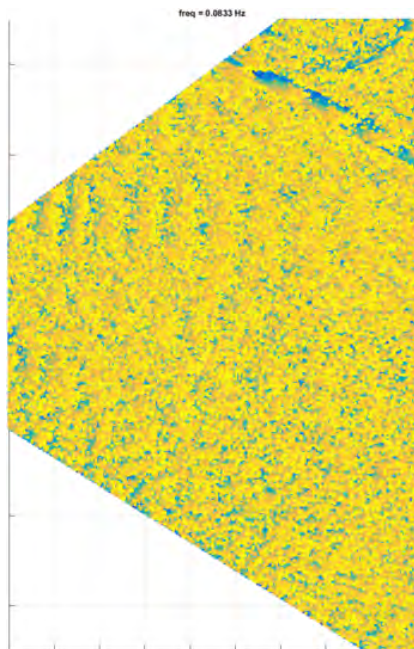


Figure 56: Wave Phase Analysis at 0.0833 Hz for Dataset 1.1

pairs for bathymetry estimation was set at 4. Furthermore, the smoothing length scales were chosen to be three meters (1 time the spatial scale of the input data) in the x direction and three meters in the y direction. Subsequently, the increase in tomographic smoothing parameter mean that the area of the tile from which a specific depth is analyzed increases when taking coordinates farther offshore. This is indicated by the Kappa parameter and is kept as small as possible (1.01) for the base settings. The algorithm was set to allow brute force decimation to be able to speed up the analyzing process and the maximum number of pixels per tile that was used was 80. The frequencies to be analyzed that were used represented the frequencies common to the relatively sheltered North Sea in front of the coast of the Netherlands from 3 second waves to 12 second waves. The number of frequencies to research was kept at 4, as increasing this number generally does not decrease the error and increases the computation time.

4.3.2 First Results

After the entire above mentioned process was completed, first results were found (see figure 57). The first subplot shows the water depths as calculated by the drone imagery. The second part indicates the water depths as measured by jetksi echo sounder. To give visual support, the perimeter of the reference measurements are indicated by a white line in the first subplot. Qualitatively, the measurements show similar results. Subsequently, the third subplot shows the quantitative difference between the first two subplots (drone measurements - reference measurements). It indicates a white color for areas where the difference between the two measurements ranges between -0.30 m and 0.30 m. From this image it can be distracted that for a large part of the analyzed area the drone images compute water depths which are larger then the reference measurement and therefore overestimates the water depth. Furthermore, in the bottom corner of the image a red colored area seems persistent. This indicates that there seems to be a skewness in the error signal at coordinate $X = 600$ ranging from an overestimation where Y is approximately -200 to an underestimation where Y is approximately 200 .

The algorithm calculated a water depth for a large part of the grid that was used as input. However, especially in the two sharp corners of the trapezoidal projection, cBathy's internal quality parameters were not sufficient and therefore no data was plotted.

To quantify these findings, a verifying area was determined over which 4 different quality indicators were calculated. Firstly the root mean squared error (rmse) computes the difference between the bathymetry as calculated by the drone imagery and the reference bathymetry after which the average is taken. For rmse computations, coordinates with a higher deviation from the reference measurement are given a higher weight than coordinates that more accurately represent the real water depth. In this way, differences in bathymetry accuracy are quantified in a more extreme manner. Furthermore, to be able to correct for water depth, the relative root mean squared error (rrmse) divides the root mean squared error by the average water depth over the specific area, as accuracies in shallower water might at first sight seem better than offshore. Also, as an indicator whether the water depth is over or underestimated in a certain area, the mean error is given. Thereafter, a standard deviation is calculated which generally shows the noise in the error from point to point. Whereas the standard deviation is reviewed, it is not shown in the figures.

As reference measurements stopped around 600 meters offshore, the Y limit of the total verify-

ing area was automatically accounted for. The X limits of the verifying area were distinguished as the width of the base of the projected trapezoid (ranging from approximately $Y = -200$ until $Y = 200$), which changes a little for the different datasets. This was chosen because when mapping the bathymetry of an area that covers a long stretch of coast, datasets would be taken subsequently and with the base side by side to be able to have a comprehensive map without gaps between the different recording. Therefore, the base of the trapezoid would be the bottleneck. In this scenario, the oblique part of the projection will always have an overlap with the next measurement. After the error of the total area was quantified, three more specific sub-areas were indicated (see figure 57, subplot 3) to give a better overview in which regions of the induced bathymetry errors will in/decrease and in what way. The first area was specified as the first 200 meters offshore in the Y direction with the width of the base of the projection in the X direction. This area is supposed to identify the general bank-area.

First results show that there is a discrepancy in the computed water depths farther offshore between coordinates that were captured by the left

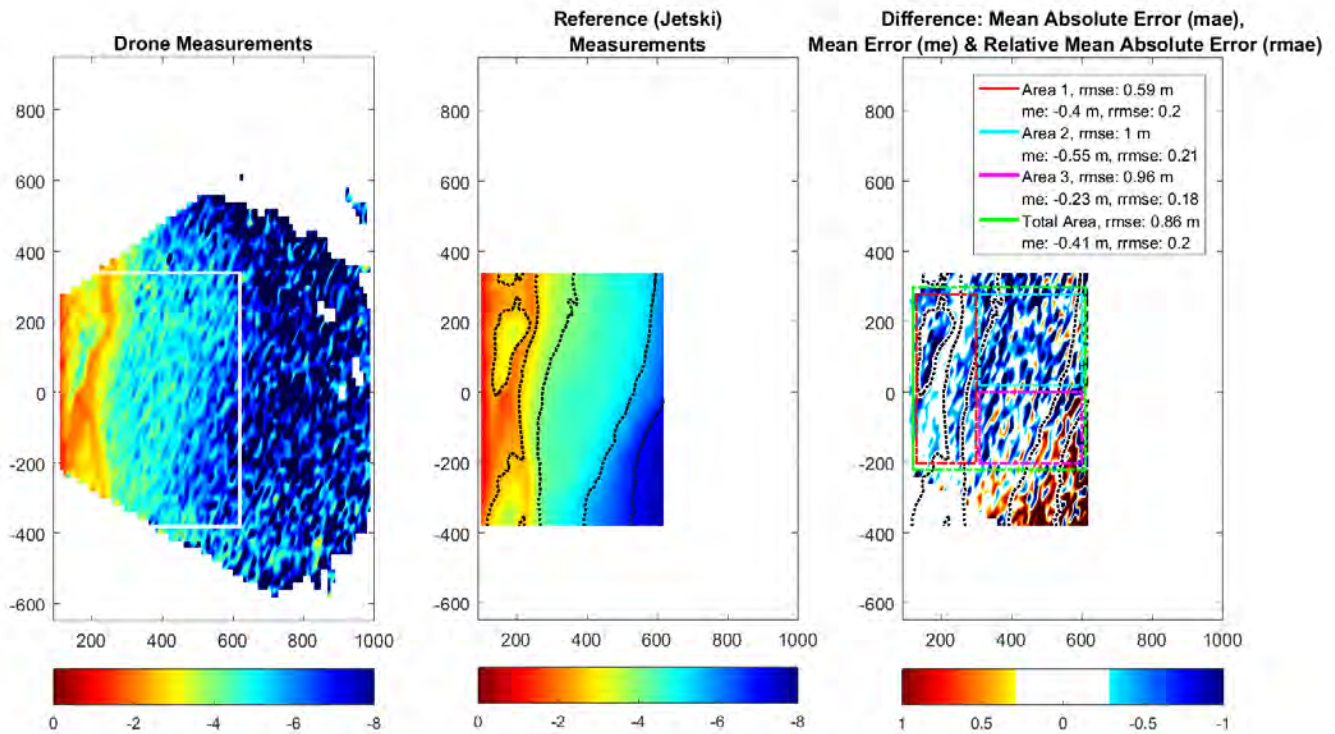


Figure 57: Result of Base Scenario for Dataset 1.1

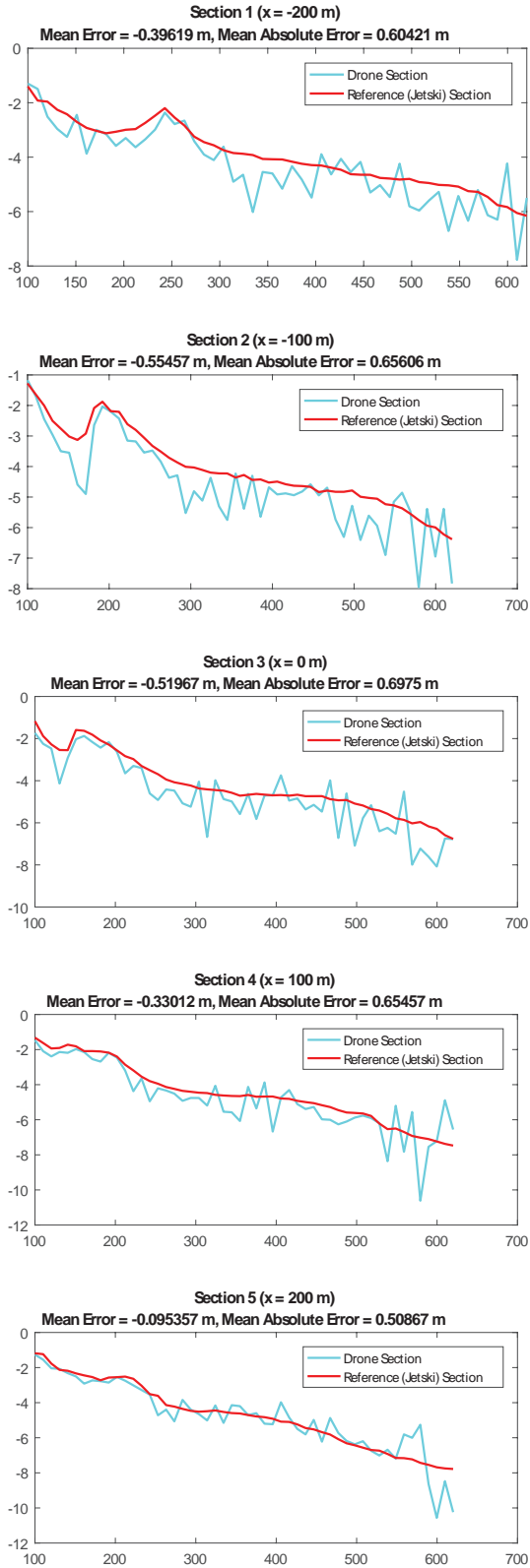


Figure 58: Cross Sections of Results with Base Settings for Dataset 1.1

side of the video and coordinated captured by the right side of the video. Therefore, the area farther offshore from the previously indicated bank area was split by the $Y = 0$ coordinate line. The other Y limit of these areas was once again indicated by the width of the trapezoids base. The areas are located in the far left and far right of the camera image respectively. In this way, inconsistencies between the quantified quality parameters in the Y direction of the data can be analyzed.

Figure 58 shows 5 cross shore transacts which are spaced every 100 meter between -200 and 200 in the alongshore. It shows that although the morphological elements of the coastal systems are computed relatively accurately, there is still a large amount of noise in the computed signal. This can probably be attributed to the use of low tomographic smoothing parameters in this base scenario. Furthermore, similar to observations regarding figure 57, relative to the reference transacts, the water depth in the sections seems to increase from the left to the right part of the captured image. Especially in areas farther offshore more variance in the water depths as computed by cBathy is found. Also the transacts show that contrary to the findings of Wengrove et al. (2013), the cBathy calculations are generally deeper than the reference measurements. Where in the third subplot, figure 57 indicates a 60 cm error window in white, it can be noticed that while large parts of the bathymetry seem to be in the 60 cm range, there are no large continuous areas with this low margin of error. This is also shown in the sections plotted in figure 58, where the drone measurements show a noisy signal. It is estimated that an increase in the tomographic smoothing will at least partly reduce the noise in the signal.

Table 7: Accuracy of Total Area using Base Scenario

Data set	rmse (m)	rrmse (m/m)	me (m)	Std Dv
1.1	0.86	0.20	-0.41	0.76
1.2	0.96	0.22	0.08	0.96
2.1	1.30	0.30	0.64	1.1
2.2	1.00	0.24	-0.07	1.0

In the top right part of subplot three in figure 57, a quantification of the water depth accuracy is found. As shown in figure, the root mean squared error of the first dataset with above mentioned base settings was found to be 0.86 meter. For the other three comparable datasets, the errors of the total

Table 8: Accuracy of Area 1, 2 and 3 using Base Scenario

Data set	Area 1				Area 2				Area 3			
	rmse (m)	rrmse (m/m)	me (m)	Std Dv	rmse (m)	rrmse (m/m)	ME (m)	Std Dv	rmse (m)	rrmse (m/m)	me (m)	Std Dv
1.1	0.59	0.20	-0.40	0.42	1.00	0.21	-0.55	0.85	0.96	0.18	-0.23	0.93
1.2	0.71	0.22	-0.26	0.66	0.95	0.20	-0.35	0.88	1.20	0.22	0.85	0.85
2.1	0.74	0.25	0.05	0.74	0.70	0.15	0.00	0.74	1.90	0.34	1.60	1.10
2.2	0.76	0.26	-0.37	0.67	1.10	0.23	-0.48	1.0	1.20	0.23	0.65	1.10

area are shown in table 7 and the errors of the sub-areas are shown in table 8. The table shows that dataset 1.1 generates the best results. Followed by datasets 1.2 and 2.2 which share similar results. The highest errors can be found for bathymetries which is inverted using dataset 2.1.

4.4 Fine Tuning cBathy Settings

As efforts have yet to be made with respect to optimization of the settings of the cBathy algorithm, it is assumed that this is the most obvious potential accuracy booster at this stage. Therefore, the following part of the report elaborates on the endeavor to increase the accuracy of the computed bathymetry when altering the settings. In sequence, settings are adjusted and compared to the base results. This analysis is done to find the optimal cBathy settings for future UAV bathymetry mapping.

Spacing for Analysis Points In the base scenario, the cross and alongshore spacing of the analysis points were respectively 10 and 20 meters. To analyze the influence of this parameter on the eventual water depth accuracy, changing the spacing from (10, 20) to (10, 10) yielded significantly different results. For dataset 1.1, on the total area, the root mean squared error increased by almost 40 centimeters which was especially attributed to the increase in error for area 3. As different areas yielded different changes in RMSE, the results did not have a clear difference in accuracy over the total area. As these particular settings are not extensively researched, further investigations are needed.

Analyzed Wave Frequencies Although the debugging mode showed that the frequencies between wave periods of 3 and 12 seconds seemed to accurately portray the North Sea’s wave climate, to be comprehensive a larger wave spectrum is analyzed in one of the fine tuning tests. After analyzing the

same input data on wave periods between 2 and 18 seconds, results show that whilst the mean error seems to decrease with 8 mm, the root mean squared error increases by 1 mm for dataset 1.1. On the other hand, for datasets 1.2 the opposite seems the case. Where the mean error is larger for the broader spectrum, the rmse decreases from .96 to .88 m.

For dataset 2.1, every area performed marginally worse. Furthermore, when taken the total area into account, dataset 2.2 reacts the same to the changed frequencies as dataset 1.1. However, when taken the smaller areas into account, analyzing a broader wave climate seems to yield better results for area 3 whereas the results are worse for area 2.

It should be noted that the different specified areas react differently to the changes in analyzed wave frequencies. Also, differences have been established between datasets that were recorded less than half an hour after each other and therefore a significant change in wave climate is not assumed. Hence, it can be concluded that increasing the wave frequencies to a broader domain does influence the results quite significantly. However, the results seem ambiguous as they differ from area to area.

Tomographic Domain Smoothing A parameter that can decrease the error in the computed bathymetry for some datasets is the tomographic domain smoothing. Essentially determined as the desired spatial resolution of the bathymetry, the Lx and Ly parameters in the base scenario are specified as 1 time the spacing for analysis points (dxm & dym). As the grid of the analysis points has length scales of 10 by 20 meters in the cross and longshore, this means that the smoothing length for selecting the subset of pixels to influence the analysis for a specific point is 10 by 20 meters. One could imagine that this is rather small as wave lengths are in the order of magnitude of approximately 30 to 100 meters at a water depth of 8 meters.

Therefore, the cBathy algorithm was ran again

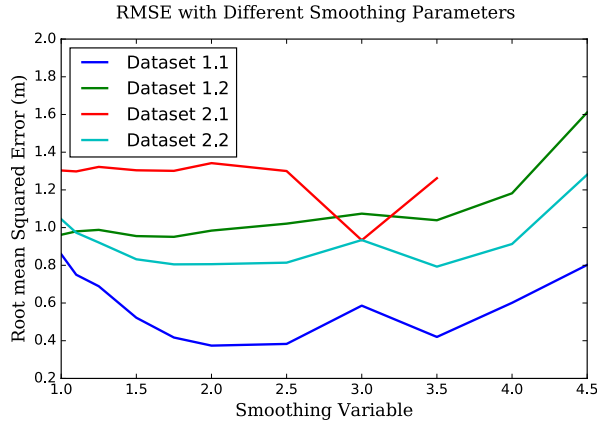


Figure 59: Total Area RMSE for Different Tomographic Domain Smoothing Parameters

with increased spatial smoothing scales. Values between 1 and 4 times the analysis grid size (10 to 40 meters in cross shore direction and 20 to 80 meters in long shore direction) were used. Figure 59 shows the total de/increase in root mean squared error for the total areas of the different datasets when altering the tomographic domain smoothing variable. The rmse for dataset 1.1 decreases the most to 0.37 for a smoothing factor of 2.0 times length scales of the analysis points. It should be noted that for dataset 2.1 when using the smoothing parameter value of 4 and 4.5, the internal quality control values of the algorithm were not met for large part of the mapped bathymetry. Therefore, no data was plotted. The figure shows that apart from deviations for a smoothing variable of three times the grid size (30m in X direction and 60m in Y direction), datasets 1.1 and 2.2 increase in water depth accuracy with an optimum for values around 2 and 2.5 times the grid size. On the other hand, datasets 1.2 and 2.1 do not seem to differ as promisingly. Therefore, it can be concluded that for some reason, these datasets are less tuneable. Also when increasing the smoothing parameter, visually the morphology seemed less rippled than when using the values of the base result. This can be attributed to a more similar water depth when including neighboring coordinates as the overlap in analyzed wave fields is larger.

Figure 61 shows the bathymetry as calculated by the cBathy algorithm when using a smoothing value of 4.5 times the grids size (so 40 meters in the cross shore for this scenario). It clearly shows that there are some unrealistically shallow areas farther offshore. Also the bathymetry in the fore-

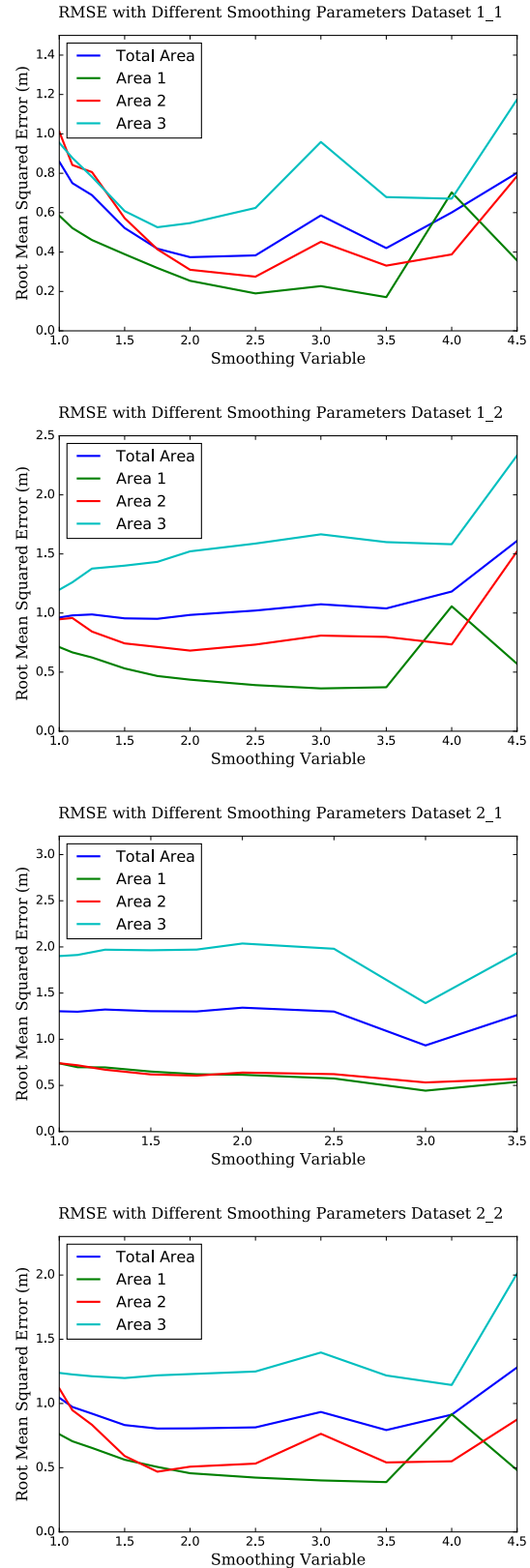


Figure 60: RMSE per Area for Different Smoothing Parameters for all Datasets

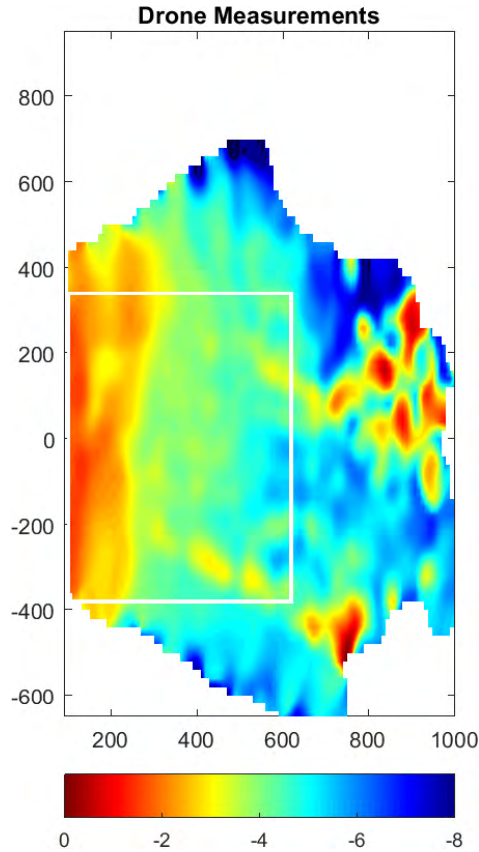


Figure 61: Bathymetry Dataset 1.1 (Smoothing = 4.5)

shore seems less pronounced. This can also be observed from the error in area 1 in subplot 1 of figure 60. When using an area of analysis which is too large, wave celerities close to the shore and wave celerities far offshore are combined into a water depth yielding very similar (blurry) water depths throughout the area of interest. Also the edges of the input data seem to include some sort of computational error yielding unrealistically shallow areas far offshore.

To analyze the influence of the domain smoothing parameters on the different sub areas, figure 60 shows the rmse for the individual areas for each dataset. From this figure it can be taken that smoothing parameters of three and higher generally yield more ambiguous and therefore unpredictable results. Also, as can be distracted from the steep red line in dataset 1.1 and 2.2, for a smoothing variable increasing from 1 to 2.5, especially area 2 gets increasingly accurate. When regarding area 2 and 3, the increasing accuracy can be attributed to a decrease in the observed ripples that are more evident farther offshore. The increasing smooth-

ing parameters filters the ripples ending up with a more accurate water depth for these locations.

Kappa Variable Similar to the tomographic domain smoothing variable, the kappa variable increases smoothing. However, the difference is that the kappa variable increases the smoothing when taking analysis points increasingly farther offshore.

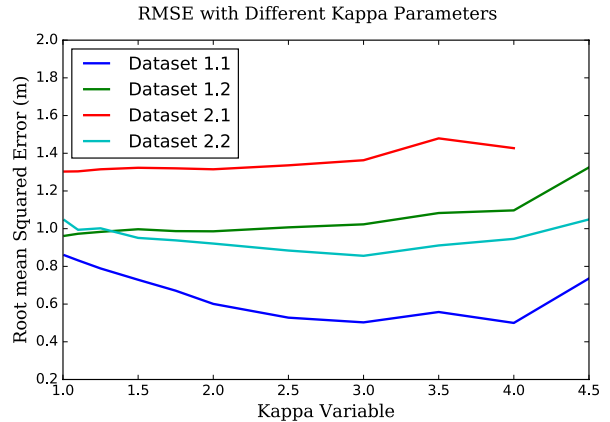


Figure 62: Total Area RMSE for Different Kappa Parameters

Like the previous section, the cBathy algorithm was ran with the exact settings as used in the base scenario but with a differing kappa parameter. Figure 62 shows the results of changing the kappa parameter for the 4 different datasets. Again, for dataset 2.1, not every kappa variable yielded results due to not passing the internal quality control of cBathy. In general increasing kappa shows similar results as changing the smoothing variable. Dataset 1.1 increases in accuracy for a kappa value increasing until around 3. Although less significant, also dataset 2.2 shows a slight improved performance in the same region. Furthermore like the section above, the other two datasets show no increase in performance and for kappa values higher than three the results seem less predictable. It should be noted that altering the kappa values yield less of an improvement in accuracy when compared to changing the smoothing variable for the total area of interest.

Subsequently, figure 63 shows the depth error in the different areas for the datasets when changing the kappa parameter. From this figure it can be concluded that of the above mentioned tuneable datasets (1.1 and 2.2), especially area 2 seems to increase in accuracy. As farther offshore the smoothing increases, for area 2 (and 3) it is really similar to

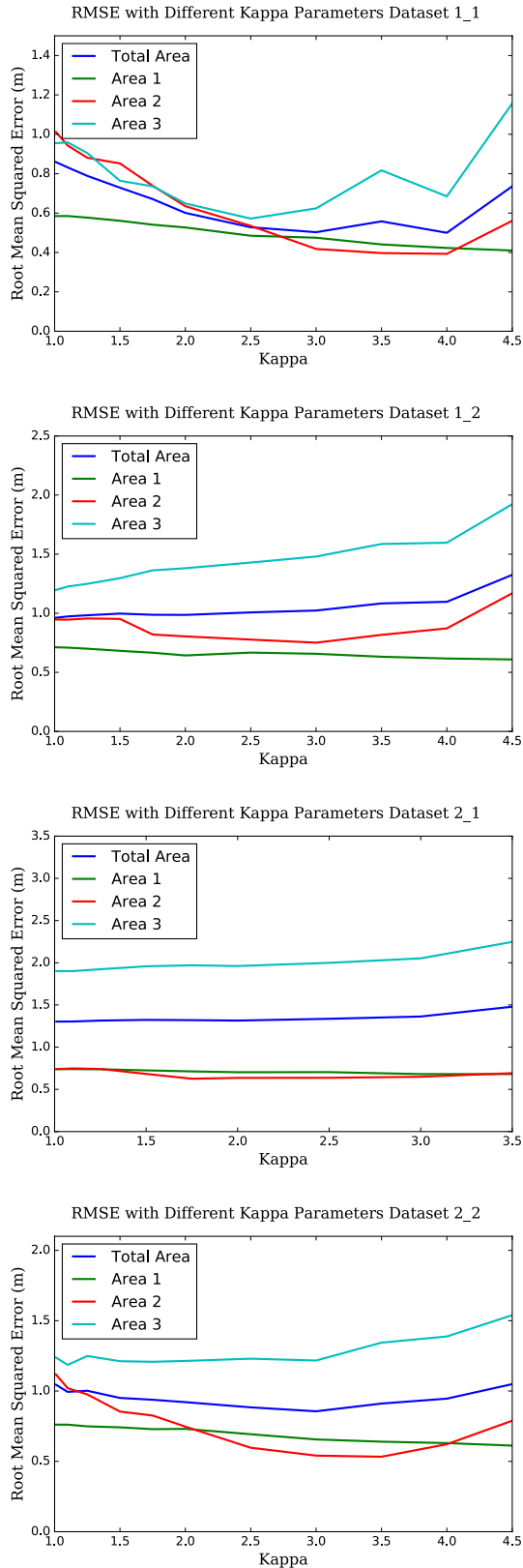


Figure 63: RMSE per Area for Different Kappa Parameters for all Datasets

the scenarios with an overall increased smoothing variable as shown in figure 60 which also showed an increase in performance. Furthermore, the relatively straight green lines for area 1 are probably a result of the smoothing not increasing enough that close to the shore to be able to increase accuracy. Also remarkable are the straight lines for every area in dataset 2.1. It does not seem to matter which value for kappa to use for the accuracy of any area in datasets 2.1 and 1.2.

Visually, from figure 64 it can be noted that, just like in figure 61, increasing the kappa value too much yields strange results farther offshore. It indicates unrealistically shallow areas around $X = 800$. It seems that, just like what was shown in figure 62, increasing the kappa value too much makes the calculations prone to error and even unstable.

When comparing the results from the smoothing analysis with the results from the kappa value analysis, it seems that for well performing datasets, all sub areas are benefited by increasing smoothing. Subsequently, it is shown that for these drone datasets a low or high smoothing value yields worse results than an intermediate one (an analysis area of around 20 to 25 meters in cross shore direction). Therefore, using a large Kappa value does not yield good results. Because, on the one end of the bathymetry (close to shore) it is using a smoothing value that is too low, whilst on the other end (farther offshore) it is using a smoothing value that is too large. Therefore, generally results are worse than using a standard (optimized) smoothing value for the complete dataset.

Optimizing the Smoothing Parameter in Combination with the Kappa Value

The previous paragraphs elaborated on the optimum values for the smoothing parameter and the kappa parameter. From the plotted transects in the results section it can be argued that the coordinates farther offshore are more prone to ripples. As above it is described that too much smoothing results in unstable bathymetries, the smoothing variable used to analyze the kappa value is a little bit on the low end of the optimum as described above. Therefore, for a smoothing variable of 1.75 by 1.75 and 2.00 by 2.00 (so 17.5 m by 35 m and 20 m by 40 m) the Kappa parameter is increased and the root mean squared error is shown in figure 65. The figure shows that increasing the Kappa value does not seem to yield smaller errors. Therefore, from the datasets of this research it can be argued that the recommended value for drone footage is a smoothing value of 2.00 times the spacing for the analysis

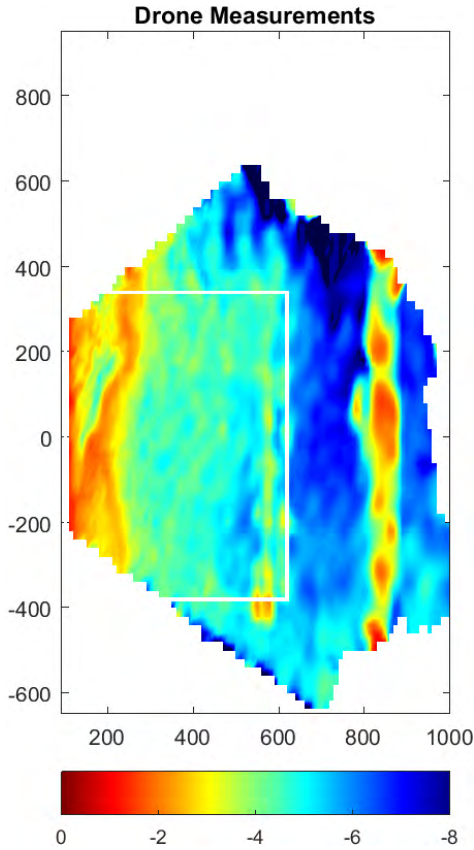


Figure 64: Bathymetry Dataset 1.1 (Kappa = 4.5)

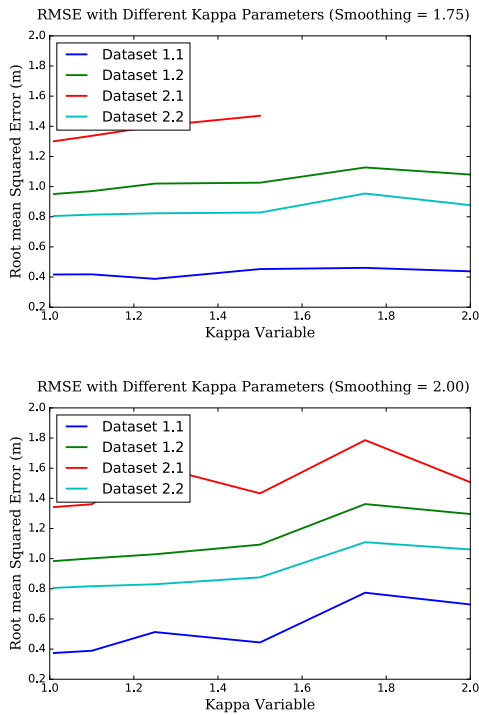


Figure 65: RMSE Total Area for Different Kappa Parameters for all Datasets

points. In this case, the smoothing length scales are 20 meters in the cross shore direction and 40 meters in the alongshore direction. Furthermore it is recommended to keep the Kappa value low (in this case 1.01).

Decimation To compute a large quantity of analyses, in the base scenario brute force decimation was used to speed up to process. During fine tuning, after disabling decimation some of the errors were observed to decrease by tenths of millimeters. As at this point the errors were still in the region of half a meter or even 1.5 meters, the alteration of the decimation parameter is not considered to have a significant influence on the final results for these particular datasets.

95% Confidence Interval After the computation of a water depth on a specific point, the cBathy algorithm also indicates its own quality parameter. Based on the analysis of the input data a 95% confidence interval is calculated. Figure 66 and 67 indicate a large confidence interval of more than 1 meter for basically the whole area in datasets 1.1 and 2.1. Subsequently, when increasing the smoothing parameter, the cBathy algorithm has indicated a higher quality parameters throughout the datasets. Figure 68 and 69 only show a high value for the 95% confidence interval for areas offshore. In previous sections it is shown that the bathymetry error is significantly lower for dataset 1.1 when using smoothing parameters of 2.50. However, it also shows an increase in error for dataset 2.1. It would be assumed that as the error especially increases in the areas with Y values lower than 0, also the confidence interval would increase.

The same discrepancy between water depth error and confidence interval is seen for dataset 1.2 and although less significant in dataset 2.2. The algorithm indicates that sufficient hydrodynamics movements have been captured by the dataset and therefore it is able to compute a bathymetry. However, it either has not enough information, or is unable to identify the most important wave frequencies.

Another striking feature is that the algorithm has more confidence in the offshore regions where it is performing worse (with negative Y values) than in the regions with positive Y values. When taking a look at the dataset qualitatively, accordingly more waves can be detected in the region of area 3 than for the region of area 2. Although they are not displayed in this section, similar results are found

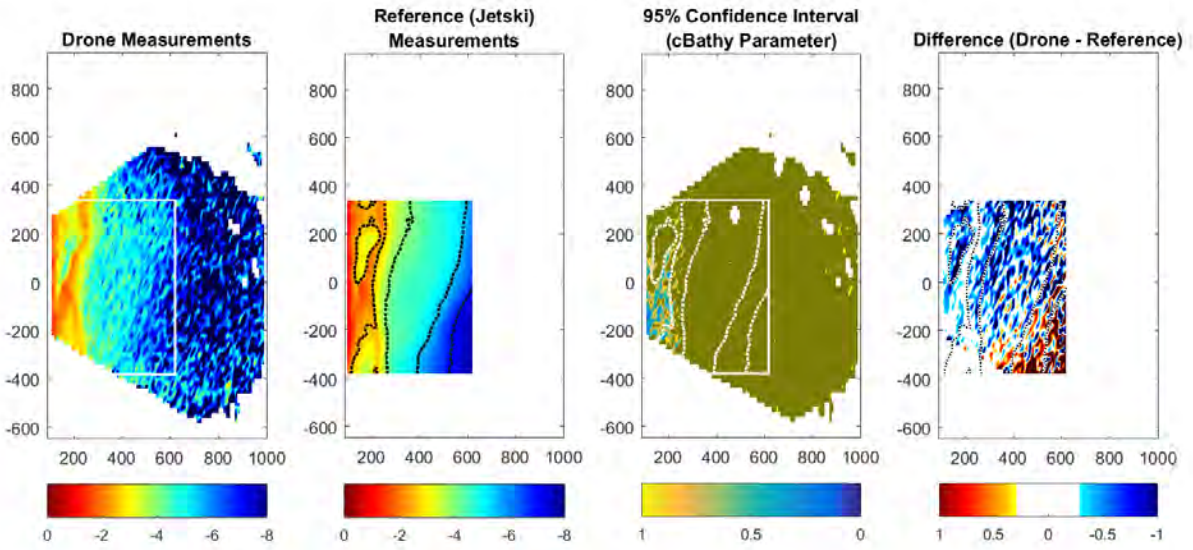


Figure 66: Bathymetry and Quality Parameters Dataset 1.1 (Smoothing Parameter: 1.00 by 1.00)

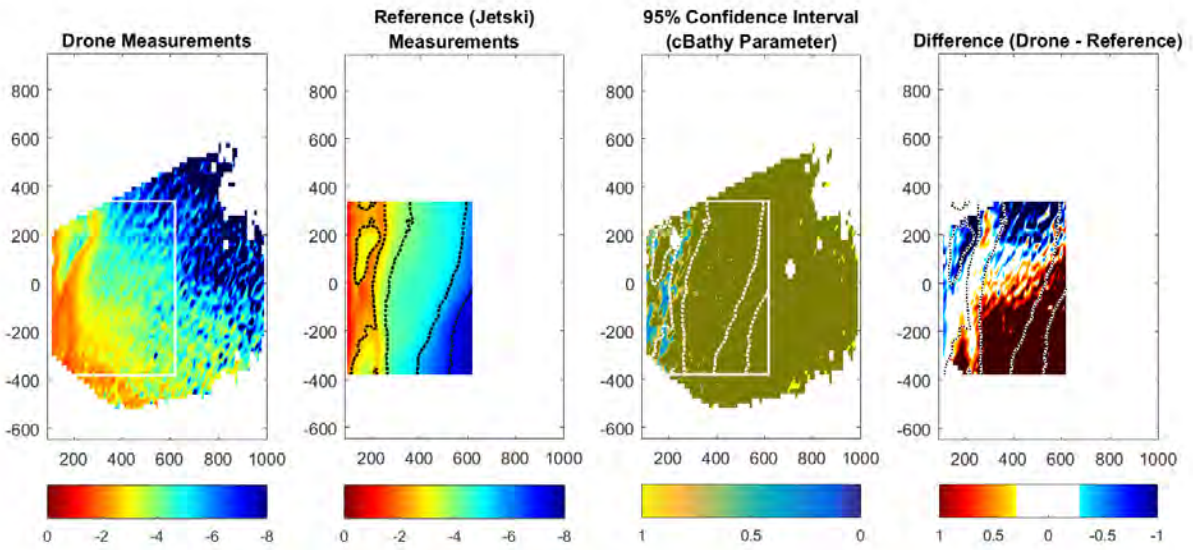


Figure 67: Bathymetry and Quality Parameters Dataset 2.1 (Smoothing Parameter: 1.00 by 1.00)

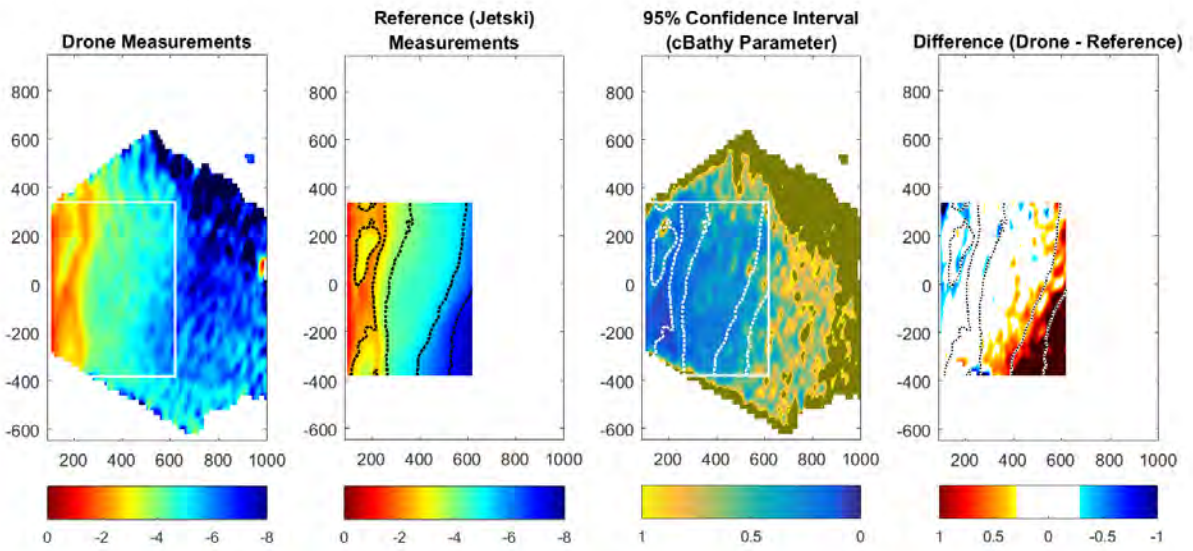


Figure 68: Bathymetry and Quality Parameters Dataset 1.1 (Smoothing Parameter: 2.50 by 2.50)

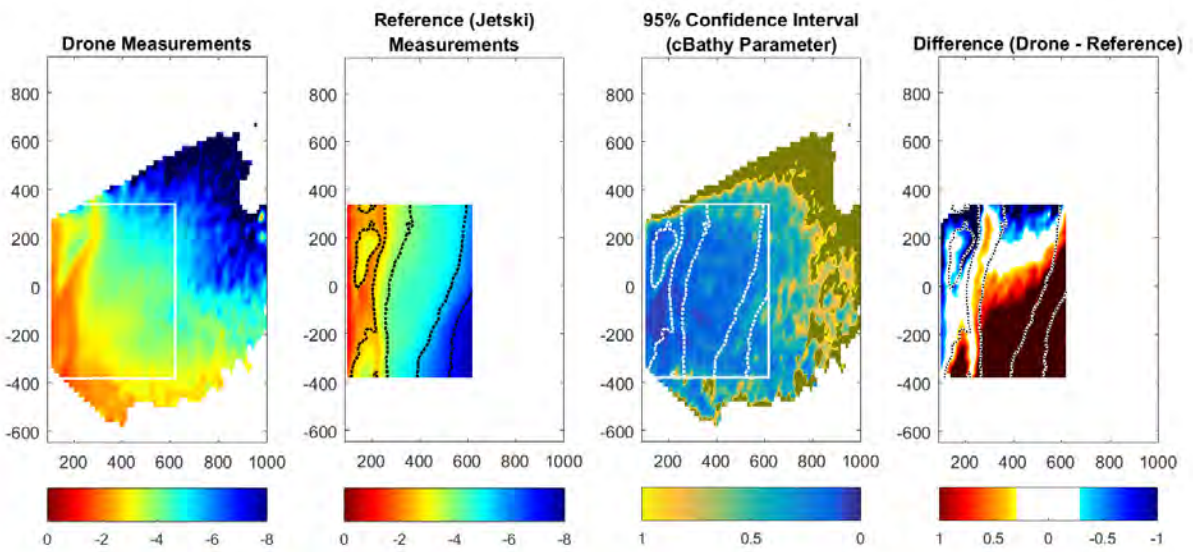


Figure 69: Bathymetry and Quality Parameters Dataset 2.1 (Smoothing Parameter: 2.50 by 2.50)

for dataset 1.2 and 2.2. Even though this seems to be the case, the areas are performing worse.

Conclusions cBathy Parameters Optimization The tests regarding the different settings for the cBathy algorithm show that for drone videos, the setup of the smoothing variable seems to be the most important. For these tests, smoothing variables of 2 to 2.5 yielded best results. Furthermore, from these tests it could be argued that the use of the kappa variable for increased smoothing increasingly offshore results in too little smoothing close to shore and too much smoothing far offshore (around 600 m or further). It can also be concluded that for some reason in areas on the right side of the recorded video, the significant underestimation in water depth of the cBathy algorithm is not shown in its 95% confidence interval.

4.5 Summary

The results of this report show that on one occasion, the accuracy of the inverted bathymetry is fairly accurate. With a root mean squared error of 0.37 meters, the best dataset accurately described the bottom as it is in the real world. Visually, the nearshore pattern shows similar features between the drone bathymetry and the jetski bathymetry.

However, for mapped water depths to be valuable for coastal monitoring purposes, it should be guaranteed that a certain accuracy is reached for every recording that is taken. These results show a large discrepancy between the accuracies of the different recordings and therefore cannot be used without a reference bathymetry. If the margin of error could be brought down to 0.20 meters, it could serve some coastal monitoring purposes. The following section of the report will more specifically go into the data that is used and tries to find explanations for the discrepancy between the accuracies.

5 Discussion

As the previous section showed a large discrepancy throughout the depth inversion accuracies between different datasets, this section searches for an explanation. At first, different parameters in the data preparation process are analyzed in terms of their impact on the eventual accuracy. Subsequently, further analyses are done regarding the wave signals that the cBathy algorithm is observing.

As shown in section 4, first results yield bathymetries for the four datasets. For these measurements, the layout was fairly similar. However, there are significant differences between the accuracy. As dataset 2.3 had a much different setup, also the discussion part of this report will focus on dataset 1.1, 1.2, 2.1 and 2.2. From these measurements, dataset 1.1 and 2.1 had a similar layout with two rows of ground control points (GCPs) located on the beach and a relatively larger portion of beach observable in the footage. However, as section 4 of this report indicates, dataset 1.1 is performing the best out of all 4 whilst dataset 2.1 is performing worst. Furthermore, similar to results as found by Wengrove et al. (2013), the cBathy algorithm seems to perform worse in deeper water than in the bank area. However, when looking at the root mean squared error divided by the water depth (rmse), table 8 shows that especially in area 2 the computed bottom for some datasets is more accurate than in area 1 (the shallow bank area). Subsequently, comparisons between mean error (me) in area 2 and 3 show a skewness in the bathymetry error. The datasets as observed in this research seem to underestimate water depth in area 2, whereas they overestimates the depth in area 3. The difference between the two areas is that the water in area 2 is generally shallower than in area 3, which is exaggerated by the cBathy algorithm. Also, the absolute rectification errors were found to be lower for the best performing dataset 1.1. The last possible accuracy explanation could be given by the longshore tidal current which was present during some of the recordings whilst being negligible during others.

As the accuracy of the bathymetry is important for research institutes as well as for governmental bodies, an indication will be given what part of the error can be contributed to which part of the depth inversion process. This section will discuss which parts of the inversion process as described in the methodology and results section can be tuned to yield better results. Afterwards, quantitative parameters regarding the intermediate steps are discussed on their potential impact on the end result.

First the rectification process is taken into account after which measurement setup is elaborated. Subsequently, the report focuses on analyzing the wave signal. Thereafter, the errors contributors will help give an indication on interesting topics to investigate in future research. Lastly, potential helpful drone depth inversion practices are elaborated.

5.1 Rectification Process Parameters

Apart from the settings in the cBathy algorithm as shown in the previous section of the report, also the implementation of the rectification process has a wide variety of different options. This section of the report elaborates the effect the rectification parameters have on the depth inversion effectiveness and tries to find an explanation for the differing inversion accuracies. It regards changing the grid size and frequency among other changing variables. As the changes of these variables are more time consuming than changing the cBathy settings, for most of the sampling alterations only dataset 1.1 is used with cBathy settings according to the base scenario.

Spatial Sampling A potential influential factor for the overall accuracy is the grid size used for input data. The base scenario used a grid of 3 meters by 3 meters in the cross and alongshore direction. Whereas decreasing the grid size, more information is available for analysis, the computation time gets exponentially longer. On the other hand, as the wave lengths are far longer than three meters, not a giant difference in accuracy is expected. The amount of points that need to be rectified and also analyzed by the algorithm increases by a factor 4 when decreasing the grid size by a factor 2. For this analyses grid with a spatial length of 6, 5, 4, 3 and 2 in both the cross as in the alongshore are used. Attempts to use a 1 by 1 meter grid failed due to a limitation in computing power.

Table 9 shows the results of the spatial resolution analysis for dataset 1.1. It shows that the difference between a grid size of 2, 3 or 4 meters does not change the outcome of the bathymetry in a clearly better way for either one. It does show that a 5 by 5 grid yields worse results whereas a 6 by 6 grid does not show any results whatsoever. From these results it can therefore be recommended to use a grid size of 4 by 4 or smaller, depending on available computing power and time.

Subsequently, the difference between grid sizes of 2 and 3 meters seems to yield different results for the offshore areas. A 2 by 2 grid in this dataset

Table 9: Depth Inversion Accuracy (RMSE) for Different Rectification Grid Sizes for Dataset 1.1

Grid Size	Total Area rmse (m)	Area 1 rmse (m)	Area 2 rmse (m)	Area 3 rmse (m)
2 by 2	0.88	0.59	0.94	1.10
3 by 3	0.86	0.59	1.00	0.96
4 by 4	0.90	0.61	0.98	1.10
5 by 5	1.00	0.65	1.00	1.4
6 by 6	_*	_*	_*	_*

*The cBathy algorithm was not able to map a complete bathymetry.

performs better in the area with positive Y values. On the other hand, the 3 by 3 grid performs better in the area with negative Y values. These discrepancies could probably be attributed to a better transfer of the wave signal from the recordings to the rectified grid data. However, the specifics are not yet understood.

Image Frequency As Argus station use a sampling frequency of 2 Hz, for the base scenario of this research the same rate was used. As the shortest wave analyzed in this research is 0.333 Hz, the refreshment rate is plenty to capture the full spectrum of the waves generates offshore. However, as the camera in Argus towers have a fixed direction and in the homography only has to adjust for the tide, the sampling is considered to be much steadier than the drone images. Therefore, one could argue that when using more images per second, there is more data to average and filter out the rectification instabilities and analyze hydrodynamic movements. Therefore, the same settings as for the base scenario have been used to compute a bathymetry with the only exception of using a sampling rate of 6 Hz instead of 2 Hz.

Table 10: Depth Inversion Accuracy (RMSE) for Different Image Frequencies for Dataset 1.1

Image Freq.	Total Area rmse (m)	Area 1 rmse (m)	Area 2 rmse (m)	Area 3 rmse (m)
2 Hz	0.86	0.59	1.00	0.96
6 Hz	0.81	0.60	0.92	0.91

The results are displayed in table 10. It shows that for the offshore areas, the root mean squared error decreases. This could be an indication that the cBathy algorithm is indeed able to the extra data to better estimate wave movements. The influence of the sampling rate is only researched quantitatively for 1 dataset. Therefore, the findings should be taken as an indication and further research is required.

Amount of GCPs Used As for practical purposes the use of less ground control points would be desirable, the minimum amount of 4 GCPs were used for the base scenario. However in dataset 1.1, 8 ground control points per image were automatically detected. Therefore, one could argue that using all of the points would yields a better and more stable rectification as the algorithm has more information to solve the homography.

Table 11: Depth Inversion Accuracy (RMSE) for Different Image Frequencies for Dataset 1.1

No of GCPs	Total Area rmse (m)	Area 1 rmse (m)	Area 2 rmse (m)	Area 3 rmse (m)
4	0.86	0.59	1.00	0.96
8	0.81	0.59	0.85	0.99

Table 11 shows the difference in rmse for the two situations. It shows that, similar to increasing the sampling frequency, the use of more ground control points overall yields better results. However, it should be noted that only in area 2 the error actually decreased.

Conclusions Whilst yielding similar gains, unlike the sampling rate, increasing the amount of ground control points does not significantly increase the computer processing time. However, it does make the efforts in the field more intensive. From experience, it could be argued that increasing the sampling rate would be the preferred when choosing between the two. This is because the reduction in computer processing time does not weight up to the reduction in measurement effort. However, it should be noted that for a large area increasing the image frequency might result in datasets that are too large for regular computers. In such a case, the computers random-access memory (RAM) seems to be the bottleneck.

Furthermore, whereas some of the rectification process parameters seem to yield better results, it should be noted that a specific explanation remains unknown. When altering one of the parameters in the early stages of the data preparation process, the errors (or decrease in errors) cascade down to the eventual depth inversion accuracy. Therefore, it is assumed that the data transfer is more effective for some of the above mentioned parameters. These findings give an indication on which parameters to review when trying to increase depth inversion accuracy.

5.2 Measurement Setup

Because there was a time constraint with respect to the amount of datasets that could be acquired on one day, limited tests were done in terms of drone location with respect to the area of interest. The methodology section of this report elaborates on advantages of different measuring setups in term of the viewing angle and drone position. In terms of rectification accuracy there seemed to be an indication that using an alongshore viewpoint (dataset 2.3) could potentially yield good results. However, as cBathy computations showed unusual results, this research focuses on finding the cause of the difference between the first 4 datasets. Furthermore, the other 4 measurements were taken in a similar fashion. The first datasets of each day had a location farther inland from the second dataset. These four dataset are not enough to make any significant conclusions in terms of the influence of the measurement setup on the bathymetry error. However, the fact that two similar scenarios yield such different results (dataset 1.1 and 2.1) indicate that it might not be the measuring setup that contributes to the largest part of the error.

5.3 Wave Signal

To give an indication of which parts of the UAV bathymetry mapping method can be contributed to which part of the error in the computed water depths, the above described analyses can be combined with an analysis of the detected wave signal. The following section elaborates on the detected wave frequencies and indicates whether the algorithm is able to use them in the water depth calculations. The signal is specifically analyzed on three individual locations, after which the entire area is taken into account. Furthermore, different cBathy internal quality parameters are investigated.

5.3.1 Signal Analysis for Specific Locations

In the first part of the signal analysis, the base dataset is elaborated. The analysis reviews wave signals as observed and modeled by the cBathy algorithm for some specific locations within the area of interest. Firstly, a section with coordinates in the center of the dataset is analyzed. An area of 25 by 25 meters around coordinate (0, 400) is indicated after which the cBathy algorithm will show the most dominant wave frequencies. As described in section 3.5.2, for these wave frequencies an observed wave field is shown for which the angle of incidence and the magnitude is analyzed. With these found values a wave field is modeled which should represent the observed wave field. If these images converge, it can be argued that the specific frequency is accurately detected. Furthermore, the skill value represents the amount of variance in the observed wave field that can be described by the modeled wave field. Therefore, it gives a good indication of the effectiveness of the analysis.

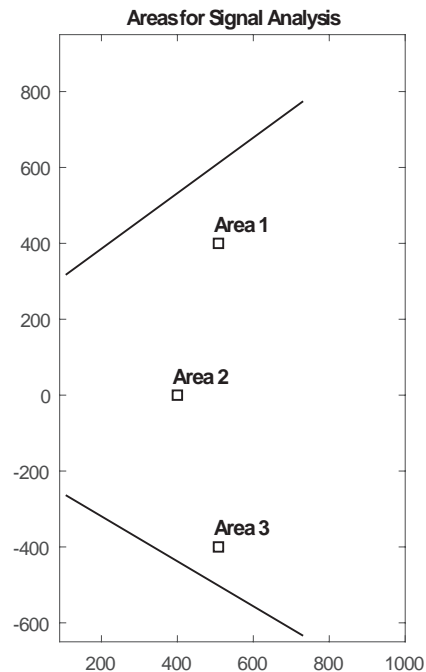


Figure 70: Three Areas at which Signal Analysis is Performed

Also areas around the (500, 400) coordinate and the, generally worse performing, (500, -400) coordinate the analysis is done. Figure 70 indicates the locations of the specific areas. At these locations, the algorithm indicates four different sub areas. As for all of these sub areas the 4 most dominant wave frequencies are denoted, a total of 16 overlapping

frequencies are analyzed. Four of these 16 frequencies (fB) for dataset 1.1 around coordinate (400, 0) are shown in table 12. The table also indicates analyzed parameters like the wave number (k), angle of incidence (a), skill value, temporary depth ($hTemp$) and the error in computed temporary depth ($hTempErr$). The skill parameter indicates how accurate the different wave frequencies describe the surface motions. As there seems to be a clear difference in performance when comparing area 2 with area 3, especially these two locations are compared in the following analysis.

It should be noted that throughout the datasets the wave front has a sharp angle with the coast. As the cBathy algorithm generally assumes waves to penetrate the coastal regions relatively perpendicular, the signal analysis should be able to indicate whether the correct wave estimations are made given the angle in these datasets.

Dataset 1.1 The coordinate in the center of the area of interest (area 2) gets elaborated first. Table 12 shows the dominant frequencies for 1 of the 4 sub areas in area 2. For 3 of the 4 sub areas, the algorithm indicates the 0.1233 Hz as the most important frequency. Thereafter the 0.2033, 0.1633 and 0.1833 Hz frequencies seem to be important. Figure 71 shows an example of a predicted wave phase corresponding to observed wave phase with a skill value of 0.92 (see table 12). Therefore, the wave is accurately analyzed. In area 2, the identified important frequencies seem appropriately consistent throughout all of the 4 sub areas. Namely, for all of the sub areas, the two most important frequencies were estimated to be either 0.1233, 0.2033 or in one case 0.1633.

When looking at area 3 (see 4 of the 16 frequencies in table 13), the amount of different frequencies identified as either the most or the second most important was larger (4). This could indicate that to the algorithm it is less clear which of the part of the wave spectrum is most important for depth inversion.

Furthermore, when regarding the area around coordinate (400, 0), the skill quality parameter indicates a value of 0.9 or above for most of the 16 wave frequencies, indicating that a large percentage of the variance can be explained by fitting the local phase data. On the other hand when looking at the skill value for coordinate (500, -400), for a part of the values it decreases to 0.8 or 0.7 even reaching 0.3 in 1 of the 16 occasions. Values under 0.5 are automatically dismissed and every value above 0.5 is considered to be good enough to use

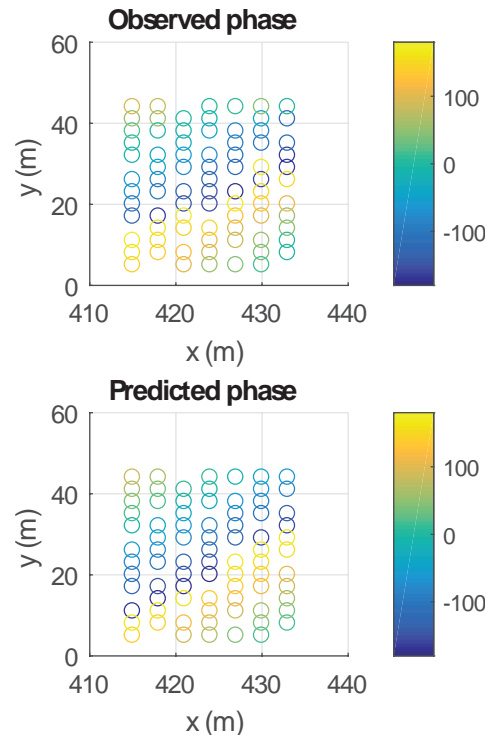


Figure 71: Phase Analysis 0.2033 Hz Dataset 1.1
Coordinate (400, 0) (see Freq 3 of table 12)

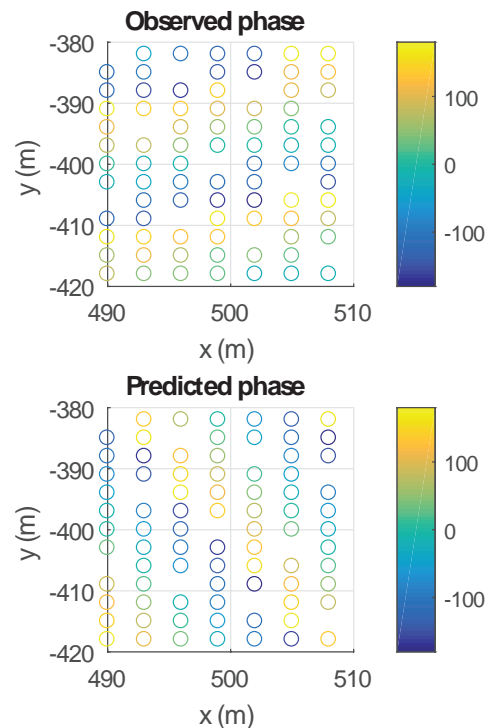


Figure 72: Phase Analysis 0.2633 Hz Dataset 1.1
Coordinate (500, -400) (see Freq 4 of table 13)

for depth estimation. Finally for the 0.2633 Hz wave frequency the algorithm is unable to accurately predict the phase. Figure 72 shows an image of the detected and the predicted wave front. When it tries to make a prediction, there seems to be a 70-90 degree angle between the actual wave front compared to the predicted wave front. In this case the skill value decreased to approximately -0.6 and is therefore dismissed.

Table 12: Debugging Values Dataset 1.1, coordinate (400, 0)

	Freq 1	Freq 2	Freq 3	Freq 4
fB (1/s)	.1633	.1233	.2033	.1833
k (1/m)	.1594	.1176	.1934	.1692
a (rad)	-.50	-.56	-.86	-.54
skill (-)	.9346	.9232	.9223	.9103
hTemp (m)	5.118	4.902	6.688	6.476
hTempErr (m)	9.04	10.69	12.35	11.51

Table 13: Debugging Values Dataset 1.1, coordinate (500, -400)

	Freq 1	Freq 2	Freq 3	Freq 4
fB (1/s)	.1833	.2233	.1633	.2633
k (1/m)	.1638	.2323	.1525	.4215
a (rad)	-.80	-.91	-.81	.39
skill (-)	.9160	.9405	.8487	-.6394
hTemp (m)	7.152	5.628	8.898	1.440
hTempErr (m)	13.24	6.50	8.90	1.44

On the other hand, for area 2, the algorithm was unable to resolve a satisfactory solution more often than for area 3. When this occurs, the algorithm returns NaNs for the specific frequency. The amount of unresolved wave solutions plotted for the central area was 3 out of 16 whereas the other area yielded only 1 out of 16 unresolved frequencies. In theory, when there are enough other modeled wave frequencies with high skill values, an accurate water depth can still be computed.

Subsequently, when looking at the preliminary depth the cBathy algorithm estimates at area 1, it seems that the variance in the depth estimations as indicated by the algorithm per frequency is lower than for area 3. It ranges between 4 and 8 meters for all of the 12 frequency values, whereas in the latter location it ranges from 2 to 12 meters. This indicates that the algorithm is more confident in

the analyzed wave field for area 3 than from area 1. As the final depth calculation in phase 2 of the cBathy algorithm does not use these preliminary depths, this does not have to be a problem. However, it does give an indication for the confidence in the eventual computed depth. Also, similar to the lower skill value, the estimated error in the preliminary water depth seems to be larger for the poorly performing area. This is again merely an indication for depth inversion accuracy.

From this analysis it is shown that the worse performing area 3 seems to consist of wave data that is slightly harder to detect for the cBathy algorithm. However in theory, enough high skill values are found to compute an accurate water depth.

Dataset 1.1 vs Dataset 2.1 The first datasets on the two days were filmed in a fairly similar setting which included the recording of two rows of ground control points on the beach. However, there was around 22 hours in between the measurements. Therefore, conditions like the tide, the wave climate had changed. When comparing the worse performing dataset 2.1 with dataset 1.1 the focus lies on area 3. This is because especially in this area, dataset 1.1 performs significantly better than dataset 2.1. This part of the report tries to find an explanation for the discrepancy in bathymetrical accuracy.

When looking at the area 2, the wave frequency that is most important according to the cBathy algorithm is 0.1233 Hz for the first day and 0.1633 Hz for the second day. The second most important frequency on the second day is 0.2233 Hz where on the first day it was 0.2033. Further dominant wave frequencies also indicate that the wave field on the second day consisted of slightly shorter waves than on the first day. This is in accordance with the visually estimated wave lengths in the results section and is later also shown in figure 75. In the image it is shown that the most dominant wave frequency was generally larger for the first day when compared to the second day. Furthermore, the dominant wave frequencies in area 3 became less obvious for both datasets 1.1 and 2.1. Instead of having 3 different frequencies indicated as being either the most or the second most important frequencies for the 4 different sub areas in the worse performing area 0.1233, 0.1433, 0.1633, 0.1833, 0.2033 and 0.2233 Hz are all indicated as being either the most or second most important. This increase from 3 to 6 different frequencies indicates that the algorithm is not as effective in the analysis for this part of the dataset.

Table 14: Debugging Values Dataset 2.1, coordinate (400, 0)

	Freq 1	Freq 2	Freq 3	Freq 4
fb (1/s)	.1633	.2233	.1833	.1433
k (1/m)	.1948	.2386	.2057	.1586
a (rad)	-.79	-.84	-.81	-.62
skill (-)	.9445	.8610	.9289	.9184
hTemp (m)	3.178	5.129	3.826	4.221
hTempErr (m)	3.89	7.14	4.23	7.12

Table 15: Debugging Values Dataset 2.1, coordinate (500, -400)

	Freq 1	Freq 2	Freq 3	Freq 4
fb (1/s)	.1833	.1633	.2433	.2033
k (1/m)	.2435	.1862	.6747	.3049
a (rad)	-1.02	-.97	.16	-1.10
skill (-)	.8716	.7985	-.7853	.8682
hTemp (m)	2.568	3.527	0.547	2.006
hTempErr (m)	2.00	3.95	0.22	1.16

When looking at the skill level between area 2 and 3 areas, the data in the center area seems to yield better values. Like dataset 1.1, this area in dataset 2.1 indicates values consistently around 0.9. Subsequently, like for dataset 1.1, the data from day two also has significantly lower skill levels for area 3. The values range from 0.4 to 0.8, with predominantly values of 0.7. It should be noted that within the 4 sub areas there are also three negative skill values which indicate a completely erroneous wave phase prediction by the algorithm. An example of the erroneous phase prediction is shown in figure 73. All three of these negative skill values are attributed to the 0.2433 Hz wave frequency, resulting in the conclusion that especially the algorithm has difficulties with analyzing sharp angled short waves.

Furthermore when regarding dataset 2.1, area 1 yields three unresolved wave frequencies, whereas area 2 and 3 only yield 1 and 2 respectively. As this analysis focuses on three really specific locations, this does not mean that there is a general trend of unresolved wave frequencies. Area 1 still yields good results probably because there are sufficient other wave frequencies that accurately model the water surface elevation. Also, the preliminary depths that are estimated by the signal analysis

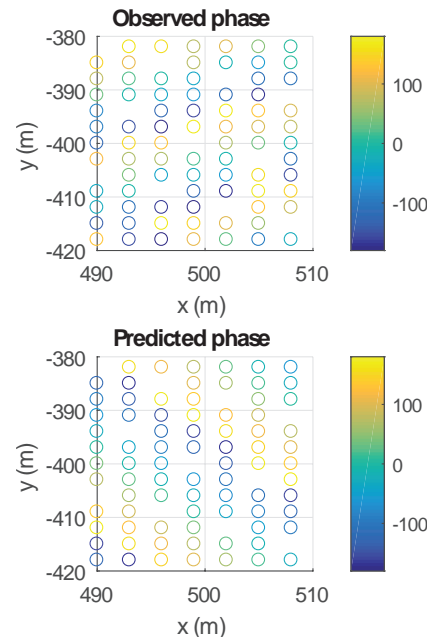


Figure 73: Phase Analysis 0.2433 Hz Dataset 2.1 Coordinate (500, -400) (see Freq 3 of table 15)

show that for both area 2 and 3, dataset 1.1 yields higher values than dataset 2.1. Whereas dataset 1.1 indicated between 4 & 8 meters of depth for area 2, dataset 2.1 yields between 3 & 5 meters. For area 3 it shown respectively between 0.2 & 12 meters and 0.5 & 4. As these specific areas are only a small subset of the total area, this could be a coincidentally.

When looking at the magnitude of the wave number as detected by the algorithm, it seems that generally for different sub sections similar results are found when comparing the specific frequencies. However, for the 0.2433 Hz frequency that was falsely predicted, the wave number changes up to a factor 2 for the different sub areas. This can probably be attributed to the fact that the phase prediction has a significant error as shown in figure 73.

From these results it can be distracted that the wave detection has difficulties with the relatively short waves (approximately 4 seconds) with a sharp angle of incidence. This error in the algorithm is known, and therefore the current state is not particularly specified on short wave coasts. On the other hand, the fact that even the poorly performing areas shown high skill values means that the algorithm is accurately observing a signal.

Area 1 As the previous parts of the signal analysis have mainly considered area 2 and 3, the area around coordinate (500, 400) is briefly elaborated

in this section. This area scores intermediate to high in terms of the skill values when compared to the other 2 areas. Furthermore, the indicated wave frequencies that are considered to be most important are fairly consistent throughout the 4 sub areas area (500, 400). In dataset 1.1 the frequencies 0.1233, 0.1433 and 0.1633 are consistently indicated as most important. The dominant wave frequency was even more consistent for dataset 2.1. For all of the 4 sub areas the 0.1433 Hz frequency was indicated as most important and the 0.1833 Hz frequency as second most important. For these reasons it is assumed that the signal in the left hand side of the image is of almost the same quality as the signal in the center of the image. Also when according to the quantitative analysis in the results section, this area seemed to perform relatively good.

Locational Signal Analysis Conclusions The previous section showed that across the analyzed datasets, the signal that was observed by the cBathy algorithm seemed better in the center area than in the area around coordinate (500, -400). The area around coordinate (500, 400) was intermediate in terms of quality of wave frequency analysis. As area 2 falls directly in the center of the envelope of the 4 used ground control points, it is assumed that the rectification quality was better both in terms of absolute error and stability. Therefore, the optical signal probably had the least distortions in terms of rectification errors. This gives an indication to research the influence of rectification errors.

Even though the wave analysis seemed to perform worse for area 3 when compared to area 2, the algorithm still theoretically found sufficient frequencies for an accurate depth estimation. Therefore, it seems that the observed optical signal did capture sufficient wave parameters for the algorithm to compute an accurate bathymetry.

5.3.2 Spatial Parameters of Signal Analysis

To be able to visualize the above mentioned analysis and consider larger spatial scales, figure 74 shows the most important wave frequency as indicated by the cBathy algorithm for datasets 1.1, 1.2, 2.1 and 2.2 for every coordinate in the rectified area. Furthermore, figure 75 illustrates the skill values of these wave frequencies. Subsequently, figure 76 indicated the second most important wave frequency for all the datasets and figure figure 77 again shows its skill value.

The first figure shows that for a large amount of

contiguous coordinates of dataset 2.1 and 2.2, the wave frequency that is estimated to be most important is the same. It seems that on the second day, especially the 0.1433 Hz frequency is indicated as a dominant signal. On the other hand, the dominant wave frequency as indicated by the phase 1 analysis seems to differ more severely throughout the datasets on the first day. Whether a severely differing dominant frequency throughout a dataset is advantageous is unknown. One could argue that multiple frequencies can yield more data throughout the frequencies and that thereby more wave data can be used to calculate bathymetry. On the other hand, as the wave climate is not estimated to differ severely throughout a section of 2500 squared meters, a more evenly indicated dominant wave frequency shows that the algorithm is better able to analyze the right frequencies. The quantitative analysis from the results section invigorates the former. Furthermore, the fact that the datasets taken on the same day show similarities could indicate that the wave climate on day one was in fact less monotone than on day two.

The second most important wave frequency is shown to differ more severely throughout the coordinates for all of the datasets. Another striking feature of figure 74 and 76 is that the areas of contiguously similar wave frequencies all border in a North-South direction. It could be that the wave direction is to be attributed as in a dataset of 15 minutes some wave groups could be more prevalent than others. Another explanation could be the direction of the sun rays, which came from the South. However, with the current data no specific conclusions can be drawn.

Subsequently, figure 75 shows the quality (skill) value that the cBathy algorithm indicates for the different coordinates. The skill value is directly related to the wave frequency as indicated for that specific coordinate. According to the algorithm, a value converging to 1 indicates an increasingly accurate water depth estimation. Also, skill values below 0.5 are indicated as insufficient and therefore are rejected. The figures show that the skill value below area 3 of the poorly performing dataset 2.1 have low values. This should mean that the identified wave frequency should not be taken into account during the phase 2 single depth estimation. It should be noted that the low skill values are generally located outside the extend of the reference bathymetry (white lines). As within the reference bathymetry the skill values are predominantly high, the algorithm should be able to compute accurate water depths. The fact that this is not the case

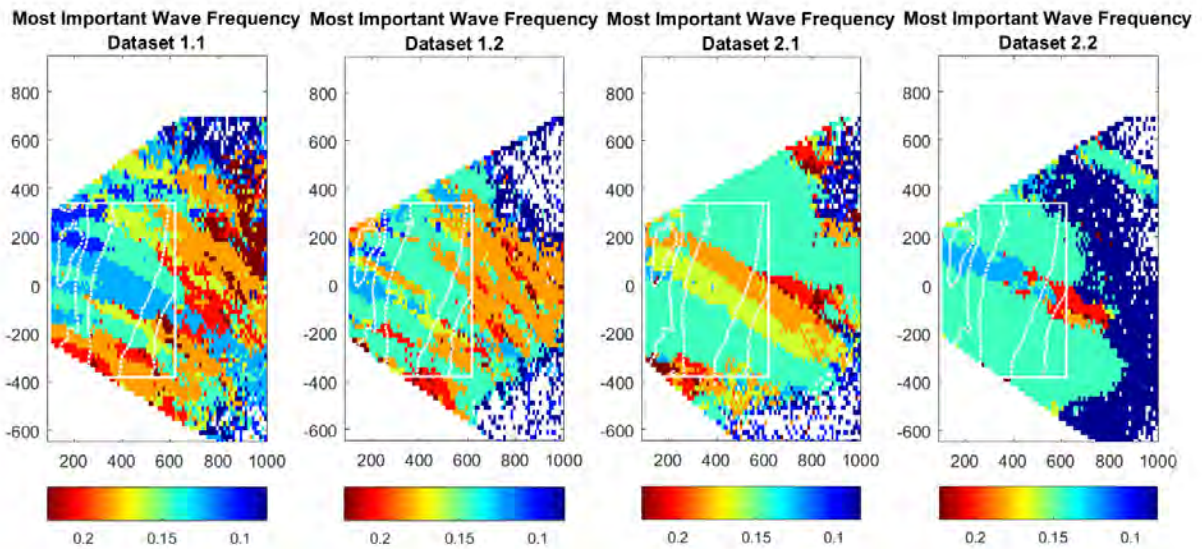


Figure 74: Most Important Frequencies (Smoothing Parameter: 2.00 by 2.00)

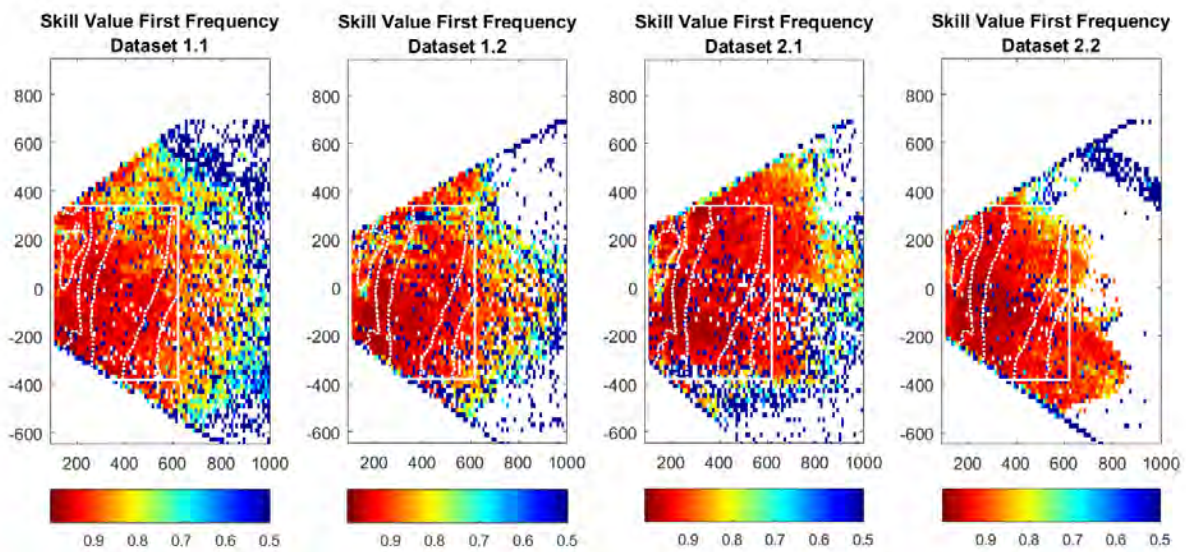


Figure 75: Skill Values of First Frequencies (Smoothing Parameter: 2.00 by 2.00)

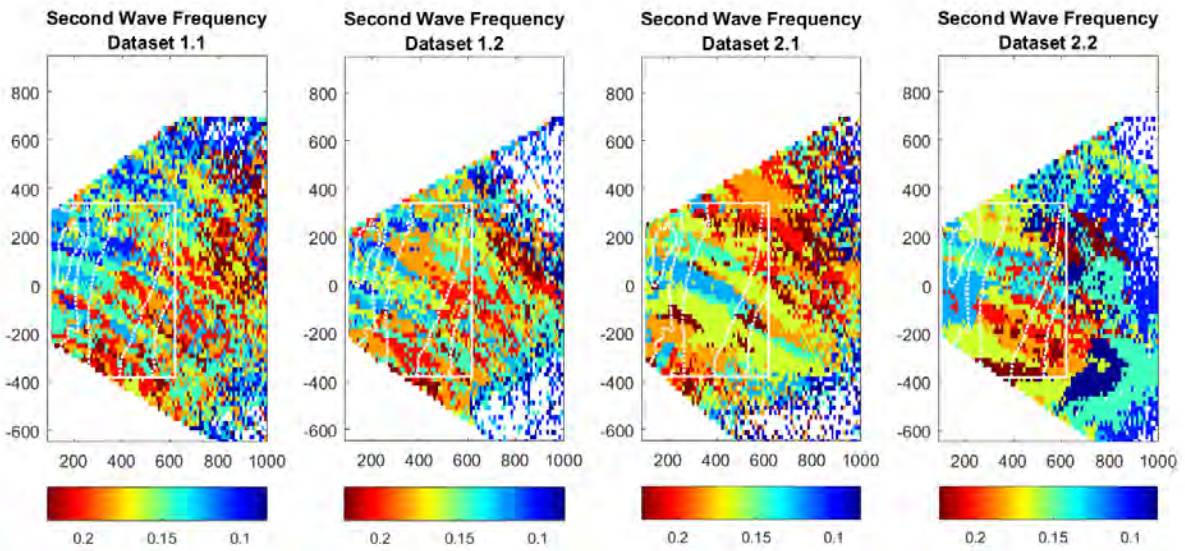


Figure 76: Second Most Important Frequencies (Smoothing Parameter: 2.00 by 2.00)

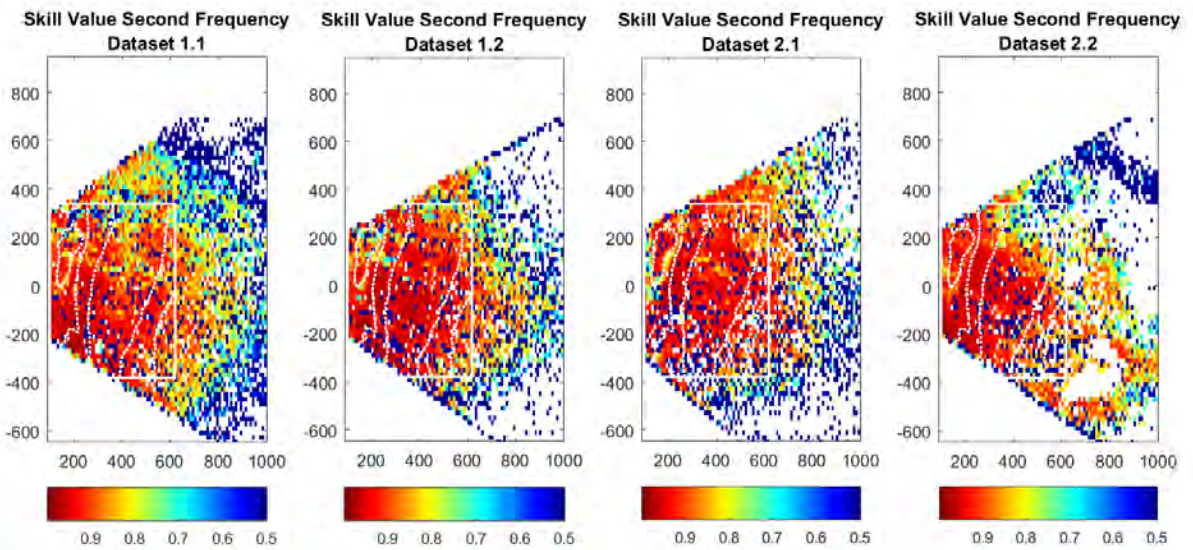


Figure 77: Skill Values of Second Frequencies (Smoothing Parameter: 2.00 by 2.00)

could again be an indication that whilst the optical signal is accurately analyzed, the signal does not correctly portray the physical signal.

Figure 76 indicates that the second most dominant wave frequency is less coherent throughout the coordinates. However, similar to the first wave frequencies in figure 74, waves on the second day seem to be less noisy than on the first day. Also like according to the first frequencies, the colors indicate that in some areas shorter waves are more predominant than in other areas.

When comparing the spatially indicated skill values to the error plots in the results section (third subplot in figure 68 & 69), it is concluded that in the area with a reference bathymetry present both the skill values and the estimated errors indicate an accurate wave field mapping and therefore also a good bathymetry inversion. The figures do show that the lower skill values in the areas with negative Y coordinates outside of the reference bathymetry also add up to a higher estimated depth error for some parts. On the other hand, also for dataset 1.1 the estimated error seems noisier in area 3. These findings indicate that the datasets score similarly in terms of analyzing the optical signal. Hence, they confirm the observation in the results section which found the datasets to be qualitatively similar in terms of visually observable wave fields. Subsequently, provided that the optical signal represents the physical signal the datasets should also perform similar with respect to depth inversion.

5.3.3 Conclusions Signal Analysis

The data elaborated in this section indicates that within the datasets that are used for this research the wave fields in the optical signal are generally analyzed in an accurate manner. However, at the worst performing sub area in the worst performing dataset, skill values as indicated by the cBathy algorithm are for some coordinates lower than for different areas. Even though this is the case, according to the internal quality parameters, the cBathy algorithm yield good phase 2 single depth estimates.

Furthermore, relatively short waves with a steep angle of incidence are more often analyzed in an erroneous way then waves with an angle more oblique to the shore.

Even though the quality was a little worse for areas below the (500, -400) coordinate, figures 68 & 69 in the previous chapter and figures 75 & 77 already showed a low error estimate for both the well and the badly performing areas. Because the skill values are generally high throughout the datasets

it can be concluded that the cBathy algorithm is accurately observing a signal. Also the low depth error as shown in the results section contributes to this observation. However, when compared to the reference bathymetry, the eventual water depths indicate a large error for areas that seem to be performing well in terms of skill values. Therefore, the question rises whether the observed optical signal is portraying the physical signal of wave motions. When looking at the input data in retrospect, there seem to be two possible explanations for the discrepancy between the optical and the physical signal. Either the tidal current influences the wave length, or the large rectification errors attribute the wrong location to an accurate optical signal.

5.4 Influence of Longshore Current

The current induced by the tide was shown in section 4.1. It showed that the tidal current during dataset 1.1 differed severely from the current during dataset 2.1. As the algorithm is written for primarily obliquely incoming waves, the influence of longshore currents is not assumed to interfere with the cBathy algorithm significantly. Therefore, the longshore current is not corrected for. As the waves during this research were coming steeply from the north and were opposing by the tidal current, the longshore current might have influenced the calculations. Therefore, a brief analysis of the potential influence is done. Lee and Mizutani (2007) researched the influence of current on waves. They showed that a current that travels in opposite direction of waves reduces their observed wave number.

Table 16: Wave Length Reduction due to Opposing Current as found by Lee and Mizutani (2007)

Wave Period (s)	Current Velocity (m/s)	Wave Height (cm)	Wave Length (m)	Reduction (%)
1.8	0	5.0	2.895	0
1.8	-4	5.0	2.790	3.6
1.8	-6	5.0	2.650	8.5
1.4	0	5.0	2.154	0
1.4	-4	5.0	2.060	4.4
1.4	-6	5.0	1.931	10.4
1.0	0	5.0	1.373	0
1.0	-4	5.0	1.279	6.8
1.0	-6	5.0	1.134	17.4

In table 16, it is shown the wave length of waves with a period of 1, 1.4 and 1.8 seconds decreases by 17.4, 10.4 and 8.5 percent respectively in terms of wave length when changing the flow from 0 to -6 m/s. As the wave periods that were prevalent during the field survey of this report were generally larger, the reduction in wave length is assumed to be lower than 8.5 percent. However, to calculate an extreme value a reduction of 8.5 percent is chosen for this analysis.

The current during dataset 2.1 was estimated to be around 0.7 m/s opposing the wave that were incoming form the North. The wave number is related to the wave length in the following way.

$$k = \frac{2\pi}{L} \quad (24)$$

This means that if the wave length would decrease by 8.5 %, according to above mentioned research, the estimated wave number would increase by the same percentage. Subsequently according to the dispersion relation (equation 23) the estimated water depth would have decreased by approximately 15 %. This gives an indication that the opposing tidal current did influence the calculations. However, as 15 % is assumed to be an extreme number, the actual influence would be smaller. As the error for the poorly performing are in dataset 2.1 is over 1 meter for areas that actually have 5 meters of depth, the error is over 20 %. Therefore, the opposing tidal current cannot be accounted for the large error in dataset 2.1.

When looking at the distribution of the tidal flow across the upper shoreface, figures 78 & 79 show the tidal current during datasets 1.1 and 2.1 respectively. As the algorithm does not take currents into account and dataset 1.1 was recorded around flow reversal, this should not influence the results. On the other hand, figure 79 shows that due to the breakwater of the Scheveningen harbor, for strong tidal flow, the tidal currents throughout the area of interest differ severely. The currents that oppose the incoming waves are much larger for the right hand side of the recorded imagery than for the left hand side (see figure 79). This would mean that in area 3, the estimated depth would be relatively lower than in area 1. This is also observed in the quantitative analysis. Hence, this might partially explain the skewness in the depth signal for dataset 2.1.

However, this would mean that due to the strong tidal current farther offshore, also in that location the estimated water depths would be smaller than the real depths. As there is no reference data for

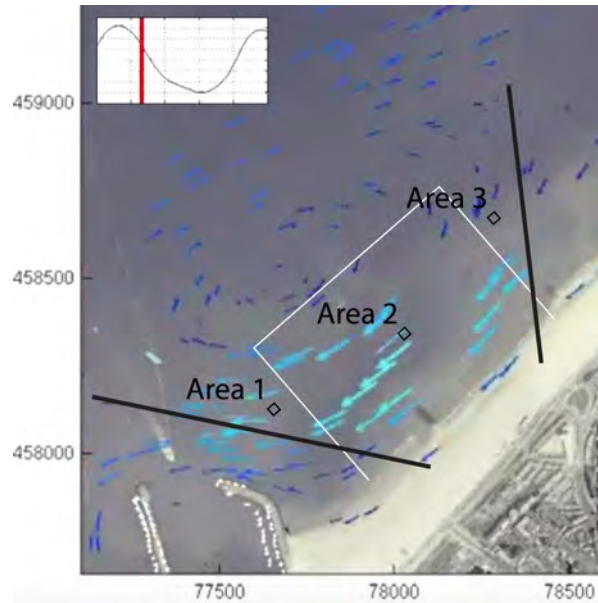


Figure 78: Tidal Currents Scheveningen During Dataset 1.1 (and 1.2) with Drone View and Reference Bathymetry Location

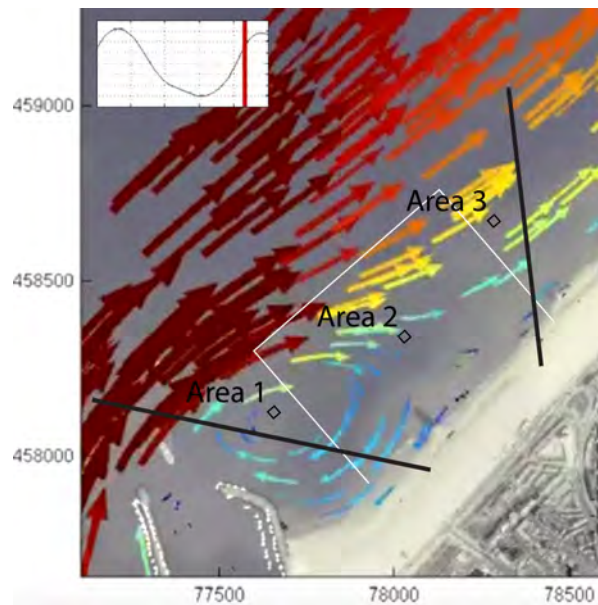


Figure 79: Tidal Currents Scheveningen During Dataset 2.1 (and 2.2) with Drone View and Reference Bathymetry Location

this part of the bathymetry, the relative depth error can not be quantified.

On the other hand, the opposing current can not explain the small depths around area 3 which similarly also observed for dataset 1.2. Dataset 1.2 was recorded approximately 30 minutes after dataset 1.1 and therefore the tidal currents were not significantly different.

Conclusion Current Interference The analysis of the tidal currents shows that when only comparing datasets 1.1 and 2.1, the currents could be identified as a contributor to the bathymetrical error. However, around area 3 also dataset 1.2 shows errors that are in the order of magnitude of the computed depth. As during this recording no significant tidal currents were present, other causes for the optical signal not representing the physical signal should be researched.

5.5 Absolute Rectification Error

As discussed in this chapter, the algorithm accurately models the severity of different observed wave frequencies. Apart from the opposing tidal current interference with the wave signal which was dismissed, no other physical aspects were found that could potentially negatively influence the physical signal (the actual wave motions). Therefore, it is assumed that the optical signal does not represent the physical signal in an accurate manner. When regarding the results chapter, one of the errors that had the largest discrepancy between the datasets was the absolute rectification accuracy (see section 4.2.5). It was shown that the average error for the floating ground control points during the best dataset ranged between 15.5 and 19.5 meters. On

the contrary, the absolute errors for the worse performing dataset 2.1 were 28.7 and 37.7 for GCPs 1 and 2 (GCPs 3 and 4 were not identifiable). Apart from the total error being larger, a large error in the Y direction was observed which was virtually undetectable for dataset 1.1. Therefore, the rectification process for dataset 2.1 is considered to have added a distortion in the optical signal which might have resulted in the low accuracy of the eventually inverted bathymetry. Another observation that seems to reinforce this hypothesis is the fact that especially outside the envelope of the GCPs used for rectification the errors seemed to increase. This could be attributed to the rectification error increasing exponentially when considering coordinates increasingly farther away for the envelope.

5.5.1 GCP Usage

To detect whether the errors in the geometry are a significant contributor to the bathymetry accuracy, the rectification algorithm needs to be changed in a way that could potentially decrease distortions in the projection. In an effort to accomplish this, for dataset 1.2 the amount of GCPs used was increased from 2 water GCPs and 2 beach GCPs to 4 water GCPs and 2 beach GCPs. Subsequently, for dataset 2.2, both the water and beach GCPs were increased to 4. After the amount of GCPs that were used for these datasets was increased, the error counter-intuitively also increased to 1.2 and 1.0 meters RMSE respectively. The large increase indicated that changing GCPs configuration significantly influences the accuracy of the method. The unexpected increase in error motivated a more elaborate investigation. In this section, several different GCP configurations will be used for an extensive analysis.

Table 17: Absolute Rectification Error (Real Location - Estimated Location) Reduction with Resulting Bathymetry Accuracy for Dataset 2.1 (for GCP layout see figure 44)

Version Number GCPs Used (water, beach)	GCP 1		GCP 2		RMSE			
	abs (m)	(<i>x, y</i>) (m)	abs (m)	(<i>x, y</i>) (m)	Total Area (m)	Area 1 (m)	Area 2 (m)	Area 3 (m)
V1: (2, 2)	28.7	(-19.8, 20.6)	37.7	(-30.5, 22.0)	1.3	0.62	0.64	2.0
V2: (2, 8)	18.4	(-15.9, 9.1)	7.0	(6.1, -3.4)	1.0	0.44	0.67	1.5
V3: (0, 8)	29.3	(15.3, 24.9)	18.9	(18.5, 3.7)	1.2	0.37	1.0	1.6
V4: (1, 8) (*gcp 1)	12.1	(-7.8, 9.2)	17.5	(15.8, -7.6)	1.3	0.49	0.91	1.9
V5: (1, 8) (*gcp 2)	19.0	(-8.9, 16.7)	5.6	(4.3, 3.5)	0.87	0.38	0.62	1.3

Whereas for datasets 1.1, 1.2 and 2.2 four ground floating ground control points were automatically detected, dataset 2.1 had only 2 water GCPs that were available together with 8 beach GCPs. After adding every beach GCP available to the geometry calculation, in contrast to the observations for the previous datasets, the error significantly decreased from 1.3 to 1.0 meters RMSE. This gave an indication that the floating GCPs might negatively influence the geometry calculation which in turn yields worse depth estimates. It could be that the GPS loggers located on the floating GCPs were not accurate enough to be used for depth inversion practices. However, as the location registered by these loggers stayed within a couple of meters between dataset 1.1 and 1.2, the discrepancy in accuracy cannot be explained solely by a large GPS error. To be more thorough, more tests were done regarding the used GCPs for dataset 2.1. Table 17 shows the reduction in absolute rectification errors³ for dataset 2.1 when altering the amount of floating and beach GCPs used. It also shows the changes in bathymetry error. As the rmse error differs with almost half a meter for the total area, the results in the table reinforces the above mentioned indication that the computation of the homography during the rectification stage of the method does have a large influence on the eventual results.

Especially the skewness (an overestimation on the left hand side of the video and an underestimation of the right hand side of the video) in the bathymetry that was observed in the base results seems to be influenced by the calculation of the geometry. Figures 80, 81, 82, 83 and 84 show the resulting bathymetries as computed when using the different GCP versions in accordance with table 17. Qualitatively, it shows that the bathymetry skewness decreases when increasing the amount of beach control points used. This can be argued because the water around coordinate (500, -400) is not computed to be as shallow as in figure 80 and the water around coordinate (500, 400) is not as deep. Furthermore, an attempt to compute a bathymetry when only using the 8 control points situated on the beach (figure 82) resulted in an even greater reduction in bathymetry skewness which is indicated by the smaller difference in water depth errors when comparing area 2 and 3 in table 17. Whereas this indicates that the projection might not be as dis-

³Whereas this section will indicate that the two floating GCPs might not contribute to better geometry calculations and therefore might not have an accurately estimated position, they are merely used as a reference point when comparing the projections of different versions.

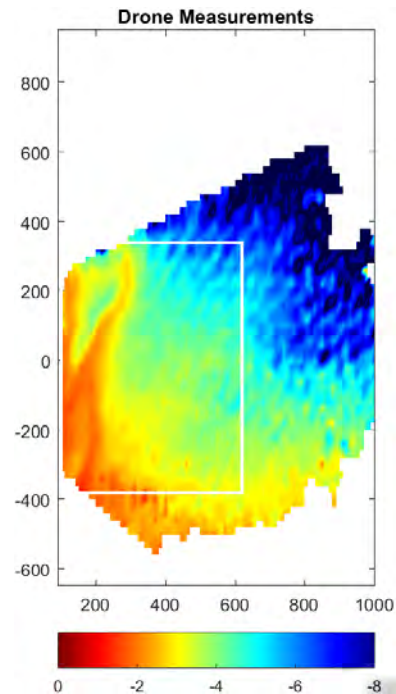


Figure 80: Bathymetry According to Dataset 2.1 when using Version 1 (GCPs 1, 2, 9 & 12)

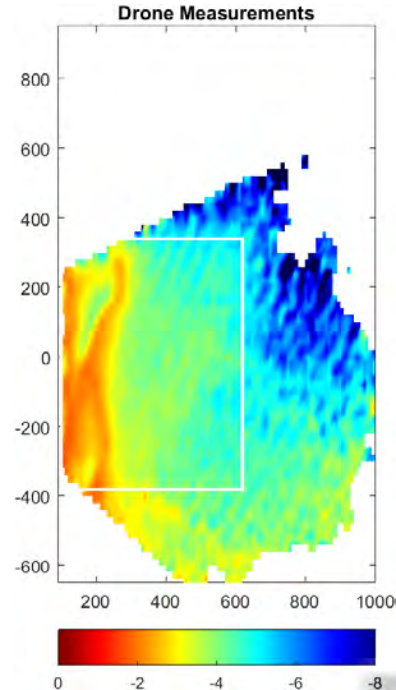


Figure 81: Bathymetry According to Dataset 2.1 when using Version 2 (GCPs 1, 2, 5, 6, 7, 8, 9, 10, 11 & 12)

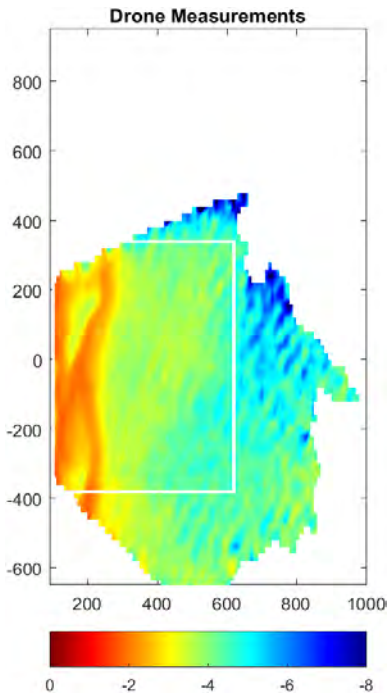


Figure 82: Bathymetry According to Dataset 2.1 when using Version 3 (GCPS 5, 6, 7, 8, 9, 10, 11 & 12)

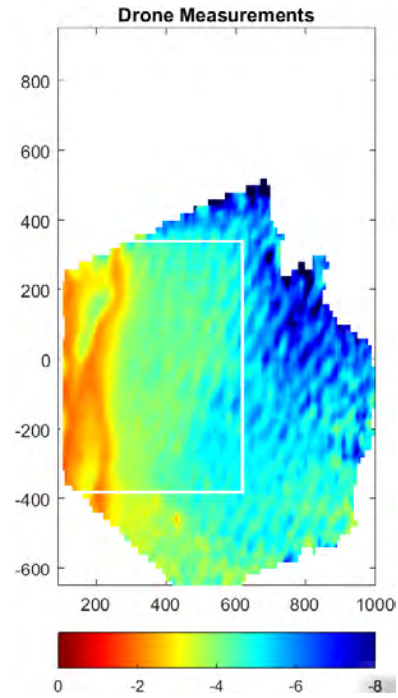


Figure 84: Bathymetry According to Dataset 2.1 when using Version 5 (GCPS 2, 5, 6, 7, 8, 9, 10, 11 & 12)

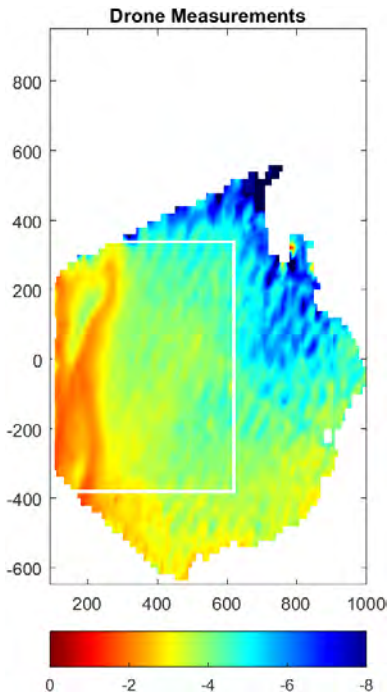


Figure 83: Bathymetry According to Dataset 2.1 when using Version 4 (GCPS 1, 5, 6, 7, 8, 9, 10, 11 & 12)

torted as for the previous versions, the lack of distance between the GCPs in the cross shore direction might have led to an underestimation of the wave length throughout the entire area and therefore computing relatively small water depths for the whole area of interest. This underestimation of the wave lengths can be argued because the rectification error in the x direction as shown in table 17 significantly increased for this version. Another indication to attribute a significant part of the bathymetry error to the projection distortion is given when regarding versions 4 and 5. These versions were compiled as version 3 yielded a smaller skewness but a larger standard underestimation of spatial scales in the cross shore direction. This is why it was argued that using only 1 floating GCP might solve the cross shore spatial scale error whilst not distorting the projection as much as when using both floating GCPs. Therefore, in versions 4 and 5 all 8 beach GCPs were used in combination with only 1 floating GCP. As the rectification error in longshore direction only based on the accurately measured beach GCPs (version 3) yielded larger error for GCP 1 than for GCP 2 (see table 17), it was predicted that version 5 would yield better water depth estimates and lower bathymetry skewness than version 4. This hypothesis was reinforced

when table 17 showed that the estimated location error for floating GCPs 1 and 2 differed significantly for version 4. Whereas GCP 1 was overestimated in cross shore direction by around 8 meters, GCP 2 was underestimated in the same direction with almost 16 meters. This distorted projection is arguably the cause of the lower bathymetry accuracy of version 4 when compared to version 5.

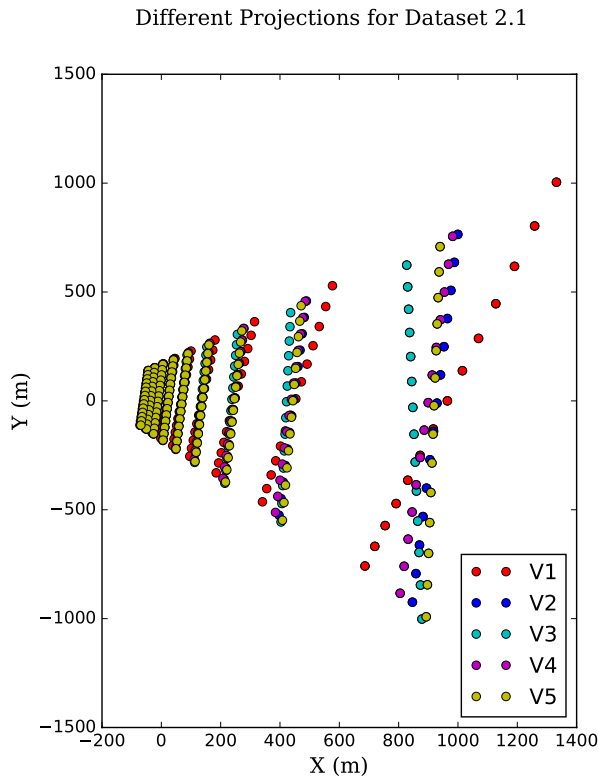


Figure 85: Different Projections of the Same Frame for Different GCP Versions (see table 17) of Dataset 2.1

To quantify and visualize the above findings, for an arbitrary frame in the video captured for dataset 2.1 the different projections are calculated per GCP version and displayed in figure 85. The figure illustrates the geographical location of a subset of pixels (the projection) taken from the image (in this case image 150) in accordance to the homography as calculated using the five different GCP versions. It is clearly shown that the same pixel of the same image of the same dataset is displayed on a completely different location when using different GCP versions. It shows a projection for version 1 which is completely different from the projection of version 3. This erroneous projection of a certain pixel can influence the water depth in two ways.

1. The water depth is calculated in an erroneous way due to an over or underestimation of the wave length
2. The calculated depth is plotted on a wrong location

The following part will elaborate and compare these two errors.

5.5.2 Wrongful Wave Length Estimation

As the same pixel of a certain frame is calculated to have a significantly different location when using different GCP configurations, the size of that particular pixel will also be different (see figure 21 in the methodology section). Table 18 shows the pixel dimensions for pixel (836, 575) and the pixel (2760, 550). These pixels were chosen as they represent the projected pixels around coordinates (600, 300) and (600, -300).

Table 18: Pixel Dimensions in Cross Shore Direction for the Different Versions van GCP Setup in Dataset 2.1

Version Number	Pixel A (836, 575) Size (m)	Pixel B (2760, 550) Size (m)
1	2.61	2.08
2	2.13	2.29
3	1.79	2.19
4	2.07	2.17
5	2.04	2.35

The table shows that the pixel portraying the (600, 300) coordinate is significantly larger for version 1 when compared to the other versions. This means that of the same waves that are observed around this particular pixel, the wave length according to version 1 is observed to be larger. The larger wave length yields a higher wave celerity. The higher wave celerity subsequently results in a larger computed water depth according to the following dispersion relation.

$$h = \frac{1}{k} \operatorname{arctanh}\left(\frac{\omega^2}{gk}\right) \quad (25)$$

The equation shows that the water depth is related to the inverse hyperbolic tangent of the frequency squared divided by the wave number. As the erroneous projection only changes the wave length whilst keeping the frequency the same, an increase in wave length (a decrease in wave number)

causes the water depth to increase as the arctanh increases according to figure 86.

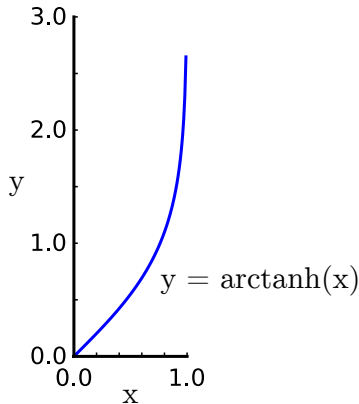


Figure 86: Inverse Hyperbolic Tangent

For instance for a wave with a length of 50 meters and a period of 9 seconds ($\frac{\omega^2}{gk} = 0.40$), the inverse hyperbolic tangent relation is semi-linear. This means that an increase in observed wave length linearly increases the inverse hyperbolic tangent. As the hyperbolic tangent is multiplied by $1/k$, which represents 2π divided by the wave length (equation 15), the relation becomes quadratic. Hence, an error in the projection represents a quadratic error in the water depth estimation.

5.5.3 Plotting the Depth at the Wrong Location

A second error that is introduced by a distortion in the projection regards plotting the calculated depth as computed for a specific coordinate at the wrong location. As the error is captured in the coordinates, the wrongly calculated water depth as described above is also attributed to its wrong location. This for instance results in water depths being plotted farther away from the shore (see figure 87) for the area around coordinate (800, 400) for GCP version 1. As apart from features like breaker bars the water generally gets deeper when taking coordinates farther offshore, this error will lead to an underestimation of the water depth for parts that are stretched out by the wrongful projection.

The two above mentioned error inducing factors as a results of projection distortion have an opposing influence on the depth of the eventual computed bathymetry. To get an indication whether the water depths are going to be under or overestimated, the dispersion relation (equation 25) is compared to the slope of the transact. As elaborated above, an increasing wave length exponen-

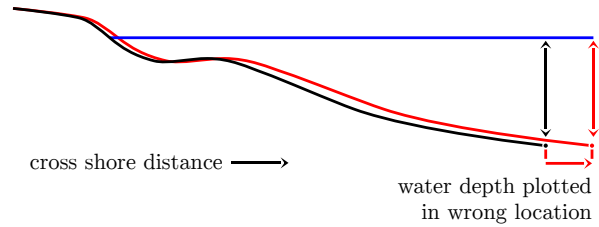


Figure 87: Water Depth Plotted in wrong Location

tially increases the computed water depth. On the other hand, the water depth of a profile generally gets less steep when taking locations increasingly offshore. Therefore, the reduction in water depth due to the overestimated pixel location is argued to be less significant when taking locations farther offshore. Hence, the under or overestimation in wave length is argued to be a more predominant factor than the attribution of a water depth to the wrong location. Subsequently, a location where the pixel coordinates are overestimated is argued to overestimate water depth and a location where the pixel coordinates are underestimated is argued to underestimate water depth. This is also clearly visible in figure 80, where the area around coordinate (800, 400) is stretched out and deep and the area around coordinate (800, -400) is more squeezed together and shallow.

Water Level A hypothesis which could potentially explain the algorithm being unable to calculate an accurate geometry is a discrepancy between the measured water level and the actual water level. Therefore, as a test, the water level as observed by the Rijkswaterstaat measuring device in the Scheveningen harbor was altered by adding and subtracting 20, 40 and 60 centimeters. These test were done by using 8 GCPs on the beach and 2 in the water because in this way it could verify whether the geometry error between the water and beach GCPs was caused by the water level. As an artificial change of observed water levels cannot be done when computing bathymetries without reference data, only the influence of the water level on the skewness in the bathymetry is regarded. After running the UAV bathymetry mapping method with the altered water levels, the skewness in the bathymetry signal was prevalent. This indicates that the water level was not the cause of the geometry problem.

Optimizing GCP Configuration for Datasets

1.2 and 2.2 The previous section has shown that the use of both beach and water GCPs for dataset 2.1 is likely to cause an error when computing the projection of the captured video on a three dimensional map. The results chapter showed that although not as strongly prevalent as in dataset 2.1, also dataset 1.2 and 2.2 suffered from a skewness in the bathymetry. Hence, it was assumed that this was caused by the same geometry error as for dataset 2.1. Therefore, it is argued that also for datasets 1.2 and 2.2 a potential accuracy increase can be accomplished by changing the GCP usage. Either only beach or only water gcps could be used to indicate whether this is the case. As for these datasets only one row of beach GCPs was visible in the video imagery, the cross shore component of the rectification could not be determined in an effective manner when using only beach GCPs. Therefore, of both datasets the bathymetry was computed using only the four water based control points. Reinforcing the above geometry indication, the root mean squared error decreased to 0.58 and 0.68 meters respectively. However, as the water based control points were situated farther away from the camera, the accuracy of the nearshore area (area 1) did decrease to root mean squared errors of 0.60 and 0.79 meters respectively. It was also found, that the skewness in the bathymetry as found in the results section disappeared. This reinforces the indication that using a combination of water and beach GCPs results in a distorted projection.

5.5.4 Summary Geometry Error

After the suspicion was raised that the projection did not represent the three dimensional coordinates in an orderly manner, an investigation was done into the use of different ground control point configurations. It was found that the error contribution induced by the erroneous projection was significantly larger than the error which were contributed by other parts of the UAV bathymetry mapping process. Using different control points yielded different projections for the exact same arbitrary frame. A subsequent qualitative analysis showed that the observed skewness in the error of the bathymetry could indeed be explained by the distortions in the projection which were present in the base scenario analyzed in the results section. Because the input data did not represent the wave climate in a correct way, the cBathy algorithm itself could not be tested to its limits.

5.6 UAV Bathymetry Mapping Performance

In this research, the cBathy algorithm seemed to perform well. For a large extend of the area of interest, the waves that were analyzed seemed to represent the optical signal correctly. Also, one of the datasets yielded relatively accurate results with an overall rmse of 0.37 meters. As the method used in this research was built from scratch, there are still several optimizations that can be investigated. This indicates that the UAV bathymetry mapping method can potentially be a valuable tool for water depth calculations.

During the bathymetry calculations using the base scenario of standard settings, the error of the method was still rather large. Some optimizations in especially the cBathy settings increased the overall accuracy. It was shown that the rectification calculations still included a large error. Eventually, also the geometry calculation was significantly improved by only using the four floating control points for datasets 1.2 and 2.2. As for dataset 2.1 two of the four floating GCPs could not be detected, the same mitigation was not possible. Therefore, the use of 8 beach GCPs and 1 floating GCP decreased the geometry error in the best way. The final bathymetry accuracies are displayed in table 19.

Table 19: Bathymetry Accuracy for all Datasets after the Geometry Error is Mitigated

Data set	Total Area rmse (m)	Area 1 rmse (m)	Area 2 rmse (m)	Area 3 rmse (m)
1.1	0.37	0.25	0.31	0.55
1.2	0.58	0.60	0.62	0.52
2.1	0.87	0.38	0.62	1.3
2.2	0.68	0.79	0.69	0.52

For the scenarios in which floating and beach control points are combined, the table still indicates a larger error for area 3 when compared to the other areas. This indicates that a discrepancy between the three dimensional location of the pixels and the projection is still present, resulting in a similar bathymetry tilt as was observed for the base scenarios in the results section.

As the final control point configurations could not be known beforehand, these root mean squared errors do not represent the accuracy of the bathymetry as would be expected when measuring without reference data. However, they do give an indication

of the potential error once the UAV bathymetry mapping method is developed more extensively. As for a usable bathymetric indication an error in the order of magnitude of 20 centimeters is required, these figures indicate that the UAV bathymetry method is still unsuitable for coastal monitoring.

5.7 cBathy Adjustments

As the cBathy algorithm has been written to accurately map water depth for the east coast of the United States, it works well when analyzing swell waves. However, as the wave climate at the North Sea is less steady and consists to a larger extent of short wind induced wave frequencies, the algorithm is argued to be less accurate for the Dutch coast.

When cBathy was ran at Argus systems, so called short wave anomalies have been observed. The reduction of pixels (the decimation parameter) to increase computation speed in some cases causes the algorithm to be unable to identify short waves. This is because the spatial scales between the pixels became larger than the (short) waves. Anomalies in computations with data from the Duck Argus station showed unrealistically shallow areas as a result of this. Another cBathy problem regarded wave angle analysis. As was observed in this research, the analysis of the angle of incidence of the waves was in some incidences unstable for waves with a steep angle of incidence resulting in a modeled wave phase with a large error in the angle of incidence.

A new version of the cBathy algorithm takes care of these issues as the area used for the analysis of one particular coordinate is not prefixed like in the version of the algorithm that is used for this research. In the new version, the area used for wave analysis is extended when analyzing coordinates increasingly offshore. Because the amount of data taken into account is generally lower due to the smaller analysis area, for computational performance, there is no need for the decimation of pixel anymore. Furthermore, the robustness of the angle of incidence analysis is increased in the new version.

Where in the data for this research, some steep wave angles were analyzed in an incorrect way, these updates to the cBathy algorithm are estimated to increase accuracy for dataset 1.1. However, as the geometry error is strongly present for the other datasets, the updated algorithm would arguably yield a minor reduction in rmse. Hence, the cBathy improvements should be tested once the geometry errors are solved. The erroneous analysis of short

waves with a sharp angle if incidence as shown in section 5.3 also indicates that the second cBathy adjustments can potentially have a significant impact on the total accuracy of the method.

On the other hand, using a larger area for depth inversion when analyzing coordinates increasingly farther offshore (represented by the Kappa value) did not seem increase the performance of the method in this particular research. Therefore, it should be investigated whether the new version of the algorithm increases depth accuracy for UAV bathymetry mapping as conducted in this research.

5.8 Future Research

For this research the whole drone depth inversion process was extensively researched. The next part will elaborate on recommended future research to increase the effectiveness of the method as used in this research.

5.8.1 Testing cBathy

At the start of the research it was estimated that the depth inversion algorithm cBathy would be the largest contributor to the bathymetry error. However, as an incorrect geometry is found to be the largest error contributor to the method as described in this report, the algorithm was not tested to its limits. When using the same method, it is advised to put effort into solving the geometry in a more accurate manner. Once the pre-processing of the data is done in a more effective manner, the cBathy algorithm can be tested to its full extend. As drone footage renders different datasets due to the difference in stability and higher altitude, it would be interesting to compare its bathymetry accuracy with Argus stations. This can be investigated by flying a drone directly over an Argus station and record a dataset at the same time. Subsequently, of these datasets a bathymetry can be calculated by the cBathy algorithm which can be compared to ground truth. A video from the Argus station could also be analyzed exactly in the same way as the drone footage, including for instance calculating the geometry for every individual frame. This process could yield valuable information about the specific difference in accuracy between the two methods.

5.8.2 Variance Decrease

For coastal monitoring purposes, a large variance between the accuracies of the UAV bathymetry mapping is detrimental. When acquiring data for spe-

cific purposes, a specific accuracy has to be guaranteed for the data to be usable. Therefore, the variance between accuracies yielded by the different datasets should be decreased. As a large part of the variance was attributed to the error in the rectification, simply creating a better algorithm for the data preparation part of the process is estimated to yield better results in terms of variance. This is reinforced by the final two bathymetry errors of datasets 1.2 and 2.2. The error between the beach and water based GCPs was eliminated by only using the water GCPs. This yielded root mean squared errors with a discrepancy of 10 centimeters. As this research was unable to use data from both floating and beach GCPs, not the full potential of the method could be used. A more standardized geometry calculation is estimated to yield better results. Therefore it is recommended to investigate a more effective way to calculate the projection of the images.

On the other hand, this research is limited as all of the data was acquired on two subsequent days with similar conditions. Therefore, whereas the variance between the accuracies could be reduced by increasing the effectiveness of the rectification part of the UAV bathymetry mapping process, it does not guarantee the same variance between datasets which were acquired during days with different weather conditions.

5.8.3 Accuracy Increase

Once the variance between different measurements is decreased, the data can potentially become usable for coastal monitoring purposes. For which purposes it can potentially be used will be determined by the eventual accuracy. When the general accuracy standard of the International Hydrographic Organization (IHO) of 25 centimeters is reached, the data becomes usable for long term monitoring of coastal features or for giving an general indication of a bathymetry at the start of a comprehensive survey. If the accuracy could ever reach a root mean squared error below five centimeters, it could even be used for sediment budget calculations. In the next part of the report, some ways of increasing accuracy are described.

Eliminating the Rectification Error In this report the rectification error was only mitigated and not eliminated entirely. As it showed that the accuracy of the computed bathymetries increased significantly when using only control points on the beach, it could be argued that there are still large

gains that can be made once the rectification process works in a more effective manner. Whereas the best dataset in this research yields a fairly accurate bathymetry, there is still some skewness observed when comparing it to ground truth. Also, although smaller than for the other datasets, the absolute rectification error in the results section still showed a large value. This arguably indicates that the bathymetry error could be smaller than the 0.37 meters found, once the geometry error is decreased.

Kalman Filter Another way of increasing the total accuracy of the UAV bathymetry mapping method includes using a Kalman filter in combination with multiple measurements of the same area. This is a practice that has been used for a while in combination with data acquired by the Argus stations. The filter uses the quality parameters which are indicated for every depth calculation. In this way, locations where the cBathy algorithm effectively found wave patterns to base the calculations on are separated from the locations where the waves are less evident. When using multiple datasets taken on the same location, these quality parameters are used to increase accuracy across the domain.

This process does increase the labor intensity of the method. Therefore, it is recommended to research whether a Kalman filter increases the performance of the method and if this is the case an optimal number of surveys of the same area can be indicated.

Improved cBathy Another promising development is the creation of the new version of cBathy as described in part 5.7. In a personal communication with the creator of the algorithm Rob Holman it was indicated that for Argus data the new version of the algorithm significantly increased the total accuracy. It is recommended to research whether this is also the case for drone measurements.

5.9 Practices

There are virtually endless possibilities to use the UAV bathymetry mapping method. An investigation regarding several cBathy settings and data sampling parameters has shown their effects on the accuracy of the bathymetry that was computed. Based on these findings, the following section shows practices that can potentially increase the accuracy of the method.

5.9.1 Drone Stability

Because Argus cameras are fixed, their projection only has to be calculated once. The fixed position yields stable projected video footage because there is no discrepancy between the location of a specific pixel in subsequent frames. For the UAV bathymetry method as used in this report, for every single frame the homography is computed. As images are distracted from the captured video by two frames per second, rectifying every individual frame adds a stability error with a two hertz frequency. Because cBathy analyses wave frequencies between 1/3 and 1/12 hertz, this reduced stability should not decrease the accuracy of the depth inversion algorithm.

On the other hand, the stability of drone footage is ever increasing. An increased stability means that changes in the coordinate that can be linked to a specific pixel in the recorded footage is very small. This means that instead of calculation the coordinate of every single pixel for every single frame, the same homography could be used for subsequent frames. This means that especially the computation time of the rectification algorithm can be decreased significantly. It should however be taken into account that the frequency of the homography calculation should not interfere with the frequencies that are analyzed by the cBathy algorithm. For instance on the Dutch coast, where the analyzed wave lengths are in between 3 and 12 seconds, the calculation of the homography can for instance be done every 15 seconds.

Virtual Image Stabilization A way of stabilizing the video footage is virtual image stabilization. This can potentially be used when recording imagery during more extreme weather conditions or when using a drone less capable in terms of image stabilization.

Through analyzing rectification stability, a couple of findings were done in terms of potential stabilization practices for the drone depth inversion process. The stability analysis in the results section indicated that throughout the measurements a significant amount of noise could be detected in the geographical location when taken a random pixel from the UV domain and analyzing its location. As the rectification consists of assigning a geographical coordinate to a pixel (UV) coordinate, it does not necessarily have to be a physical ground control point. The below proposed image stabilization method works similar to stabilization methods being used to filter shaky images recorded

by hand held (and therefore moving) consumer devices. However, instead of matching pixel color, pixel coordinates are used.

After calculating the homography of a specific frame based on 4 points in that image of which the location is known, the geographical location of every single pixel in the image is estimated. When taking a random image, their location throughout the time series can be indicated at which point just like in the stability analysis of the results section noise is detected. The noise is indicated by filtering out sudden, unrealistic location changes of a specific pixel using a Savitsky Golay (Savgol) filter. The filter signal does include the longer term movements of the pixel location, which is necessary because unlike Argus cameras, the drone camera does not have a fixed aim. On the other hand, the 1 hertz noise caused by the rectification is filtered out. In this way, in theory every single pixel in the video domain (4096 * 2160 pixels) can be smoothed after which a more stable rectified video is computed. However, computing about 9 million Savgol filters is a time consuming job. Therefore, instead of calculating the filter every single pixel, only 4 have to be stabilized after which with the use of the internal camera parameters a new homography can be calculated for every frame. The 4 stabilized pixels can be indicated as virtual ground control points. The proposed stabilizer basically computes the homography of frame n with the use of all of the computed homographies for the frames surrounding it (a couple of seconds earlier ($n - 1, 2, 3$) and a couple of seconds later ($n + 1, 2, 3$)). It should be noted that the proposed stabilization method does not decrease the absolute error of the rectification. However, it does make it more stable from one frame to the other. Therefore, one of the potential implementations could be to have 4 fixed GCPS on land which are easy to setup and use these points to rectify a video. This video will be unstable as the area between the 4 points is relatively small. However, using virtual GCPS, the instability can be adjusted for. This practice has been done in this research en qualitatively (visually) it seems to yield a stable rectified video. On the other hand, in this practice cross shore spatial scales are difficult to verify.

The same process could potentially also be implemented in terms of drone position of viewing angle. As the rectification process used in this research calculates the position of the drone for every individual frame, strong differences in drone position of viewing angle from one frame to the next can be assumed to be untrue and adjusted for. Fur-

thermore, also the homography of frame n could be used as a basis to calculate the homography of frame $n + 1$ and thereby the footage might increase in stability.

The Use of Ships as Ground Control Points

Another method to decrease the need for floating ground control points is to use ships as ground control points. According to maritime law, ships over a certain length are required to broadcast their location every second while moving. If the drone camera is aimed in such a way that the ships are visible, they can be automatically detected and the broadcasted location can be used for rectifying the video. Generally, when analyzing a location that is increasingly far offshore, the rectification instability increases significantly. This can be contributed to the small errors in the solution for the homography are multiplied by the distance because of the geometrical conditions. As the ships are located far offshore, it can be argued that this method would yield stable results especially for the location of the area of interest.

5.9.2 Limitations

Because the UAV bathymetry mapping method in total consists of a large amount of steps, it is difficult to isolate different influential parameters. Due to changing weather conditions, measuring setups and rectification accuracies, the input data is different for all of the datasets. Therefore, even though this research attempted to keep the steps consistent throughout the datasets, differing final results indicate that there are still significant differences in the data. The sheer volume of potentially minor changes throughout the process resulted the differences in the data to add up and yield variable results. Therefore, these field experiments can only give an indication of which steps in the process are important as suggested by these specific measurements. The variable input parameters could not be isolated in an evident way and therefore results are not as specific as was aimed when starting the research. Only after a significant amount of research gets put into this specific subject a comprehensive database can establish more specific error contributors and guidelines for future use.

Conditions During Measurements The conditions during the measurements that were analyzed in this report were largely kept as constant as possible. The amount of fog during the two testing days was visually comparable and the wave

height was also similar. Due to differences in tidal phase, water level did change throughout the measurements. These specific conditions should be attributed to the results in this report and therefore statements made in this research could be different for similar measurements done with altering conditions. Again, more data needs to be gathered and compared before more generic conclusions and recommendations can be made.

6 Conclusions & Recommendations

This section starts with a summary of the thesis. The general results are briefly discussed after which the hypothesis is reviewed. After answering the research questions, the report concludes with recommendations on how future studies can contribute to the UAV bathymetry mapping method.

Summary To be able to increase efficiency regarding the acquisition of bathymetric data, this research aimed at contributing to the development of the UAV bathymetry mapping method working out every step in the process and investigating its accuracy. The research utilized video footage acquired by a Unmanned Aerial Vehicle to compute water depths in the nearshore of a specific location on the Dutch coast. The different videos as captured in the survey qualitatively seemed very similar. However, when comparing computed water depths with ground truth acquired using a jetski with an echo sounder, the method yielded different accuracies ranging from a root mean squared error (rmse) of 0.37 to 0.87 meters. The accuracy and especially the variance between the rmse's makes the technology in its current state unsuitable for coastal monitoring purposes. The largest contributor to the error of this method was found to be the calculation of the geometry when pre processing the video footage. A more standardized coordinate calculation is estimated to decrease variance which is required for the UAV bathymetry mapping method to in the future partly replace conventional bathymetry mapping methods.

Results This report includes bathymetries of an area 500 meters in cross shore direction and 500 meters in longshore direction at Scheveningen in the Netherlands. The bathymetries are calculated from video imagery taken by an Unmanned Aerial Vehicle. The process included three different steps. The first step involved data acquisition. Step 2 involved the rectification of the captured imagery and in the third step the water depths were computed.

The data for this research was acquired on two subsequent foggy days in February 2017. The days yielded 2 (1.1 and 1.2) and 3 (2.1, 2.2 and 2.3) usable datasets respectively. As datasets 1.1 and 2.1 as well as 1.2 and 2.2 were very similar and dataset 2.3 yielded bad results from the start, the analysis focuses on the first two datasets of each day. With weather conditions being similar and wave

height of around 0.95 meter on the first day and 0.80 meters on the second, for each dataset 2 offshore ground control points (GCPS) and 2 static GCPS on the beach were used to rectify every subsequent image that was cut from the video at a rate of 2 frames per second. The identified noise in the data as induced by step 1 and 2 of the process was established to be contributed to the foggy weather, the relatively small waves, the error in the GPS loggers positioned at the floating GCPS, the automatic GCP detection, the opposing tidal current and the geometry calculation for the image rectification. Subsequently, the water depth that is calculated by the depth inversion algorithm (cBathy) in step 3 is an estimation of which an uncertainty was expected.

The absolute rectification error ranged from 20 to 35 meters in the cross shore direction. Furthermore, an analysis to the pixel intensity of the grid that was used as input data to the cBathy algorithm showed similar values for the couples of similar datasets. The average pixel intensities of the cross section in the center of the area of interest at $Y = 0$ for dataset 1.1 and 2.1 showed a similar curve as well as the intensities for dataset 1.2 and 2.2. Regarding the standard deviation over the whole time series for the same cross section, dataset 2.2 was shown to have the largest value, while the other three datasets seemed comparable.

After fine tuning the parameters of the cBathy algorithm, the UAV bathymetry mapping method yielded root mean squared errors ranging between 0.37 (dataset 1.1) and 1.3 (dataset 2.1) meters for the predetermined area of interest 500 meters in cross shore and 500 meter in longshore direction. The datasets which yielded the best and the worst accuracy were seemingly identical in terms of visibility, ground control points used and their average analyzed pixel intensities. A discrepancy was found between the depth inversion accuracy of three different sub areas as compared to the total area of interest. In general the area closest the shore (the bank area) yielded more consistent results with a RMSE ranging from 0.25 meters for dataset 1.1 to 0.62 meters for dataset 2.2. The area farther offshore on the left side of the captured recording also seemed to perform well. The RMSE in this particular area ranged from 0.32 meters for dataset 1.1 to 0.64 meters for dataset 2.1. Whereas its RMSE was generally larger than the RMSE in the bank area, after dividing the error by the average water depth that area, it even seemed to perform better in most instances. On the other hand, for the offshore area on the right hand side of the recorded

video, the algorithm seemed to constantly underestimate water depth. Subsequently, after comparing the signal in three specific points, it was shown that around the poorly performing area the cBathy algorithm did not correctly model the specific wave frequencies as well as in other areas. However, as for every area it was shown that there were enough frequencies modeled in a correct manner, the algorithm should have been able to compute water depths with a higher accuracy than observed.

Fine tuning data sampling parameters indicated a potential increase in accuracy in several occasions. Whereas decreasing the grid size of the input matrix from 3 by 3 to 2 by 2 meters did not seem to yield better results, increasing the sampling rate from a 2 Hz to a 6 Hz frequency for the base (pre fine tuned) scenario did decrease the the rmse by 0.05 m. Especially in the areas farther offshore the accuracy increased. As the rectification noise is higher farther offshore, this decrease in error could arguably be contributed to the algorithm being able to filter out the noise in a more effective way. Also, as it increases the information available to resolve the same number of degrees of freedom, increasing the amount of ground control points used for the rectification process from 4 to 8 resulted in a 0.05 m decrease of the rmse. Also, increasing the spatial resolution of the data which is used to compute water depths does not seem to influence the observed signal and depth inversion in a positive way.

An investigation in the large rectification errors showed that the largest contributor to the total error with these particular measurements was an incorrect calculation of the geometry in the rectification process. Using different combinations of GCPs for the calculation of the geometry yielded significantly different mapped projections. It was shown that there was a large discrepancy between the location of a specific pixel according to the different GCP scenarios. This finding showed that the end result of the UAV bathymetry mapping method as it was performed in this research is sensitive to the usage of differing GCPs for the geometry calculation. For dataset 2.1, increasing the sheer amount of GCPs used therefore decreases the total rmse from 1.3 to 0.87. Subsequently, only using the four floating GCPs when using the UAV depth inversion method for datasets 1.2 and 2.2 decreased their rmse to 0.58 and 0.68 meters respectively. A reduction of almost half a meter.

Main Question: Is it valuable to intensify researching efforts regarding UAV bathymetry mapping for future use in coastal monitor-

ing? The results from this research show that it is possible to map a bathymetry with an rmse of 0.37 meters. As this is a relatively accurate bathymetry, the UAV bathymetry mapping method shows potential. How, for the data to be valuable, a low variance is desirable. Therefore, the discrepancy between the total accuracies of the different datasets renders the method unsuitable for coastal monitoring purposes for the current state of the technology.

Sub Question 1: What is the depth inversion accuracy in the current state of the technology for coastal conditions in the Netherlands? After the geometry error was taken into account, the eventual accuracy ranged from 0.37 to 0.87 meters rmse for an area of around 2500 square meters for dataset 1.1 and 2.1 respectively. The rmse's of dataset 1.2 and 2.2 were 0.58 and 0.68 meters respectively.

Sub Question 2: Does the depth inversion process yield consistent results within 0.2 meters root mean squared error? The the depth inversion results seem promising. However, the discrepancy between the rmse of the different datasets makes the technology in its current form unsuitable for coastal monitoring purposes. For the measurements used in this research the observed difference between the rmse of dataset 1.1 and dataset 2.1 was half a meter. Once the variance in the eventual accuracies is brought down, the data becomes more valuable and maybe eventually usable.

Sub Question 3: Which step in the UAV depth inversion process is the largest contributor to the water depth error budget? In this research, an error in the calculation of the geometry when converting the two dimensional video the a three dimensional projection was found to be the largest contributor to the overall water depth error. However, as it should be noted that different image rectification strategies might yield different results, other UAV bathymetry mapping efforts might stumble upon errors in different parts of the process. This is due to the large quantity of steps in the process.

Sub Question 4: On which aspect of the UAV bathymetry mapping method should future research be focused to increase its accuracy? In future attempts, especially the error variance

needs to be brought down. The reduction in variance can be established when sensitive areas like the geometry calculations are more standardized. Clear quality benchmarks should be established for every step in the process to be able to use the data without a reference bathymetry.

Recommendations It can be concluded that the algorithm is able to compute water depths with 0.37 meters root mean squared error. However, it is also shown that there is a large variance between four datasets which were very similar in terms of measuring setup and pixel intensities. On beforehand the bottleneck of the UAV depth inversion method was estimated to be the bottleneck in compiling an accurate bathymetry. However for the method used in this research, the rectification part of the process was a larger contributor to the total error budget. Therefore, to optimize the method used for this research, it is advised first increase the accuracy of the rectification. Thereafter, the depth inversion algorithm can be tested more thoroughly. Also, investigations regarding the data sampling and settings to be used for the depth inversion algorithm gave some indications for potential incremental improvements. These tests were done with the already well performing dataset 2.1. As these incremental improvements are only interesting when the bathymetry is already relatively accurate, provided that the rectification is calculated correctly, future research can investigate whether the indicated incremental improvements are valid for datasets recorded during differing conditions.

To become a widely adopted method in the future, the consistency of the UAV depth inversion method has to be improved. The lack of consistency is considered to be a larger drawback than its 0.37 meter rmse accuracy. If in a future scenario the variance in rmse's between different datasets could be decreased to 0.2 meters, the data could be usable for coastal monitoring purposes. Subsequently, efforts can also decrease the absolute error after which current jetski measurement technologies could be partly replaced. An existing method to decrease variance in bathymetry accuracy uses a Kalman filter. For every location the cBathy algorithm calculates quality control parameters, which seems to perform well. These parameters indicate whether the cBathy algorithm is confident that the optical signal is analyzed in a correct way. When multiple datasets are captured for the same area, the chance of at least one good wave field estimation for a specific coordinate increases. This is a method currently used for Argus stations, and is

assumed to work equally well for drone measurements. The downside is that each individual drone flight is labor intensive when compared to the Argus system. A potential strategy when using the Kalman filter would be to subsequently measure stretches of beach with a width of around 400 meters (approximately the width of the base of the projection) for the entire stretch of coast that needs to be measured. Thereafter, this process could be repeated a couple of times until there is enough data for the Kalman filter process to yield consistent results. It is therefore recommended to research how many measurements of 1 specific stretch of coast are necessary to be able to compute consistent bathymetry accuracy when using a Kalman filter. Even though repeating the measurements is a time consuming job, it is still estimated to be more cost and labor efficient than the current jetski measurements. Another strategy would be to overlap the measurements making the effective depth inversion area narrower. Provided that the wave and lighting conditions are sufficient, these strategies make sure that for every coordinate in the area of interest there is a high chance of a good skill value for the estimated water depth and therefore a consistent accuracy.

If these future implementations could decrease accuracy variance and eventually even total water depth errors, the UAV method can replace jetski measuring methods in some occasions. When compared to jetski depth measurements, there are significantly more factors throughout the measuring process that contribute to an error in the computed water depth. Therefore, it would involve extensive efforts to achieve a similar accuracy. Whereas it is not estimated that this will happen in the near future, the drone measurements could serve in situations where a five centimeter accuracy is not specifically required. For a first estimation of the layout of a specific area of interest or for generating input data for computational models, the drone measurements could be suitable.

The power of Argus stations lies in its near-continuous monitoring. As continuous monitoring of a specific coastal regions with UAV's would require a lot of repetitive efforts, for long term projects Argus station would be more desirable. However, for situations where only a bathymetric snapshot is required, its flexibility could make UAV bathymetry mapping a desirable solution. As worldwide there are only a couple jetskis equipped to measure water depth, the sheer number of drones available indicates a future with a wide range of applications.

References

- Aarninkhof, S. G. J. (2003). *Nearshore bathymetry derived from video imagery*, volume PhD.
- Aarninkhof, S. G. J., Turner, I. L., Dronkers, T. D. T., Caljouw, M., and Nipius, L. (2003). A video-based technique for mapping intertidal beach bathymetry. *Coastal Engineering*, 49(4):275–289.
- Algrain, M. and Quinn, J. (1993). Accelerometer based line-of-sight stabilization approach for pointing and tracking systems. *Control Applications*.
- Barrick, D. E. (1980). Accuracy of Parameter Extraction from Sample-Averaged Sea-Echo Doppler Spectra. *IEEE Transactions on Antennas and Propagation*, 28(1):1–11.
- Birkemeier, W. A., ASCE, A. M., and Mason, C. (1984). The Crab: A Unique Nearshore Surveying Vehicle. *Journal of Surveying Engineering*, 110(1):1–7.
- Brouwer, R. L., de Schipper, M. A., Rynne, P. F., Graham, F. J., Reniers, A. J. H. M., and MacMahon, J. H. (2015). Surfzone Monitoring Using Rotary Wing Unmanned Aerial Vehicles. *Journal of Atmospheric and Oceanic Technology*, 32(4):855–863.
- Chen, J.-f. and Fuh, C.-s. (2005). *Image stabilization with best shot selector and super resolution reconstruction*. PhD thesis.
- Chereau, R. and Breckon, T. (2013). Robust motion filtering as an enabler to video stabilization for a tele-operated mobile robot. *Proc. SPIE Electro-Optical Remote Sensing, Photonic Technologies, and Applications VII*.
- Chickadel, C. C., Holman, R. A., and Freilich, M. H. (2003). An optical technique for the measurement of longshore currents. *Journal of Geophysical Research*, 108(C11):1–17.
- Davidson, M., Van Koningsveld, M., de Kruif, A., Rawson, J., Holman, R. A., Lamberti, A., Medina, R., Kroon, A., and Aarninkhof, S. G. J. (2007). The CoastView project: Developing video-derived Coastal State Indicators in support of coastal zone management. *Coastal Engineering*, 54(6-7):463–475.
- Davis, C. O., Bowles, J., Leathers, R. A., Korwan, D., Downes, T. V., Snyder, W. A., Rhea, W. J., Chen, W., Fisher, J., and Bissett, W. P. (2002). Ocean PHILLS hyperspectral imager : design , characterization , and calibration. *Optics Express*, 10(4):2–11.
- de Vries, S., Hill, D. F., de Schipper, M. A., and Stive, M. J. F. (2011). Remote sensing of surf zone waves using stereo imaging. *Coastal Engineering*, 58(3):239–250.
- Dill, A. J., Garcia, M. H., and Albert, J. V. (1995). Video-Based Particle Tracking Velocimetry Technique For Measuring Flow Velocity in Porous Media. *Civil Engineering Studies*, (48).
- Dugan, J. P., Piotrowsky, C. C., and Williams, J. Z. (2001). Water depth and surface current retrievals from airborne optical measurements of surface gravity wave dispersion. *Journal of Geophysical Research*, 106(C8):16903–16915.
- Fujita, I., Muste, M., and Kruger, A. (2017). Large-scale particle image velocimetry for flow analysis in hydraulic engineering applications Large-scale particle image velocimetry for flow analysis in hydraulic engineering applications Vélocimétrie par image de particules a grande échelle (LSPIV) p. *Journal of Hydraulic Research*, 1686(April).
- Fujita, I., Watanabe, H., and Tsubaki, R. (2007). Development of a non intrusive and efficient flow monitoring technique : The space time image velocimetry (STIV). *International Journal of River Basin Management*, 5124(April).
- Gorsline, D. S. (1966). Dynamic characteristics of west Florida Gulf Coast beaches. *Marine Geology*, 4:187–206.
- Guenther, G. C., Cunningham, A. G., Larocque, P. E., and Reid, D. J. (2000). Meeting the Accuracy Challenge in Airborne Lidar Bathymetry.
- Herrera, C. D., Kannala, J., and Heikkilä, J. (2012). Joint depth and color camera calibration with distortion correction. *IEEE Transactions on Pattern Analysis and Machine Intelligence*, 34(10):2058–2064.
- Holland, K. T. (1992). *The Statistical Distribution of Swash Maxima on Natural Beaches*. PhD thesis.
- Holland, K. T., Holman, R. A., Lippmann, T., Stanley, J., and Plant, N. (1997). Practical use of video imagery in nearshore oceanographic field studies. *IEEE Journal of Oceanic Engineering*, 22(1):81–91.

- Holland, K. T., Lalejini, D. M., Spansel, S. D., and Holman, R. A. (2010). Littoral environmental reconnaissance using tactical imagery from unmanned aircraft systems. *Ocean Sensing and Monitoring II*, 7678:767806–767806–8.
- Holland, T. K. (2001). Application of the linear dispersion relation with respect to depth inversion and remotely sensed imagery. *IEEE Transactions on Geoscience and Remote Sensing*, 39(9):2060–2072.
- Holman, R. A. (1981). Infragravity energy in the surf zone. *Journal of Geophysical Research*, 86(C7):6442.
- Holman, R. A., Holland, K. T., Lalejini, D. M., and Spansel, S. D. (2011). Surf zone characterization from Unmanned Aerial Vehicle imagery. *Ocean Dynamics*, 61(11):1927–1935.
- Holman, R. A., Plant, N., and Holland, K. T. (2013). CBathy: A robust algorithm for estimating nearshore bathymetry. *Journal of Geophysical Research: Oceans*, 118(5):2595–2609.
- Holman, R. A., Sallenger, A. H., Lippmann, T. C., and Haines, J. W. (1993). The Application of Video Image Processing to the Study of Nearshore Processes. *Oceanography*, 6(3):78–85.
- Holman, R. A. and Stanley, J. (2007). The history and technical capabilities of Argus. *Coastal Engineering*, 54(6-7):477–491.
- Holthuijsen, L. H. (2014). *Waves in Oceanic and Coastal Waters*.
- Ingle, J. C. (1966). *The Movement of Beach Sand*. Elsevier.
- Irish, J. L. and Lillycrop, W. J. (1999). Scanning laser mapping of the coastal zone: The SHOALS system. *ISPRS Journal of Photogrammetry and Remote Sensing*, 54(2-3):123–129.
- Irish, J. L., McClung, J. K., and Lillycrop, W. J. (2000). Airborne Lidar Bathymetry: The Shoals System. *Bulletin-International Navigation Association*, pages 43–54.
- Jiminez, J. A., Osorio, A., Marino-Tapia, I., Davidson, M., Medina, R., Kroon, A., Archetti, R., Ciavola, P., and Aarnikhof, S. G. J. (2007). Beach recreation planning using video-derived coastal state indicators. *Coastal Engineering*, 54(6-7):507–521.
- Johannessen, J. A. (2000). Coastal observing systems: the role of synthetic aperture radar. *Johns Hopkins APL technical digest*, 21(1):41–48.
- Komar, P. D. and Inman, D. L. (1970). Longshore Sand Transport on Beaches. *Journal of Geophysical Research*, 75(30):5914–5927.
- Kroon, A., Davidson, M. A., Aarninkhof, S. G. J., Archetti, R., Armaroli, C., Gonzalez, M., Medri, S., Osorio, A., Aagaard, T., Holman, R. A., and Spanhoff, R. (2007). Application of remote sensing video systems to coastline management problems. *Coastal Engineering*, 54(6-7):493–505.
- Kutser, T., Eloheimo, K., Hannonen, T., Harma, P., Kirkkala, T., Koponen, S., Pullianen, J., and Pyhalahti, T. (1998). Monitoring of Coastal Waters of the Baltic Sea by Airborne Imaging Spectrometer AISA. *Transactions on Ecology and the Environment*, 18.
- Lee, K.-h. and Mizutani, N. (2007). Wave-current Interaction for Waves Propagating Against Currents. *International Journal of Offshore and Polar Engineering*, 17(4):259–265.
- Leu, L., Kuo, Y., and Liu, C. (1998). Coastal Bathymetry from the Wave Spectrum of Spot Images. *Coastal Engineering Journal*, 41(1).
- Li, J., Zhang, H., Hou, P., Fu, B., and Zheng, G. (2016). Mapping the bathymetry of shallow coastal water using single-frame fine-resolution optical remote sensing imagery. *Acta Oceanologica Sinica*, 35(1):60–66.
- Lin, Y.-m. and Fuh, C.-s. (2006). Image Stabilization System on a Camera Module with Image Composition. *Images & Recognition*, 12(4):40–45.
- Lippmann, T. C. and Holman, R. A. (1989). Quantification of sand bar morphology: A video technique based on wave dissipation. *Journal of Geophysical Research: Oceans*, 94(C1):995–1011.
- Lippmann, T. C. and Holman, R. A. (1990). The Spatial and Temporal Variability of Sand Bar Morphology. *Faculty Research Publications (Oregon State University)*.
- Lippmann, T. C. and Holman, R. A. (1991). Phase Speed and Angle of Breaking Waves Measured with Video Techniques. *Coastal Sediments*.
- Lippmann, T. C., Holman, R. A., and Hathaway, K. K. (1993). Episodic, Nonstationary Behavior

- of a Double Bar System at Duck, North Carolina, U.S.A., 1986-1991. *Journal of Coastal Research*, 15:49–75.
- Litvin, A., Konrad, J., and Karl, W. (2003). Probabilistic video stabilization using Kalman filtering and mosaicing. *Image and Video Communications and Processing*.
- Lyzenga, D. R., Malinas, N. P., and Tanis, F. J. (2006). Multispectral bathymetry using a simple physically based algorithm. *IEEE Transactions on Geoscience and Remote Sensing*, 44(8):2251–2259.
- Matsushita, Y., Ofek, E., Ge, W., Tang, W., and Shum, H. (2006). Full-frame video stabilization with motion inpainting. *IEEE Transactions on Pattern Analysis and Machine Intelligence*, 27(7):1150 – 1163.
- Medina, R., Marino-Tapia, I., Osorio, A., Davidson, M., and Martin, F. L. (2007). Management of dynamic navigational channels using video techniques. *Coastal Engineering*, 54(6-7):523–537.
- Mills, G. B. (1998). International Hydrographic Survey Standards. *International Hydrographic Review*.
- Mobley, C. D., Sundman, L. K., Davis, C. O., Bowles, J. H., Downes, T. V., Leathers, R. a., Montes, M. J., Bissett, W. P., Kohler, D. D. R., Reid, R. P., Louchard, E. M., and Gleason, A. (2005). Interpretation of hyperspectral remote-sensing imagery by spectrum matching and look-up tables. *Applied optics*, 44(17):3576–3592.
- Monasse, P., Morel, J., and Tang, Z. (2010). Three-step image rectification. *Proceedings of the British Machine Vision Conference*, pages 89.1–89.10.
- Moulton, M., Elgar, S., and Raubenheimer, B. (2014). Improving the time resolution of surf-zone bathymetry using in situ altimeters. *Ocean Dynamics*, 64(5):755–770.
- Pacheco, A., Horta, J., Loureiro, C., and Ferreira (2015). Retrieval of nearshore bathymetry from Landsat 8 images: A tool for coastal monitoring in shallow waters. *Remote Sensing of Environment*, 159:102–116.
- Piotrowski, C. C. and Dugan, J. P. (2002). Accuracy of bathymetry and current retrievals from airborne optical time-series imaging of shoaling waves. *IEEE Transactions on Geoscience and Remote Sensing*, 40(12):2606–2618.
- Plant, N. G., Edwards, K. L., Kaihatu, J. M., Veeramony, J., Hsu, L., and Holland, K. T. (2009). The effect of bathymetric filtering on nearshore process model results. *Coastal Engineering*, 56(4):484–493.
- Plant, N. G., Holland, K. T., and Haller, M. C. (2008). Ocean wavenumber estimation from wave-resolving time series imagery. *IEEE Transactions on Geoscience and Remote Sensing*, 46(9):2644–2658.
- Plant, N. G., Holland, K. T., and Puleo, J. A. (2002). Analysis of the scale of errors in nearshore bathymetric data. *Marine Geology*, 191(1-2):71–86.
- Plant, N. G. and Holman, R. A. (1997). Intertidal beach profile estimation using video images. *Marine Geology*, 140(1-2):1–24.
- Rijkswaterstaat (2017a). Water Level Data.
- Rijkswaterstaat (2017b). Wave Height Data.
- Ruessink, B. G., Price, T., and Castelle, B. (2013). Finite-Amplitude Behaviour of alongshore variability in nearshore sandbars: observations and modelling. *Coastal Dynamics*, pages 1–14.
- Ruessink, B. G., Walstra, D. J. R., and Southgate, H. N. (2003a). Calibration and verification of a parametric wave model on barred beaches. *Coastal Engineering*, 48(3):139–149.
- Ruessink, B. G., Wijnberg, K. M., Holman, R. A., Kuriyama, Y., and van Enckevort, I. M. J. (2003b). Intersite comparison of interannual nearshore bar behavior. *Journal of Geophysical Research*, 108(C8).
- Ruggiero, P., Kaminsky, G. M., Gelfenbaum, G., and Voigt, B. (2005). Seasonal to Interannual Morphodynamics along a High-Energy Dissipative Littoral Cell. *Journal of Coastal Research*, 21(3):553–578.
- Sallenger, A. H., Krabill, W. B., Swift, R. N., Brock, J., List, J., Hansen, M., Holman, R. A., Manizade, S., Sontag, J., Meredith, A., Morgan, K., Yunkel, J. K., Frederick, E. B., and Stockdon, H. F. (2003). Evaluation of Airborne Topographic Lidar for Quantifying Beach Changes. *Journal of Coastal Research*, 18(1):125–133.
- Senet, C. M., Seemann, J., Flampouris, S., and Ziemer, F. (2008). Determination of bathymetric and current maps by the method DiSC based

- on the analysis of nautical X-band radar image sequences of the sea surface (November 2007). *IEEE Transactions on Geoscience and Remote Sensing*, 46(8):2267–2279.
- Smit, M. W. J., Aarninkhof, S. G. J., Wijnberg, K. M., Gonzalez, M., Kingston, K. S., Southgate, H. N., Ruessink, B. G., Holman, R. A., Siegle, E., Davidson, M., and Medina, R. (2007). The role of video imagery in predicting daily to monthly coastal evolution. *Coastal Engineering*, 54(6-7):539–553.
- Sobral, F., Pereira, P., Cavalcanti, P., Guedes, R., and Calliari, L. (2013). Intertidal Bathymetry Estimation Using Video Images on a Dissipative Beach. *Journal of Coastal Research*, SI 65(65):1439–1444.
- Son, Y. T., Lee, S. H., Kim, C. S., Chul Lee, J., and Lee, G. H. (2007). Surface current variability in the Keum River Estuary (South Korea) during summer 2002 as observed by high-frequency radar and coastal monitoring buoy. *Continental Shelf Research*, 27(1):43–63.
- Stockdon, H. F. and Holman, R. a. (2000). Estimation of wave phase speed and nearshore bathymetry from video imagery. *Journal of Geophysical Research*, 105(C9):22015.
- Stumpf, R. P., Culver, M. E., Tester, P. A., Tomlinson, M., Kirkpatrick, G. J., Pederson, B. A., Truby, E., Ransibrahmanakul, V., and Soracco, M. (2003). Monitoring *Karenia brevis* blooms in the Gulf of Mexico using satellite ocean color imagery and other data. *Harmful Algae*, 2(2):147–160.
- Taborda, R. and Silva, A. (2012). COSMOS: A lightweight coastal video monitoring system. *Computers and Geosciences*, 49:248–255.
- Teague, C. C. (1986). Multifrequency HF Radar Observations of Currents and Current Shears. *IEEE Journal of Oceanic Engineering*, OE-11(2):258–269.
- Trebossen, H., Deffontaines, B., Classeau, N., Kouame, J., and Rudant, J. P. (2005). Monitoring Coastal Evolution and Associated Littoral Hazards of French Guiana Shoreline with Radar Images. *Comptes Rendus - Geoscience*, 337(13):1140–1153.
- Trizna, D. B. (2001). Errors in bathymetric retrievals using linear dispersion in 3-D FFT analysis of marine radar ocean wave imagery. *IEEE Transactions on Geoscience and Remote Sensing*, 39(11):2465–2469.
- Turner, I. L. and Anderson, D. J. (2007). Web-based and 'real-time' beach management system. *Coastal Engineering*, 54(6-7):555–565.
- Turner, I. L., Harley, M. D., and Drummond, C. D. (2016). UAVs for Coastal Surveying. *Coastal Engineering*, 114:19–24.
- Van Dongeren, A., Plant, N., Cohen, A., Roelvink, D., Haller, M. C., and Catalán, P. (2008). Beach Wizard: Nearshore bathymetry estimation through assimilation of model computations and remote observations. *Coastal Engineering*, 55(12):1016–1027.
- Van Enckevort, I. M. J. and Ruessink, B. G. (2001). Effect of hydrodynamics and bathymetry on video estimates of nearshore sandbar position. *Journal of Geophysical Research*, 106:100.
- Van Koningsveld, M., Davidson, M., Huntley, D., Medina, R., Aarninkhof, S. G. J., Jiménez, J. A., Ridgewell, J., and de Kruif, A. (2007). A critical review of the CoastView project: Recent and future developments in coastal management video systems. *Coastal Engineering*, 54(6-7):567–576.
- Van Koningsveld, M., Stive, M. J. F., Mulder, J. P. M., de Vriend, H. J., Ruessink, B. G., and Dunsbergen, D. W. (2003). Usefulness and Effectiveness of Coastal Research: A Matter of Perception? *Journal of Coastal Research*, 18(2):441–461.
- van Son, S., Lindenbergh, R., de Schipper, M., de Vries, S., and Fuijnmayr, K. (2009). Using a Personal Watercraft for Monitoring Bathymetric Changes at Storm Scale.
- Vousdoukas, M. I., Pennucci, G., Holman, R. A., Conley, D. C., and Bartolomeo, V. S. (2011). A semi automatic technique for Rapid Environmental Assessment in the coastal zone using Small Unmanned Aerial Vehicles (SUAV). *Journal of Coastal Research*, (64):1755–1759.
- Wengrove, M. E., Henriquez, M., de Schipper, M. A., Holman, R., and Stive, M. J. F. (2013). Monitoring Morphology of the Sand Engine Lee-side Using Argus' cBathy. *Coastal Dynamics*, pages 1893–1904.
- Wijnberg, K. M. and Terwindt, J. H. J. (1995). Extracting decadal morphological behaviour from high-resolution, long-term bathymetric surveys

- along the Holland coast using eigenfunction analysis. *Marine Geology*, 126(1-4):301–330.
- Williams, W. W. (1947). The Determination of Gradients on Enemy-Held Beaches. *The geographical Journal*, 109(1):76–90.
- Windau, J. and Itti, L. (2011). Multilayer real-time video image stabilization. *Intelligent Robots and Systems*.
- Wu, J. and Juang, J. T. (1996). Application of Satellite Images to the Detection of Coastal Topography. *Coastal Engineering*, 25.
- Young, I. R., Rosenthal, W., and Ziemer, F. (1985). A three-dimensional analysis of marine radar images for the determination of ocean wave directionality and surface currents. *Journal of Geophysical Research*, 90:1049–1059.
- Zhang, Q. and Pless, R. (2004). Extrinsic Calibration of a Camera and Laser Range Finder (improves camera calibration) . *Iros*, 3:2301–2306.
- Zhang, Z. (2002). A Flexible New Technique for Camera Calibration (Technical Report). *IEEE Transactions on Pattern Analysis and Machine Intelligence*, 22(11):1330–1334.